12-2022

# Synthesis of Bioactive Heterocycles

Shaila Akter Shetu
*The University of Texas Rio Grande Valley*

# SYNTHESIS OF BIOACTIVE HETEROCYCLES

A Thesis

by

SHAILA AKTER SHETU

Submitted in Partial Fulfillment of the

Requirements for the Degree of

MASTER OF SCIENCE

Major Subject: Chemistry

The University of Texas Rio Grande Valley

December 2022

# SYNTHESIS OF BIOACTIVE HETEROCYCLES

A Thesis
by
SHAILA AKTER SHETU

COMMITTEE MEMBERS

Dr. Debasish Bandyopadhyay
Chair of Committee

Dr. Narayan G Bhat
Committee Member

Dr. Javier Macossay-Torres
Committee Member

December 2022

# ABSTRACT

Shetu, Shaila Akter, SYNTHESIS OF BIOACTIVE HETEROCYCLES. Master of Science (MS), December, 2022, 94 pp., 9 tables, 64 figures, references, 81 titles.

The Discovery of a variety of heterocyclic drugs for the treatment of cancer and other diseases (e.g, neglected tropical diseases) is a medical breakthrough and inspiring for the research community as a whole. A wide range of natural, semi-synthetic, and synthetic anticancer drugs are synthesized using various methods. Among them, β -lactams stand out as a novel class of antibiotics that has different types of biological as well as anti-cancer properties. β -lactam has become a premier and active research subject towards the development of revolutionary anti-cancer drugs. In recent years, a large amount of investigations have been done to find the anticancer effect of β -lactams. There exist clinically established synthetic methods to synthesize the beta-lactam ring. To find the better anticancer effect, many bicyclic, polycyclic starting materials have been selectively chosen to be used with the beta-lactam ring. Many endeavors conducted comprehensive biological studies to determine the anticancer activity of such synthetic β -lactams. Also, to investigate the binding effect of β -lactam, molecular docking studies have been performed. This review discusses several prominent synthetic methods of synthesis and anticancer activity of β -lactams.

# DEDICATION

I dedicate this thesis and all my academic progress made so far to my Parents and my Husband for their unwavering support and prayers and to the Almighty God for wisdom, strength, and good health.

# ACKNOWLEDGMENTS

My heartfelt gratitude goes to my mentor and committee chair, Dr. Debasish Bandyopadhyay for his insightful and unparallel mentorship, patience, and guidance. It's been a privilege and honor coming under your guidance and I am grateful for providing the platform through which this project was successfully completed. To my research committee members Dr. Narayan G Bhat, Dr. Javier Macossay-Torres, thanks for more than willing to help and for your generous expertise whenever needed. To Thomas Eubanks, thanks for always responding to our equipment needs. To my colleagues in the lab- Judith, Tanzida, and Nazmul, thanks for the help and valuable contributions.

Finally, many thanks to the office for sustainability and the University of Texas Rio Grande Valley for the financial support given through the prestigious Sustainability Fellowship.

TABLE OF CONTENTS

Page

LIST OF TABLES

Page

LIST OF FIGURES

Page

# CHAPTER I

# INTRODUCTION

## Heterocyclic drugs on neglected tropical diseases (NTDs) (Part-A)

In drug discovery research heterocycles play a significant role. A significant number of small molecule inhibitors are heterocyclic compounds. Among various classes of heterocycles, for example, aza-, oxo-, phospho-, thioheterocycles; aza- or nitrogen heterocycles are found in many pharmacologically relevant compounds natural and synthetic. Benzopyrazine (also known as quinoxaline) is a fused bicyclic scaffold in which benzene is fused with pyrazine (Bandyopadhyay & Banik, 2021). A few naturally occurring antibiotics and nutrients like vitamin B2 contain benzopyrazine moiety as a core in their structures (Figure 1). This scaffold is present as the key structural motif in many biologically active compounds, which includes anticancer (Bandyopadhyay et al., 2013; Lee et al., 2012; Qi et al., 2018), antibacterial (El-Attar et al., 2018), antitubercular (Achutha et al., 2013), anti-ebola (Loughran et al., 2016), antifungal (Carta et al., 2001) among many others. Consequently, several procedures of synthesizing benzopyrazines have been reported in the literature. A few synthetic procedures, reported in the immediate past, include the synthesis of benzopyrazines under the catalytic influence of Co3O4 nanocages based nickel catalyst (Sharma et al., 2021), iron-catalyzed transfer hydrogenative condensation (Putta et al., 2021), sodium hydroxide-mediated hydrogen-transfer (Wang et al., 2021), as well as the uses of tungstophosphoric acid-support (Kumaresan et al., 2020) , and

Co-based nanocatalyst (Panja et al., 2020)(13).

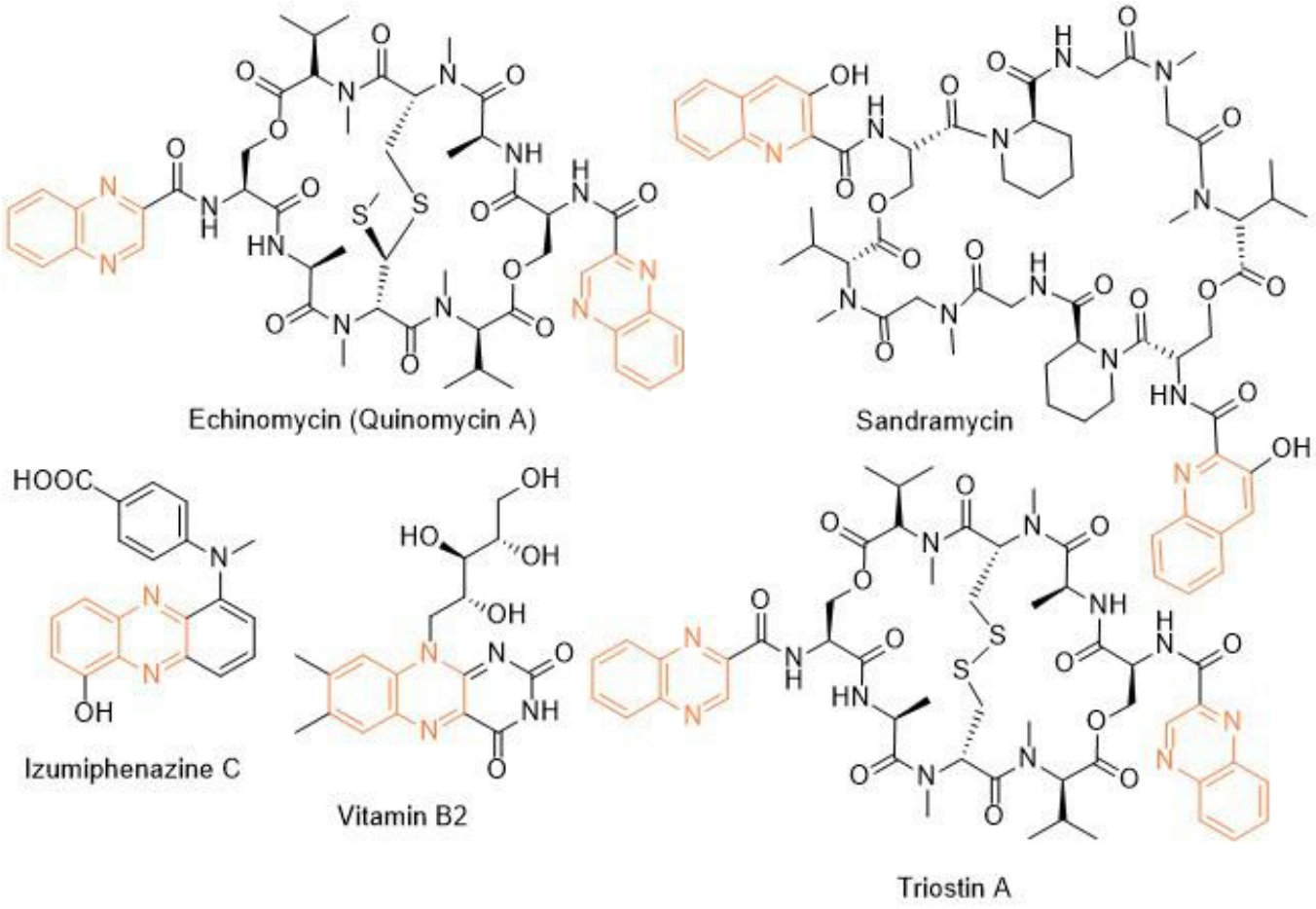


Figure 1.1: Different heterocyclic drugs used in NTDs

On the other hand, the World Health Organization (WHO) identified twenty tropical disease categories as neglected tropical diseases (NTDs). In general, the population below the poverty line are the primary sufferers of NTDs. Every year millions of people from 149 countries worldwide are being infected by NTDs that cause the waste of billions of dollars and a loss of thousands of lives. Based on the mortality and morbidity rates, Chagas' disease (named after the Latin American physician Carlos Chagas, also known as American trypanosomiasis) and leishmaniasis are two major categories of NTDs that demand immediate attention from the global community (Maheshwari & Bandyopadhyay, 2021)(14).

## Molecular Mechanism of Pancreatic Cancer and it's Inhibitor (Part-B)

### Major drivers of pancreatic cancer

Pancreatic cancer is considered as most common and the most lethal type of cancer. It is seventh most common cause of cancer-associated deaths around the World and the 3rd leading cause of cancer-related death for both men and women in the United States and is the only major cancer with a 5-year relative survival rate in the single digits (8.5%) (Are et al., 2016; Mizrahi et al., 2020). The majority of pancreatic malignancies arise from microscopic non-invasive epithelial proliferation known as pancreatic intraepithelial neoplasia that develops inside the pancreatic ducts. According to estimates, pancreatic ductal adenocarcinoma (PDAC) is the most prevalent kind of pancreatic cancer, caused 432,242 deaths globally in 2018 (Rawla et al., 2019). PDAC is a condition having genetic and epigenetic components to its onset, progression, and emergence of treatment resistance.

A multistep process leads to the development and progression of pancreatic cancer. There are four main driver genes for pancreatic cancer: KRAS, CDKN2A, TP53, and SMAD4 which introduced the concept of core signaling pathways (Jones et al., 2008). Pancreatic intraepithelial neoplasia (PanIN) lesions are precursors to pancreatic cancer, which progresses to invasive carcinoma (Ferro & Falasca, 2014; Hidalgo, 2010). PanIN lesions are further subdivided into low (PanIN-1A/B) to high (PanIN-3) grade lesions based on the degree of cellular and nuclear atypia (Hruban et al., 2000). Over time, numerous genetic changes cause histologic progression through the PanIN stages (PanIN1–3), ultimately leading to invasive adenocarcinoma. These changes include microRNAs (miRNAs), various genes that promote or

suppress tumor growth, and genetic mutations (Khan et al., 2013; Yonemori et al., 2017). In initial low grade PanIN lesions (PanIN-1), Kirsten rat sarcoma oncogene homolog (KRAS) is mutated, oncogenic miRNAs are overexpressed, and stromal associated factors are activated. In intermediate lesions (PanIN-2), Mucin 1 (MUC1) is overexpressed, and inactivating mutations in the p16/CDKN2A. Finally, late lesions (PanIN-3) are linked to inactivating mutations in tumor protein p53 (TP53), breast cancer type 2 susceptibility protein (BRCA2) (Ferro & Falasca, 2014; Golan et al., 2014; Tinder et al., 2008; Weissmueller et al., 2014).

Various small molecule inhibitors are used in combination or alone for treatment of pancreatic cancer.

**RAS inhibitors in pancreatic cancer**

Most cases of pancreatic cancer have mutations in the KRAS gene at the time of diagnosis (>80% of cases). It is found that 90% of pancreatic cancers are developed in the exocrine compartment of the pancreas and cause pancreatic ductal adenocarcinoma (PDAC). Codon 12 is accountable for 98% of PDAC mutation. Research found that codon G12D (51%) is the most aggressive PDAC subtype subsequently G12V (30%), G12A/C/S (2% each), and G12L/F (<1%) (Bryant et al., 2014). KRAS plays a vital role in developing PDAC type pancreatic cancer (Lanfredini et al., 2019). The progression of PDAC occurs due to the loss of tumor suppressor gene cyclin-dependent kinase inhibitor 2A (CDKN2A) (Schutte et al., 1997). Although KRAS mutation is undruggable and does not have any anti-KRAS therapy, some inhibitors show their effect against cancers. Inhibition of the RAF-MEK-ERK protein kinase pathway is one of the most potent factors that works against KRAS mutation. This pathway has an important role in the progression of PDAC (Waters & Der, 2018). It is also reported that iExosomes inhibit PDAC in mice by delivering RNAi. However, exosomes are therapeutically potential to control KRAS-

dependent pancreatic cancer (Kamerkar et al., 2017; Kordelas et al., 2014). Additionally, the KRAS mutation can be inhibited by using a slow-released biodegradable polymer matrix. This process works delivering siRNA as an extended-release drug to mutated KRAS (Zorde Khvalevsky et al., 2013). Another method for suppressing the KRAS mutation is Anti-RAS vaccination. These vaccines contain different mutated genes that work against KRAS mutations (Mosolits et al., 2005; Quandt et al., 2018).

Table 1.1: RAS inhibitors in pancreatic cancer

| Inhibitors | Structure | Target | Ref |
|---|---|---|---|
| AMG 510 (Lumakras or Sotorasib) | 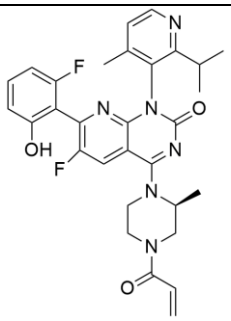 | $KRAS^{G12C}$ inhibitor | (Canon et al., 2019) |
| MRTX849 (Adagrasib) | 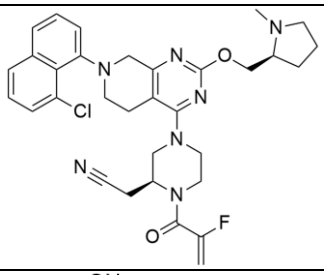 | $KRAS^{G12C}$ inhibitor | (Hallin et al., 2020) |
| ††† | 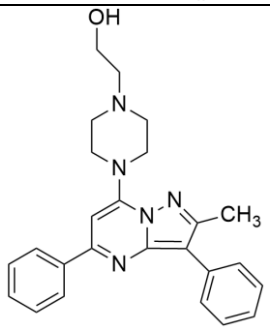 | Inhibits MAPK/RAF signaling | (McCarthy et al., 2019) |
| Deltarasin | 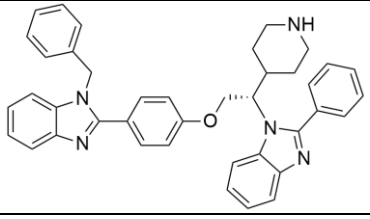 | Downregulates RAS/RAF signaling pathway | (Leung et al., 2019) |

Table 1.1: RAS inhibitors in pancreatic cancer (cont.)

| | | | |
|---|---|---|---|
| Talniflumate + Ggefitinib | 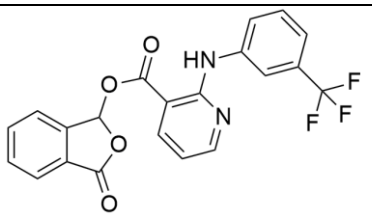 | Inhibition of 2 β-1,6 N-acetylglucosaminyltransferase (GCNT3) | (Rao et al., 2016) |
| MDC-1016 | 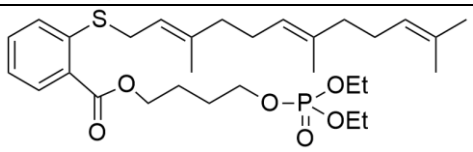 | Ras inhibitor | (Mackenzie et al., 2013) |
| Natural product | | | |
| Simvastatin | 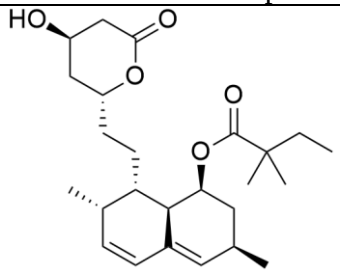 | GFP-K-Ras protein trafficking | (Gbelcová et al., 2017) |
| Avicin G | 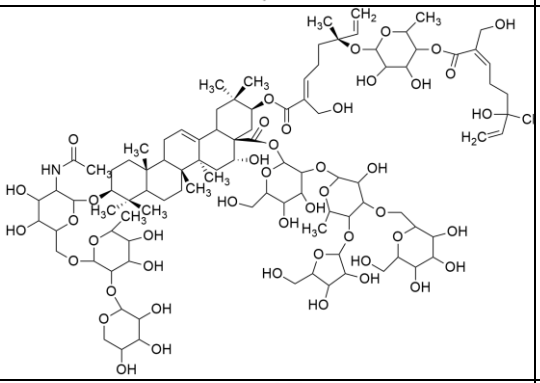 | $KRAS^{G12V}$ and $HRAS^{G12V}$ | (Garrido et al., 2020) |
| Prostratin | 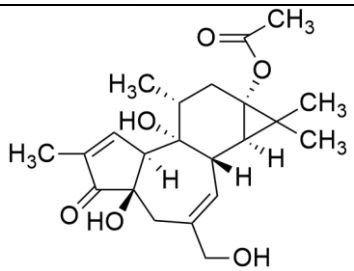 | KRAS | (Wang et al., 2015) |
| Lupeol | 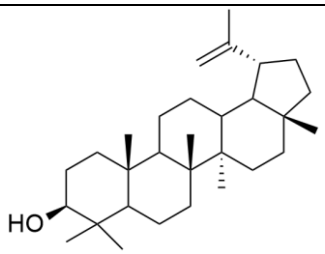 | $KRAS^{G12V}$ | (Sturm et al., 1996) |

**AMG 510 (Lumakras or Sotorasib).** The AMG 510 inhibits $KRAS^{G12C}$ type oncogene by using irreversible strategy of the His95 groove, which is close to the cystine pocket. It also downregulates MAPK signaling pathway in both pancreatic and lung cancer. But it does not affect wild-type $KRAS^{G12C}$ mutation that proves the specificity of AMG 510. After the consequent success, further study has been conducted to get a more efficacious result. Combinatorial therapy of AMG 510 with MAPK inhibitor (carboplatin) creates a more potent outcome than monotherapy. These effective outcomes induce researchers to move forward. As a result, synergistic effects are tested on the mice model, and 90% of mice qualified for complete tumor suppression. Finally, a preliminary clinical study on the human model provided 50% tumor regression. However, most of the success of these comprehensive studies goes only for $KRAS^{G12C}$ oncogene, mostly found in lung cancer (Román et al., 2018). Only 2% PDAC are responsible for KRASG12C oncogene (Melo et al., 2015).

**MRTX849 (Adagrasib).** Jill Hallin et al. (Janes et al., 2018) found very potent, selective, and covalent KRASG12C inhibitor in pancreatic and lung cancer, which is structurally and functionally close to the AMG 510. This compound exerts effectiveness in combination therapy and has remarkable potency when admin-istered only MRTX849. Thus, phase I clinical study was conducted with the single agent in two patients associated with the final stage lung and colon carcinoma. Results showed partial response to these two critical types of cancers. However, the comeback of ERK signaling and lack of inhibition of mTOR-S6 signaling makes the MRTX849 re-sponse short-termed and ineffective. The result from this study makes expectations for pancreatic cancer treatment.

**†††.** Recently, investigations found that AMG 510 is not the only small molecule inhibitor that is potent to KRAS mutation. In 2019, McCarthy et al. (Patricelli et al., 2016)

developed a new small molecule inhibitor which has the affinity to bind the allosteric binding site. This allosteric pyrazolopy-rimidine-based inhibitor (†††) binds with the allosteric p1 pocket of both wild-type and KRAS mutant. This new small molecule blocks MAPK pathway by downregulating the Raf signaling towards RAS mutation. Another advantage of this allosteric inhibition is that it is not limited to only the specific type KRAS allele. It shows benefit to wild type and GTP bound subtype KRAS oncogene. This remarkable positive result makes this allosteric inhibitor first-line therapy for tumor treatment in a different range. This small molecule allosteric inhibitor showed notably good results in lung and oral cancer cell lines that make the allosteric pyrazolopyrimidine-based inhibitor applicable for PDAC treatment.

**Deltarasin.** Recent studies found Deltarasin downregulates RAS/RAF signaling pathway by inhibiting Phosphodiesterase-δ (PDEδ) binding with hydrophobic pocket of PDEδ, resulting in inhibition of KRAS harbored pancreatic ductal adenocarcinoma (PDAC) (Cox et al., 2014; Miguel-García et al., 1998). The majority of lung cancer incidents happen for KRAS mutants (Gysin et al., 2011). As a result, Leung et al. (Zimmermann et al., 2014) first identified that deltarasin induces apoptosis significantly in both vitro and in vivo in lung cancer cells. It also induces autophagy in lung cancer cells by inhibiting MAPK/mTOR signaling pathway. It is also shown that when deltarasin is treated with 3-MA (autophagy inhibitor), it increases autophagic properties and produces more intracellular ROS levels, protecting further autophagy.

**Talniflumate.** Mucin is one of the major culprits that hinder drug delivery, and several clinical studies identified that mucin is overexpressed in KRAS-driven pancreatic cancer in mouse and human models (Evelyn et al., 2014; Kaur et al., 2013; Wallis et al., 2022; Xie et al., 2017). Enzyme 2 β-1,6 N-acetylglucosaminyltransferase (GCNT3) is recognized as a novel core mucin synthesized enzyme, and targeting this enzyme could decrease the overexpression of

mucin (Geltz & Augustine, 1998). KRAS mutation with p48Cre/+-LSL-KrasG12D/+ GEM upregulates the mucin concentration in pancreatic intraepithelial neoplasia (PanIN) and PDAC. Further study found that GCNT3 enzyme is abnormally expressed from GEM in pancreatic cancer than the normal pancreases, resulting in high mucin formation. Therefore, GCNT3 is used as the novel target to inhibit the overexpression of mucin in pancreatic cancer. Talniflumate is a mucin inhibitor with good binding capacity with GCNT3 after the in-silico validation. The docking score of talniflumate is very impressive compared to the known ligand GALB1,3GALNAC. Further study confirms talniflumate, after binding with GCNT3, inhibits the protein expression of GNCT3 and significantly decreases the overexpression of mucin. Further investigation on EGFR inhibitor (gefitinib) confirms remarkable tumor regression in PDAC and PanIN with a significant decrease in mucin expression.

**MDC-1016.** Mackenzie et al. (Mackenzie et al., 2013) synthesized phospho-farnesylthiosalicylic acid (PFTS; MDC-1016) and evaluated its efficacy, safety, and metabolism in preclinical models of pancreatic cancer. PFTS downregulates c-RAF/mitogen-activated protein–extracellular signal–regulated kinase (ERK) kinase (MEK)/ERK1/2 kinase and phosphatidylinositol 3-kinase/ AKT ultimately inhibits Ras-GTP, the active form of Ras, mechanistically, both in vitro and in vivo. PFTS transcription 3 (STAT3) inhibitors, displaying synergy in the inhibition of pancreatic cancer growth. PFTS also shows synergistic effect combination with phospho-valproic acid, a novel signal transducer and activator of transcription 3 (STAT3) inhibitor in pancreatic cancer.

**Simvastatin.** The Mevalonate intermediates, including farnesyl pyrophosphate (FPP) and geranylgeranyl pyrophosphate (GGPP), which are responsible for activating RAS proteins, potentially inhibited by statins in pancreatic cancer (Lee et al., 2003). Simvastatin treatment on

MiaPaCa-2 human pancreatic cancer cells showed 200 genes affected by simvastatin treatment. The reason is due to the interaction with FPP and simvastatin. However, it is observed that the normalization of expression of KRAS-related gene and the GFP-K-Ras protein trafficking was partially prevented by the addition of any of the mevalonate pathway's intermediates. Finally, the addition of FPP or GGPP normalized simvastatin-treated altered genes. Therefore, KRAS protein trafficking is successfully inhibited by statin treatment in pancreatic cancer (Lee et al., 2003).

**Avicin G.** The Avicin G is a plant-derived triterpenoid saponin from Acacia victoriae, mislocalizes KRASG12V from the Plasma membrane (PM), and disrupts PM spatial organization of oncogenic K-Ras and H-Ras by depleting phosphatidylserine (PtdSer) and cholesterol contents, respectively, at the inner PM leaflet (Kumar & Agnihotri, 2019). Further investigation suggests avicin G inhibits KRASG12V and HRASG12V mutation by downregulating pERK signaling pathway and pAkt, but more inhibition was observed on KRASG12V cells. Next, a cell proliferation assay was performed on human pancreatic ductal adenocarcinoma (PDAC) cells and non-small cell lung carcinoma (NSCLC) cells. Results showed significant growth inhibition for both types of the cancer cell line. Research identifies that lysosome activity is vital for KRAS-driven cancer growth, but avicin G blocks the lysosome activity by elevating lysosomal PH and inhibiting phosphorylation of ERK signaling (Kim et al., 2020; Yaqoob et al., 2020).

**Prostratin.** The Prostratin is a phorbol ester, first isolated from the bark of the mamala tree of Samoa, Homalanthus nutans (Euphorbiaceae) (Garrido et al., 2020). Prostatin inhibits KRAS and HRAS tumor growth by suppressing non-canonical Wnt/Ca2+ signaling. In comparison to KRAS and HRAS, KRAS produce more tumorigenesis, although they have a

comparable level of canonical RAS signaling. The reason for that is the ability to induce tumor initiation that is directly related to the ability of KRAS to suppress the Fzd8 mediated non-canonical Wnt/Ca2+ signaling. In KRASG12V mutation, Fzd8 was downregulated, and CaMKii level was decreased than the HRASG12V, resulting in phosphorylation of threonine 286. Therefore, prostatin (PKC activator) interrupts KRAS calmodulin-binding that increases the level of Fzd8, which inhibit KRAS mutation in pancreatic cancer cell (Garrido et al., 2020).

**Lupeol.** The Lupeol is a triterpenoid, a FPTase inhibitor, and specifically inhibits KRAS mutant, not wt KRAS. After analyzing crystal structure, Ganaie et al. identified 20 terpenoids for their KRAS binding affinity. A comprehensive study on lup-20 (Kumar et al., 2011) - en-3b-ol (lupeol) as a KRAS inhibitor performed differential scanning fluorimetry, immunoprecipitation assays, and isothermal titration calorimetry, lupeol identified as a potent KRAS inhibitor. Lupeol has a potential inhibitory effect on mutant KRASG12V. In vivo lupeol administration in mouse model showed inhibition of development of pancreatic intraepithelial neoplasia .

**RTK inhibitors in pancreatic cancer**

Receptor tyrosine kinases (RTKs) are transmembrane proteins expressed on the cell membrane that act as signal transducers. They are responsible for different vital cellular regulations that cause proliferation, apoptosis, differentiation and metabolism (Yang et al., 2021). RTK alteration happens in a wide range of cancers, emphasizing its significant role in cancer progression and as an appropriate therapeutic target. RTK comprises 58 members from 20 subfamilies. Among them, Vascular Endothelial Growth Factor Receptor (VEGF) (Itakura et al., 2000) and Insulin Receptor (IGF-IR) (Hakam et al., 2003) are overexpressed in pancreatic cancer.

Table 1.2: RTK inhibitors in pancreatic cancer

| Inhibitor | Structure | Target | Ref. |
|---|---|---|---|
| Pazopanib | 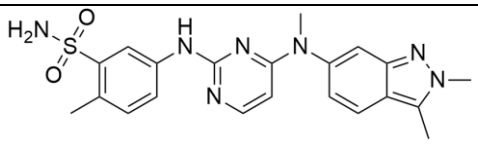 | VEGF receptors 1, 2, and 3 | (Alexandria T. Phan et al., 2015) |
| Vandetanib | 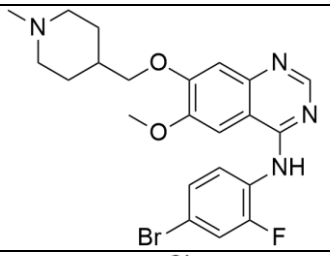 | VEGFR2, RET, and EGFR | (Middleton et al., 2017) |
| Lapatinib<br>+<br>Capecitabine | 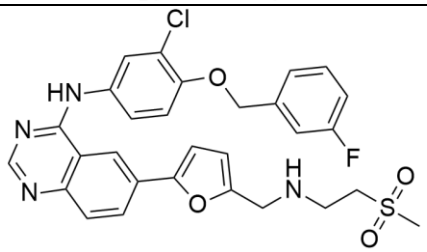 | EGFR and HER-2 | (Wu et al., 2015) |
| Erlotinib<br>+<br>gemcitabine | 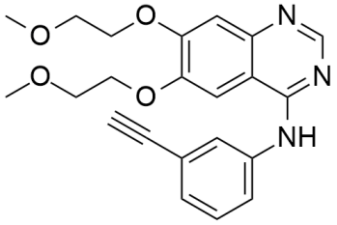 | EGFR | (Renouf et al., 2014) |
| Axitinib<br>+<br>gemcitabine | 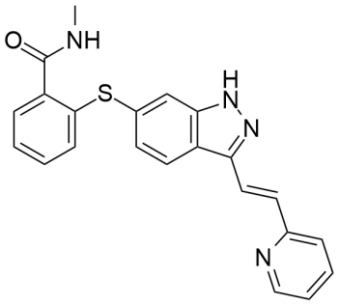 | VEGFR1, VEGFR2, VEGFR3 and PDGFRβ | (Ioka et al., 2015) |
| PD173074 | 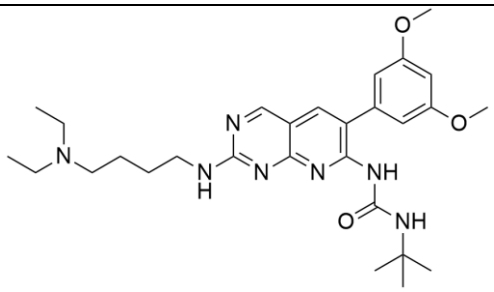 | VEGF-RII and FGF-RI | (Büchler et al., 2007) |

Table 1.2: RTK inhibitors in pancreatic cancer (cont.)

| | | | |
|---|---|---|---|
| Bemcentinib (Synonyms: R428; BGB324) | 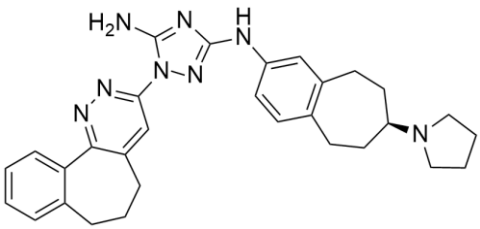 | Axl | (Ludwig et al., 2018) |
| Imatinib Mesylate | 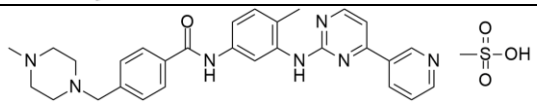 | PDGFR, c-Kit, v-Abl | (Moss et al., 2012) |
| Sunitinib | 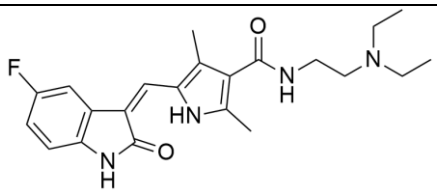 | PDGFR, FLT3, IRE1α, Kit | (Martínez-Bosch et al., 2016) |
| Sorafenib+ gemcitabine | 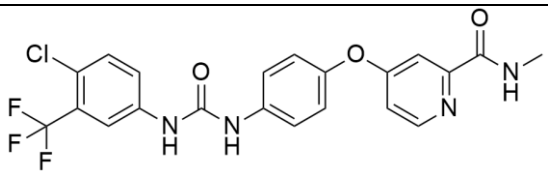 | VEGFR-2/PDGFR-beta | (Gonçalves et al., 2012) |
| Losartan+ FOLFIRINOX | 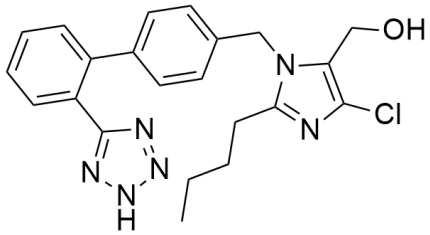 | Angiotensin receptor | (Murphy et al., 2019) |
| Galunisertib | 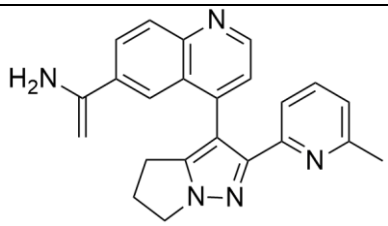 | TGF-β type I receptor (TβRI) | (Melisi et al., 2018) |
| BMS-754807 | 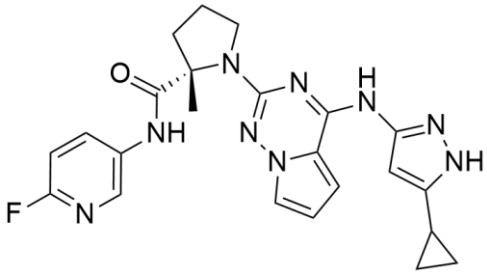 | insulin-like growth factor-1R/IR | (Carboni et al., 2009) |

**Pazopanib.** Pazopanib is a small molecule VEGF receptor 1, 2, and 3 inhibitors and is also known as orally bioavailable drug. Phan et al. (A. T. Phan et al., 2015) studied the

pazopanib effect on 52 patients counting 32 individuals with pancreatic NETs. Among them, 21 (66%), 8 (25%), and 21 (66%) had progressive disease at enrolment, received everolimus therapy, and received previous chemotherapy respectively. Finally, 21.9% of patients gave overall objective responses.

**Vandetanib.** Middleton et al. (Middleton et al., 2017) investigated combination therapy of vandetanib and gemcitabine in 381 individuals for advanced pancreatic cancer. Vandetanib is an RTK inhibitor of VEGFR2, RET, and EGFR, all of which are responsible for cancer prognosis. Results showed addition of vandetanib to gemcitabine therapy did not improve overall survival in advanced pancreatic cancer when compared to gemcitabine alone although the combination of gemcitabine plus vandetanib was generally well tolerated. The post-hoc analysis showed the development of rash increases the progression-free survival when using vandetanib which supports the idea rash might be indicative of regression of pancreatic cancer.

**Lapatinib.** The Combination therapy of lapatinib an EGFR, HER-2 inhibitor, and capecitabine a third-generation aromatase inhibitor (AI) showed a tolerable regimen for patients with gemcitabine refractory pancreatic cancer (Wu et al., 2015). However, this single-arm phase-II trial was conducted for a very small amount of patients. This study also reported severe side effects for 17% of patients although there was no cardiac side effect for all of the patients and most patients tolerated without dose adjustment (Wu et al., 2015).

**Erlotinib.** Erlotinib has been shown its beneficial effects on non-small cell lung cancer (NSCLC) as a single agent. It is also identified that this effect is limited to the patients who possess the EGFR mutation. Data from NSCLC patients demonstrated that KRAS mutation is very low in NSCLC but high in pancreatic cancer and has significantly decreased benefit from EGFR tyrosine kinase inhibitor. Renouf et al. (Renouf et al., 2014) studied 29 patients, 27 (93%)

were KRAS mutated and there was no difference in outcomes when compared with the wild-type KRAS mutation. In addition, erlotinib and gemcitabine combinations were analyzed on 117 patients, and the results indicated non-significant changes. Finally, dose escalation of erlotinib might be the indicator but it is not much effective in non-selected patients with advanced pancreatic cancer resistant to gemcitabine.

**Axitinib.** Axitinib is a selective and potent VEGF inhibitor. Ioka et al. (Ioka et al., 2015) investigated the efficacy of axitinib and gemcitabine combinedly in patients with advanced pancreatic cancer from different countries (Japan, North America, and the European Union). All the data suggested that in tolerable dose Axitinib/gemcitabine did not provide survival benefits over gemcitabine alone in patient with advanced pancreatic cancer from Japan, North America, and the European Union.

**PD173074.** PD173074 is a VEGF-RII and FGF-RI inhibitor targeting neoangiogenesis and mitogenesis. Bu¨chler et al. (Büchler et al., 2007) first identified high doses of PD173074 as a single compound and come up with preclinical evidence that small molecule inhibitor PD173074 tailored cancer therapy toward the simultaneous inhibition of angiogenesis, induction of apoptosis, and inhibition of tumor growth factor-mediated mitogenesis. In vivo study on HPAF-II and MIA PaCa-2 cell, PD173074 showed prominent inhibition of cell growth which expressed high levels of FGF-RI.

**Bemcentinib.** Bemcentinib is a small molecule inhibitor, that targets RTK in pancreatic ductal adenocarcinoma (PDAC). Axl signaling upregulates TBK1–NFkB pathway and stimulates innate immune suppression in the tumor microenvironment. In vitro analysis of six human and three mouse PDAC cell lines showed dose-dependent inhibition with $IC_{50}$ values ranging from 1-4 μmol/L. In addition, combination treatment of Bemcentinib and gemcitabine decreases cell

apoptosis, decreases cell proliferation, and reduced microvessel density in genetic KIC and syngenic Pan02 tumors (Ludwig et al., 2018).

**Imatinib mesylate.** Imatinib mesylate (IM) is a platelet-derived growth factor (PDGFRs) that is rich in the pancreatic tumor microenvironment. IM increases drug access by inhibiting interstitial fluid pressure. Moss et al. (Moss et al., 2012) investigated Imatinib mesylate and gemcitabine effect in phase 2 trial for forty four patients who possessed metastatic pancreatic cancer. Result showed that combination of IM and gemcitabine were well tolerated than gemcitabine alone but the overall survival rate was not significant in statistical information.

**Sunitinib.** Sunitinib is a tyrosine kinase inhibitor and is well known for its anti-angiogenic effect. Using Ela-myc transgenic mouse model Martínez-Bosch et al. (Martínez-Bosch et al., 2016) investigated the effects of sunitinib in pancreatic cancer. PDGFR and VEGFR were overexpressed in Ela-myc pancreatic tumors. However, treatment with sunitinib in Ela-myc had no impact on either early or advanced tumor progression and also no effect on survival or tumor burden. But in vivo study, all the subcutaneous tumors generated from tumor cell lines regressed after sunitinib treatment. All results indicated that the main barrier to sunitinib treatment in vivo is the pancreatic tumor microenvironment, which might be improved by treating in combination with drugs that disrupt tumor fibrosis.

**Sorafenib.** Sorafenib is a RTK inhibitor, that inhibits angiogenic and RAS-dependent signaling. A phase I trial showed combination therapy of sorafenib and gemcitabine had activity and was well tolerated in advanced pancreatic cancer. But the combination therapy of sorafenib and gemcitabine did not show overall survival (OS) and progression-free survival (PFS) and clinical benefit in a double-blind phase-III randomized trial for advanced-stage pancreatic cancer patients (Gonçalves et al., 2012).

**Losartan.** Murphy et al. (Murphy et al., 2019) investigated the neoadjuvant therapy of FOLFIRINOX (fluorouracil, leucovorin, oxaliplatin, and irinotecan) and losartan followed by chemoradiotherapy in locally advanced pancreatic cancer. A phase II clinical trial of losartan, an angiotensin receptor antagonist combined with the FOLFIRINOX regimen to evaluate the margin-negative (R0) resection rate. The result suggested that the treatment with FOLFIRINOX and losartan, significantly decrease plasma TSP1 and TGF-β levels indicating a high rate of R0 resection and prolonged survival rates in LAPC (Murphy et al., 2019).

**Galunisertib.** Galunisertib is an (ALK5) serine/threonine kinase inhibitor. It is the first oral small-molecule type I transforming growth factor-beta receptor to enter clinical development. Melisi et al. (Melisi et al., 2018) investigated a first line treatment of galunisertib with gemcitabine for patients associated with unresectable pancreatic cancer. The overall result suggested that Combination therapy of galunisertib and gemcitabine increase the overall survival (OS) than the gemcitabine treatment alone in unresectable pancreatic cancer. Minimal toxicity was also found with this treatment. Further evidence found from biomarker analyses that patients subgroups with higher levels of cytokines recruited macrophages or regulatory T cells that may benefit to a greater extent from treatment with galunisertib plus gemcitabine.

**BMS-754807.** BMS-754807 is a potent and reversible insulin-like growth factor 1 receptor inhibitor. Awasthi et al. investigated therapeutic potential of combination therapy of BMS-754807 and gemcitabine in PDAC (Carboni et al., 2009). BMS-754807 and gemcitabine inhibited cell proliferation in PDAC cell determined by WST-1 assay. BMS-754807 inhibited PDAC cell proliferation at 10 mmol/L of 54%, 37%, 49%, and 39% in AsPC-1, BxPC-3, MIA PaCa-2, and Panc-1 cells, respectively by dose-dependent manner. Additionally, it is also determined that combination therapy of BMS-754807 and gemcitabine increases the inhibitory

effect more than gemcitabine alone. The addition of BMS-754807 decreased gemcitabine IC50 from 9.7 mmol/L to 75 nmol/L for AsPC-1, from 3 mmol/L to 70 nmol/L for Panc-1, from 72 to 16 nmol/L for MIA PaCa-2, and from 28 to 16 nmol/L for BxPC-3 cells. BMS-754807þgemcitabine also showed strong antitumor activity by decreasing phospho-IGF-1R and phospho-AKT in tumor tissue lysates (Awasthi et al., 2012).

# CHAPTER II

# METHODOLOGY

## Synthesis of diversely substituted bioactive quinoxalines (Part-A)

In this research, World Health Organization (WHO) identified twenty tropical disease categories as neglected tropical diseases (NTDs). Chagas' disease (also known as American trypanosomiasis) and leishmaniasis are two major classes of NTDs. The total number of mortality, morbidity, and disability attributed each year due to these two categories of diseases in magnitudes is much higher than the so-called elite diseases like cancer, diabetes, AIDS, cardiovascular and neurodegenerative diseases. Impoverished communities around the world are the major victim of NTDs. The development of new and novel drugs in the battle against Chagas' disease and leishmaniasis is highly anticipated.

In this research, an ultrasound-assisted on-water green synthesis was performed to synthesize diversely substituted quinoxalines. Eleven compounds were synthesized **(Figure 2.1)** and subsequent in vitro trypanocidal and leishmanicidal evaluations were performed of these compounds. Further, it is hypothesized that the biological (trypanocidal and leishmanicidal) activity is due to the interaction and subsequent inhibition of the protozoal proteins responsible for these diseases. In addition, in silico docking study was conducted to validate the hypothesis.

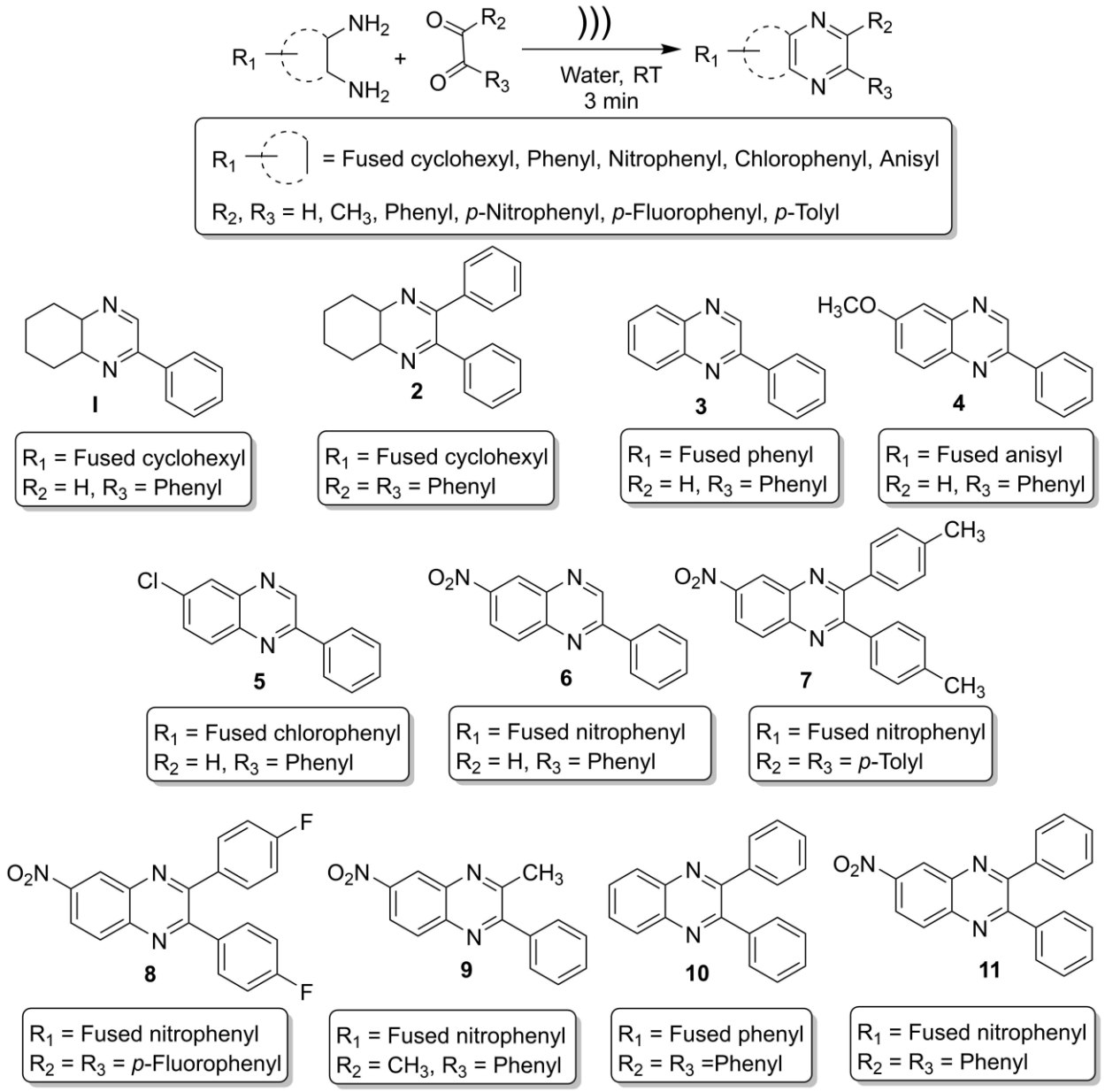


Figure 2.1: Ultrasound-assisted on-water green synthesis of diverse benzopyrazines

## General

**Materials.** All the Chemicals were purchased from Sigma-Aldrich, Inc. (St. Louis, MO) and VWR International (Missouri, TX). Solvents were purchased from Fisher Scientific International Inc. (Pittsburgh, PA) throughout the investigation.

**Ultra-sonicator.** Sonication was performed with the UP200St (200W, 26kHz) ultra-sonicator (Hielscher Ultrasonics GmbH, Germany).

**FT-IR.** FT-IR spectra were recorded on a Bruker Alpha modular Platinum-ATR FT-IR spectrometer with OPUS software, using the samples directly (neat) without making pallets.

**NMR.** FT-IR $^{1}H$ NMR (600 MHz) and $^{13}C$ NMR (150 MHz) spectra were obtained at room temperature with Bruker superconducting Ultrashield Plus 600 MHz NMR spectrometer with central field 14.09 T, coil inductance 89.1 Hz, and magnetic energy 1127.2 kJ using $CDCl_3$ or $d_6$-DMSO as solvent.

**General procedure for synthesis of quinoxalines**

In a general procedure of this on-water reaction, ortho-diamine and dicarbonyl compounds were mixed (1:1 molar ratio) in a hard glass test tube, and 1 mL tap water was added to the reaction mixture. In a model reaction, 1 mL water was taken in a hard glass test tube, and one mmol of o-phenylene diamine (108 mg) and one mmol of phenylglyoxal hydrate (134 mg) were added into the test tube. The ultrasonic probe was inserted into the test tube (reaction mixture), and the mixture was sonicated. The reaction was monitored by thin-layer chromatography (TLC) every after one minute. The most intense TLC spot was seen after three minutes. Further sonication did not increase the intensity of the product spot; rather, it reduced the product and generated gummy material. Initially, the reaction was carried out in deionized water, but no significant change in yield was observed compared to tap water. At the end of the reaction, the product looked like a chunk, and it was not soluble in water. Consequently, the product was extracted with 9 mL (3x3 mL) of ethyl acetate. The organic layer was dried over sodium sulfate and concentrated by reduced pressure distillation by a rotary evaporator. The

crude mass was passed quickly through a purification column with ethyl acetate to get highly pure (>98%) and crystalline compounds. The spectral data of the compounds are given bel

**Trypanocidal and Leishmanicidal (in vitro) evaluations**

The promastigotes of L. mexicana (MHOM/MX/ISETGS) clinical strain were used for the leishmanicidal growth inhibition assay. The clinical strain was initially isolated from a patient suffering from diffuse cutaneous leishmaniasis. The trypanocidal assay also carried out with the epimastigotes of T. cruzi (MHOM/MX/1994/NINOA). The clinical strain was originally isolated from a patient with the disease in the acute phase for this assay. Schneider's Drosophila medium, supplemented with 10% fetal bovine serum, penicillin (100 IU/mL), and streptomycin (100 µg/mL), was used to culture the parasites at 26 °C. The antiprotozoal assays were carried out in 96-well plates using dimethyl sulfoxide (DMSO) as the carrier. The standard controls and the testing compounds were solubilized in DMSO and diluted as required. All the antiprotozoal assays were performed in duplicate. Aliquots of 100 µL of compound solution and 100 µL of culture medium containing 10000 Leishmania promastigotes or 20000 *T. cruzi* epimastigotes were combined to obtain concentrations of 50, 25, 12.5, 6.25, 3.125 µg/mL, and so on. Two first-line commercial drugs nifurtimox (antichagasic drug) and miltefosine (leishmanicidal drug), were used as positive controls. Only the parasite-containing culture was used as the negative control. The plates were incubated for 72 hours at a temperature of 26 °C, and the antiprotozoal activity of the compounds was determined by direct count of parasites in a Neubauer chamber. The IC50 values (the concentration required to inhibit 50% of parasite growth were calculated (in µg/mL) by probit analysis.

### *In silico* molecular docking studies

*In silico* molecular docking was conducted following our previously published procedure (3). In brief, the ligands were prepared with their corresponding assigned atoms types and charges using ChemOffice 2015 as MOL files and converted to PDB and PDBQT sequentially following a few steps utilizing open-source and well-known graphic user interface software. Control drugs (positive controls) were imported from ChemSpider as MOL format; if not, control ligands were manually prepared from scratch. Crystal structures of the four proteins 4YPF, 1S0J, 4K32, 6QDA (biological targets in this study) were imported from RCSB (4), a member of Worldwide Protein Data Bank (wwPDB). The MOL formats of the ligands were changed to PDB format by Avogadro software (5). The ligands were saved in .pdb format and AutoDock4. AutoDockTools 1.5.6, part of AutoDock4 (AD4), were used to alter the ligands and receptors (proteins) from PDB to PDBQT formats. PDBQT format provides the molecular structure coordinate files, including atomic partial charges, atom types, torsional flexibility information, etc. The ligand files (in .pdb form) were loaded onto the AutoDockTools dashboard to detect torsion root, rotatable bonds and add gasteiger charges for atomic charges, if necessary. The receptor-binding sites were localized using the Adaptive Poisson-Boltzmann Solver (APBS) plugin for surface electrostatic calculation and Computed Atlas Surface Topology of proteins (CASTp) for a pocket that void detection on the protein surface (6). Binding site visualization was made feasible by Schrödinger Maestro, AutoDock4, PyMOL, and other software. (7,8,9). These software packages offer a complete molecular viewer and graphic user interface, which are essential for structure-based drug design and discovery. PDBQT structure formats are compatible with AutoDock Vina (10), a complementary AD4 molecular docking program, and are required to run the docking simulations. We used the Schrödinger Maestro to visualize and

preparing the PDB receptor and ligand conformation files for docking. We uploaded the receptor files to the Maestro workspace, and the binding site surface area was calculated using the Task Tree search bar and selecting Binding Surface Area Analysis. The resulting free energy binding affinities (in kcal/mol) were recorded as docking scores. These scores were considered to evaluate the strength of non-covalent interaction between different receptor-ligand conformations. A conformer with the lowest energy and highest cluster counts was regarded as the best ligand conformation that fits the binding site. The structural analysis was effectuated in Schrödinger Maestro was set to (i) visualize the formation and quantify distances of H-bonds, π-π stacking interactions, and close contacts of each ligand to the receptor of interest; (ii) obtain images of ligand-receptor residue interactions within the vicinity of the binding site, and (iii) observe the receptor surface homology through molecular dynamics simulation (11). The in silico docking study evaluated miltefosine and nifurtimox, leishmanicidal, and trypanocidal control drugs, respectively.

**Synthesis of carbazole derivative beta-lactams (Part-B)**

β-lactam is a four-membered lactam ring. Its lactam part is a cyclic amide. It is called β-lactam because the nitrogen atom is attached to the β carbon atom relative to the carbonyl group. Their advent started in 1928 when Sir Alexander Fleming first discovered “penicillin”. Fleming discovered that bacterial growth was restricted with Penicillium (7). β-lactam started its journey as an antibiotic from the beginning. Penicillin is the first β-lactam compound that has the antibacterial property (15, 16). It is proven that the β-lactam core, 6-aminopenicillanic acid is the lead compound of penicillin synthesis (17). Due to the increasing rate of bacterial resistance, the new group of semi-synthetic β-lactam has been synthesized to get the potent broad-spectrum

activity. For Example, cephalosporin which is a group of broad-spectrum β-lactam antibiotic, are mostly synthesized from semi-synthetic derivatives of cephalosporin C (18). Biosynthetic studies have shown that the β-lactam class of natural products can be divided into at least four different subgroups based on the origin of the β-lactam ring. These groups will be referred to as the penicillin/cephalosporin, the clavam, the carbapenem, and the monocyclic β-lactam compounds (Figure 1) Within these four compounds first three (penicillin/cephalosporin, the clavam, the carbapenem) are the bicyclic β-lactam compounds. Most bicyclic β-lactams are produced by fermentation or modification of fermentation-derived materials (19-21).

The Discovery of a variety of anticancer drugs for the treatment of cancer is a medical breakthrough and inspiring for the cancer research community as a whole. A wide range of natural, semi-synthetic, and synthetic anticancer drugs are synthesized using various methods. Among them, β -lactams stand out as a novel class of antibiotics that has different types of biological as well as anti-cancer properties. β -lactam has become a premier and active research subject towards the development of revolutionary anti-cancer drugs. In recent years, a large amount of investigations has been done to find the anticancer effect of β -lactams. There exist clinically established synthetic methods to synthesize the beta-lactam ring. To find the better anticancer effect, many bicyclic, polycyclic starting materials have been selectively chosen to be used with the beta-lactam ring. Many endeavors conducted comprehensive biological studies to determine the anticancer activity of such synthetic β -lactams. Also, to investigate the binding effect of β -lactam, molecular docking studies have been performed.

**Synthesis of DB-5-SAS series**

For this research, some novel beta-lactam derivatives have been synthesized using multistep synthesis process. Firstly, Schiff base (Imine) has been synthesized from aldehyde, 5-

fluoropicolinaldehyde and amine, 9-ethyl-9H-carbazole-3-amine. Using the Staudinger reaction five derivative of beta-lactam were synthesized from the previously synthesized imine. To the best of my knowledge, this is the first report that discusses the synthesis of beta-lactam from carbazole derivatives.

**General procedure for the synthesis of imines.** The chapter Amine and aldehyde were mixed in equimolar (1:1) ratio and refluxed in dry toluene using a Dean-Stark water separator. After completion of the reaction (monitored by thin layer chromatography, 2–3 hours), the solvent was removed under reduced pressure distillation (by rotavapor) and the pure imine was isolated by crystallization from dichloromethane/hexanes.

**General procedure for the synthesis of DB-5-SAS-OAC via the Staudinger reaction.** 5.706 gm of imine was taken to 500 ml round bottom flask. Then 100 ml of anhydrous DCM and 6.3 ml of anhydrous TEA were added to the similar round bottom flask which contained imine. After adding the reaction mixture was stirred for 20 minutes. Then acetoxy acetyl chloride was added dropwise. The reaction mixture was stirred 48 hours. The reaction temperature was maintained 0 to -5° C. After completing the reaction, the reaction mixture was extracted with brine solution, sodium bicarbonate, Dichloromethane (DCM), and Ethyl acetate. The pure product was isolated by column chromatography.

**General procedure for synthesis of DB-5-SAS-OH.** 1.5 mmol of acetoxy beta-lactam was taken to a round bottom flask. 10 ml of tetra hydro furan and 10 ml of deionized water were added to the similar round bottom flask. After stirring the reaction mixture at 0 to -5°C temperature, 10 ml of 6% aqueous sodium hydroxide was added to the reaction mixture. Then the reaction was monitored by thin layer chromatography every 10, 20, 30, 40, 50, and 60 mins intervals. When the reaction was completed, it was quenched by ethyl acetate. Extraction was

done using brine solution, DCM, and ethyl acetate. Pure compound was isolated using column chromatography.

**Synthesis of DB-5-SAS-OTFE beta-lactam.** 1 mmol of hydroxy beta-lactam was taken to a round bottom flask. 8 ml of dry DCM and 9mmol of try ethyl amine is added to the flask. The reaction mixture was stirred for 20 minutes, and the reaction environment was maintained 0 to -5° C temperature. After 20 min stirring 3 mmol of 2,2,2 trifluoroethane sulfonyl chloride was added dropwise to the reaction mixture. The reaction was monitored by TLC in every 30minutes interval. After completing the reaction, the reaction mixture was extracted by diluted brine solution. Pure compound was isolated by column chromatography.

**Synthesis of DB-5-SAS-OCAS beta-lactam.** 1 mmol of hydroxy beta-lactam was taken to a round bottom flask. 8ml of dry DCM and 9 mmol of triethyl amine were added to the reaction mixture. Performed 20 min starring maintaining 0 to -5° C temperature. 3 mmol of cyanoazetidine-1-sulfonyl chloride was added directly to the reaction mixture. Reaction was monitored by TLC in every 2 hours interval. Reaction completed within 18-24 hours. After completing the reaction, the reaction mixture was extracted with diluted brine solution, DCM, and ethyl acetate. Pure compound was isolated using column chromatography.

**Synthesis of (IPMS) beta-lactam.** 1 mmol of hydroxy beta-lactam was taken to a round bottom flask. 8ml of dry DCM and 9 mmol of triethyl amine were added to the reaction mixture. Performed 20 min starring maintaining 0 to -5° C temperature. 3 mmol of isopropyl methyl sulfonyl chloride was added directly to the reaction mixture. Reaction was monitored by TLC in every 48 hours interval. Reaction completed within 96 hours. After completing the reaction, the reaction mixture was extracted with diluted brine solution, DCM, and ethyl acetate. Pure compound was isolated using column chromatography.

# CHAPTER III

# RESULTS

## Green synthesis of bioactive diversely substituted quinoxalines (Part-A)

### Green synthesis of diverse benzopyrazines

Ultrasound-assisted diversely substituted benzopyrazines were synthesized, inserting a powerful sonicator probe into the reaction mixture. For the diamine and dicarbonyl compounds, various substituents based on electron-withdrawing or electron-donating ability were tested to generalize the reaction. The nitro, chloro, on the diamine represent strong and weak electron-withdrawing groups (EWG), whereas the fused cyclohexyl and methoxy groups represent mild and strong electron-donating groups (EDG). The ultimate goal was to evaluate whether the presence of these functional groups influences the nucleophilicity of the diamines. Similarly, the electrophilicity of the diketo compound was varied by introducing *p*-nitro, *p*-fluoro (EWG) or methyl (EDG) in the dicarbonyl system. The overall yield of the products indicates that the presence of EWG or EDG does not influence the reaction significantly, which in turn supports the universality of this synthetic method. Based on the available literature, this is the first example of synthesizing benzopyrazines under this condition. Our method produced excellent yields of the corresponding products (overall yield 92% or more) in a very short period. The yield of the products and the atom economy of the reactions are shown in Table 3.1. The range of atom economy in the series

varies from 76.92% to 88.89%, which undoubtedly supports the greenness of the synthetic method.

Table 3.1: The yield, and atom economy in the synthesis of benzopyrazines (1–11)

| Compound | Yield (%)* | Atom economy |
|---|---|---|
| **1** | 97 | 85.48 |
| **2** | 96 | 88.89 |
| **3** | 94 | 76.92 |
| **4** | 92 | 80.00 |
| **5** | 95 | 76.92 |
| **6** | 98 | 78.57 |
| **7** | 99 | 86.36 |
| **8** | 93 | 84.21 |
| **9** | 97 | 80.00 |
| **10** | 96 | 83.33 |
| **11** | 98 | 84.21 |

**Tripanocidal and Leishmanicidal evaluations (in vitro) of the benzopyrazines (1–11)**

We used the promastigotes of *L. mexicana* (MHOM/MX/ISETGS) clinical strain for the leishmanicidal growth inhibition assay. The clinical strain was initially isolated from a patient suffering from diffuse cutaneous leishmaniasis. We carried out the trypanocidal assay with the epimastigotes of *T. cruzi* (MHOM/MX/1994/NINOA). The clinical strain was originally isolated from a patient with the disease in the acute phase for this assay. Schneider's Drosophila medium, supplemented with 10% fetal bovine serum, penicillin (100 IU/mL), and streptomycin (100 µg/mL), was used to culture the parasites at 26 °C. Two commercial drugs, miltefosine, and nifurtimox were used as standard controls. Compound 1 demonstrated good in vitro activity against both the strains with comparable IC50 values with both the controls: miltefosine and nifurtimox. Compounds 3 and 4 showed moderate IC50 values against the L. mexicana (M378)

strain (Table 3.2). The standard biosecurity and institutional procedure were followed during the experiment.

Table 3.2: $IC_{50}$ (µM ± SD) of the benzopyrazines (**1**–**11**) against epimastigotes from *T. cruzi* and promastigote from *L. mexicana*.

| Compound | *L. mexicana (M378)* | *T. cruzi (NINOA)* |
|---|---|---|
| **1** | 12.46 ± 0.62 | 37.85 ± 0.52 |
| **2** | >100 | >100 |
| **3** | 50.86 ± 1.02 | >100 |
| **4** | 39.83 ± 0.29 | >100 |
| **5** | >100 | >100 |
| **6** | >100 | >100 |
| **7** | >100 | >100 |
| **8** | >100 | >100 |
| **9** | >100 | >100 |
| **10** | >100 | >100 |
| **11** | >100 | >100 |
| Miltefosine | — | 19.56 ± 0.61 |
| Nifurtimox | 9.32 ± 0.31 | — |

### *In silico* molecular docking of the compounds 1

*T. cruzi* Histidyl-tRNA synthetase (PDB ID: 4YPF; Koh et al., 2015) and T. cruzi trans-sialidase (PDB ID: 1S0J; Amaya et al., 2004) are considered as two major biological drug targets for American trypanosomiasis whereas Leishmanial rRNA A-site (PDB ID: 4K32; Shalev et al., 2013) and Leishmania major *N*-myristoyltransferase (PDB ID: 6QDA; Bell et al., 2020) are considered as the major biomolecular drug targets for leishmaniasis (Kelly et al., 2020). As shown in Table 3.3, compound 1 showed comparable in vitro trypanocidal and leishmanicidal activities with two standard commercial drugs; therefore, we hypothesized the inhibition of the proteins as mentioned earlier with compound 1. To validate our hypothesis, we carried out extensive molecular docking studies of compound 1 against the four proteins. The docking

scores are presented in Table 3.4. Docking interactions between compound 1 with the four proteins are shown in Figures (2a–5b).

Table 3.3: Molecular docking scores of the compound 1 and the standard controls

| Compound | Structure | Docking score* (PDB ID: 4YPF) | Docking score* (PDB ID: 1S0J) | Docking score* (PDB ID: 4K32) | Docking score* (PDB ID: 6QDA) |
|---|---|---|---|---|---|
| **1** | 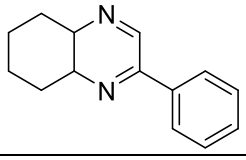 | -6.7 | -7.3 | -6.3 | -7.4 |
| Miltefosine | 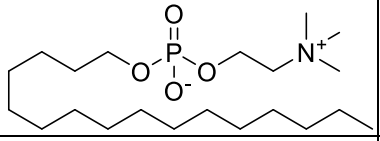 | -4.7 | -5.4 | -4.9 | -6.0 |
| Nifurtimox | 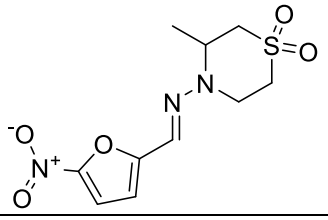 | -7.0 | -7.8 | -6.6 | -7.5 |

* Binding affinity [kcal/mol]

4YPF: Crystal structure of T. cruzi Histidyl-tRNA synthetase in complex with quinolin-3-amine

1S0J: Trypanosoma cruzi trans-sialidase in complex with MuNANA (Michaelis complex)

4K32: Crystal structure of geneticin bound to the leishmanial rRNA A-site

6QDA: Leishmania major N-myristoyltransferase in complex with quinazoline inhibitor IMP-0000811

Table 3.4: Interactions between compound 1 with the four biomolecular targets (PDB IDs: 4YPF, 1S0J, 4K32 and 6QDA)

| **Receptor** | **Binding Site Residue(s)** | **Type of Interactions** | **Hydrophobic Residues** | **Docking score*** |
|---|---|---|---|---|
| 4YPF | HID168 | π-π stacking | GLU105, ILE106, GLN109, PRO125, TRP155, ARG165, GLU167, CYS365 | -6.7 |
| 1S0J | N/A | Hydrophobic Interaction | ARG35, ARG53, ASN60, ARG93, ASP96, TYR113, TRP120, LEU176, GLU230, TRP312, ARG314, TYR342 | -7.3 |
| 4K32 | Guanine 8 | H-Bond | U9, A39, A40, A41, G43 | -6.3 |
| 6QDA | HID 219, PHE232 | π-π stacking | VAL81, GLU82, ASP83, PHE88, ARG89, PHE90, SER330, LEU341 | -7.4 |

* Binding affinity [kcal/mol]

4YPF: Crystal structure of T. cruzi Histidyl-tRNA synthetase in complex with quinolin-3-amine

1S0J: Trypanosoma cruzi trans-sialidase in complex with MuNANA (Michaelis complex)

4K32: Crystal structure of geneticin bound to the leishmanial rRNA A-site

6QDA: Leishmania major N-myristoyltransferase in complex with quinazoline inhibitor IMP-0000811

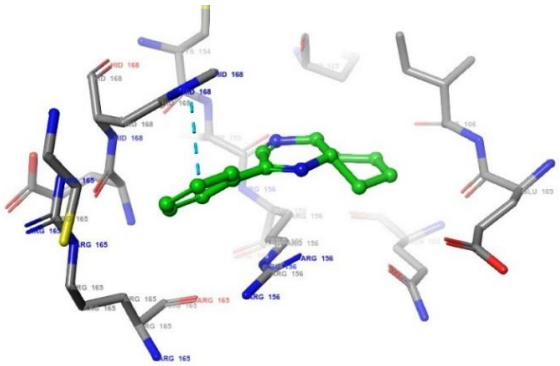

Figure 3.1a: The binding mode of the interactions between 1 with T. cruzi Histidyl-tRNA synthetase (PDB ID: 4YPF)

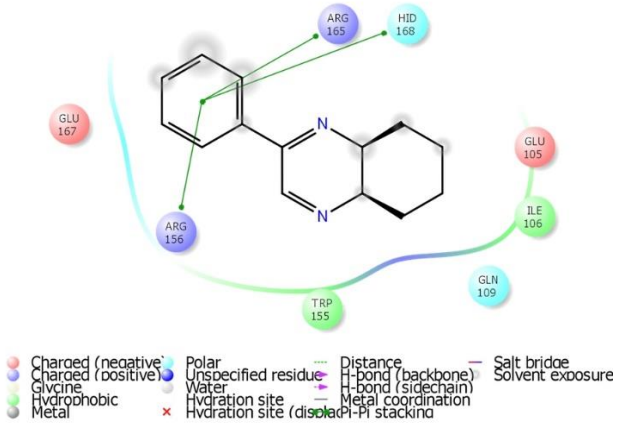


Figure 3.1b: Results of the validation of 1 inside the T. cruzi Histidyl-tRNA synthetase active sites

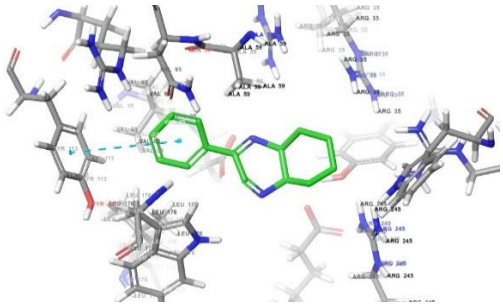

Figure 3.2a: binding mode of the interactions between 1 with T. cruzi trans-sialidase (PDB ID: 1S0J)

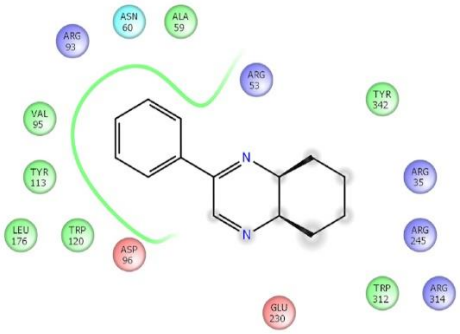


Figure 3.2b: Results of the validation of 1 inside the T. cruzi trans-sialidase active sites

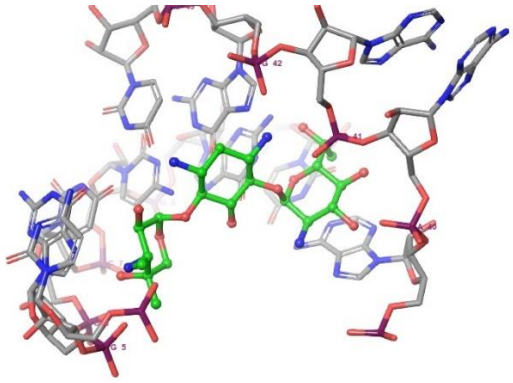

Figure 3.3a: The binding mode of the interactions between **1** with Leishmanial rRNA A-site (PDB ID: 4K32)

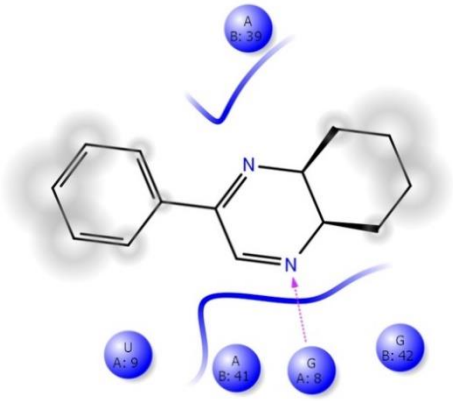


Figure 3.3b: Results of the validation of 1 inside the Leishmanial rRNA A-site active sites

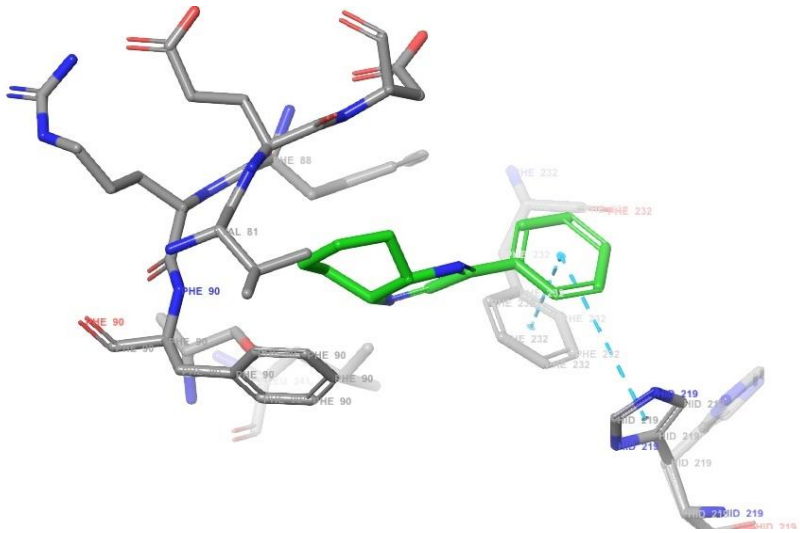

Figure 3.4a: The binding mode of the interactions between 1 with Leishmania major N-myristoyltransferase (PDB ID: 6QDA)

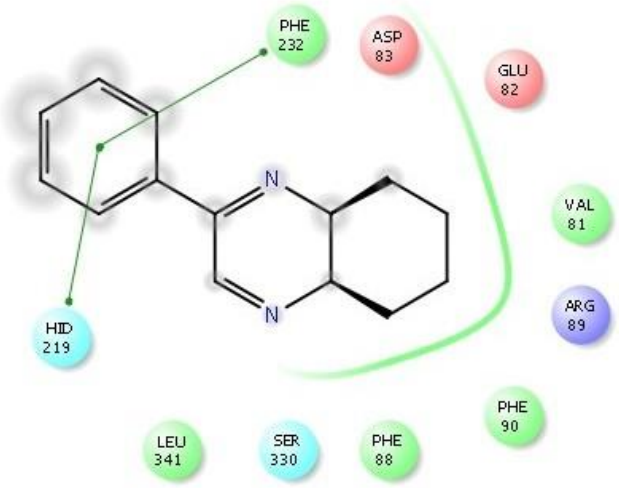


Figure 3.4b: Results of the validation of 1 inside the Leishmania major *N*-myristoyltransferase active sites

### *In silico* drug-likeness determination

Drug-likeness indicates the possibility of a molecule becoming a drug. Accordingly, a drug molecule should have a balance of various physicochemical properties like molecular

weight, hydrogen bond donor, hydrogen bond acceptor, total polar surface area, rotatable bond, hydrophilicity, lipophilicity, hydrophobicity, lipophobicity, bioavailability, half-life, etc. The druggability assessment of all the eleven benzopyrazines was performed in compliance with Lipinski's rule of five (RO5) [Lipiniki et al., 1997, 2001; Lipinski, 2004). The druggability parameters of the eleven benzopyrazines are shown in Table 4. Compound 1 shows the minimum miLogP value (2.96) out of all the eleven analogs without having any significant violations of druggability.

Table 3.5: Validation† of drug-likeness of the benzopyrazines (1–11)

| Compound | miLogP[a] | HBA[b] | HBD[c] | TPSA[d] | RB[e] | MW[f] | Violation |
|---|---|---|---|---|---|---|---|
| **1** | 2.96 | 2 | 0 | 24.73 | 1 | 212.30 | 0 |
| **2** | 4.62 | 2 | 0 | 24.73 | 2 | 288.39 | 0 |
| **3** | 3.41 | 2 | 0 | 25.78 | 1 | 206.25 | 0 |
| **4** | 3.44 | 3 | 0 | 35.02 | 2 | 236.27 | 0 |
| **5** | 4.06 | 2 | 0 | 25.78 | 1 | 240.69 | 0 |
| **6** | 3.34 | 5 | 0 | 71.61 | 2 | 251.25 | 0 |
| **7** | 5.91 | 5 | 0 | 71.61 | 3 | 355.40 | 1 |
| **8** | 5.34 | 5 | 0 | 71.61 | 3 | 363.32 | 1 |
| **9** | 3.56 | 5 | 0 | 71.61 | 2 | 265.27 | 0 |
| **10** | 5.08 | 2 | 0 | 25.78 | 2 | 282.35 | 1 |
| **11** | 5.01 | 5 | 0 | 71.61 | 3 | 327.34 | 1 |

†Molinspiration property engine v2018.10;

[a]miLogP: Moriguchi octanol-water partition coefficient, is based on quantitative structure-LogP relationships, by using topological indexes;

[b]Hydrogen bond acceptor;

[c]Hydrogen bond donor;

[d]Total polar surface area;

[e]Number of rotatable bonds.

## Carbazole derivative Beta lactams (Part-B)

### Synthesis of carbazole derivative Beta lactams (1-5)

In the present study Staudinger [2+2] ketene-imine cycloaddition reaction was performed extensively for the synthesis of carbazole derivative beta-lactams. Multistep synthesis processes are conducted to get all of these beta-lactams. In the subsequent step 9-ethyl-N-((5-fluoropyrimidine-2-yl) methylene)-9H-carbazole-3-amine has been synthesized by refluxing aldehyde and amine with toluene (Figure 3.5).

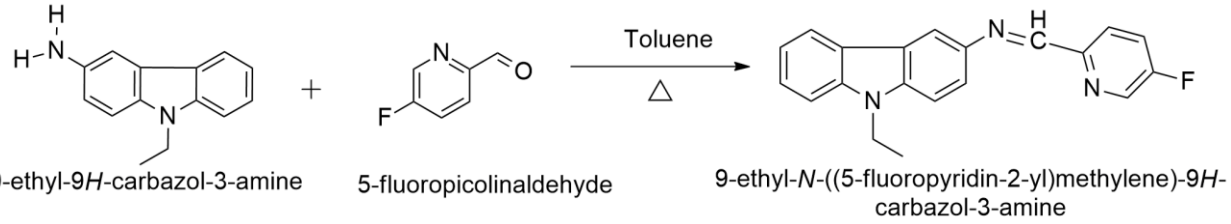


Figure 3.5: Synthesis of imine

A total of five β-lactam derivatives have been synthesized through multi-step process exploring [2+2] ketene-imine cycloaddition as the key step. After the [2+2] ketene-imine cycloaddition, DB-5-SAS-OAC (compound 1) (Figure) has been synthesized. By performing the hydrolysis acetoxy group was replaced by a hydroxyl group and produced DB-5-SAS-OH (compound 2) (Figure). Additionally, three different reactions were performed using three different sulfonyl chloride to get three derivatives of sufonyl chloride beta-lactam (Figure). Although the compounds were synthesized through a multi-step process and purified by repeated column chromatography yet good to excellent yields were isolated each case.

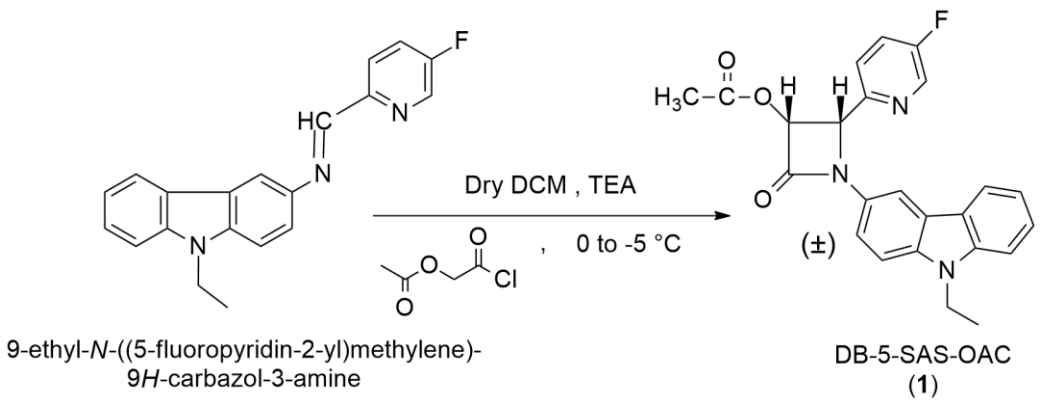


Figure 3.6: Synthesis of DB-5-SAS-OAC (1)

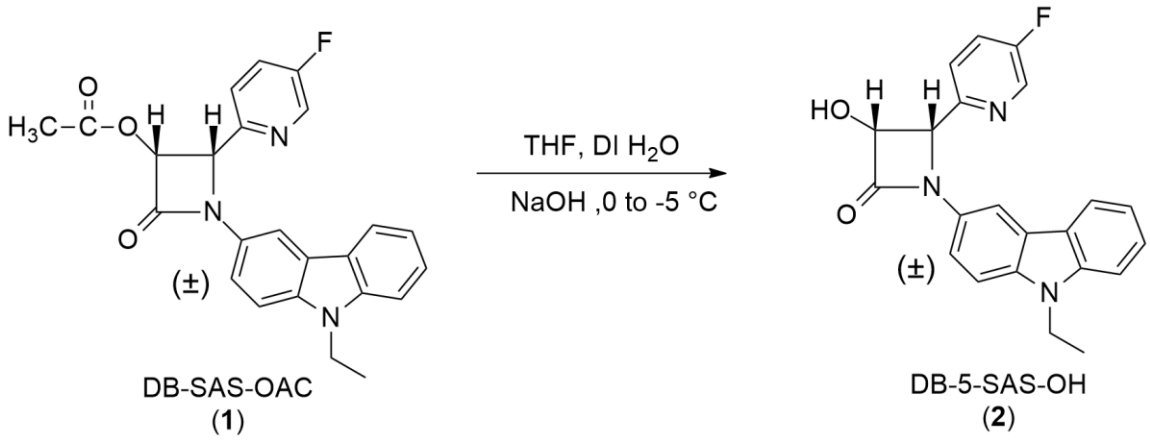


Figure 3.7: Synthesis of DB-5-SAS-OAC (2)

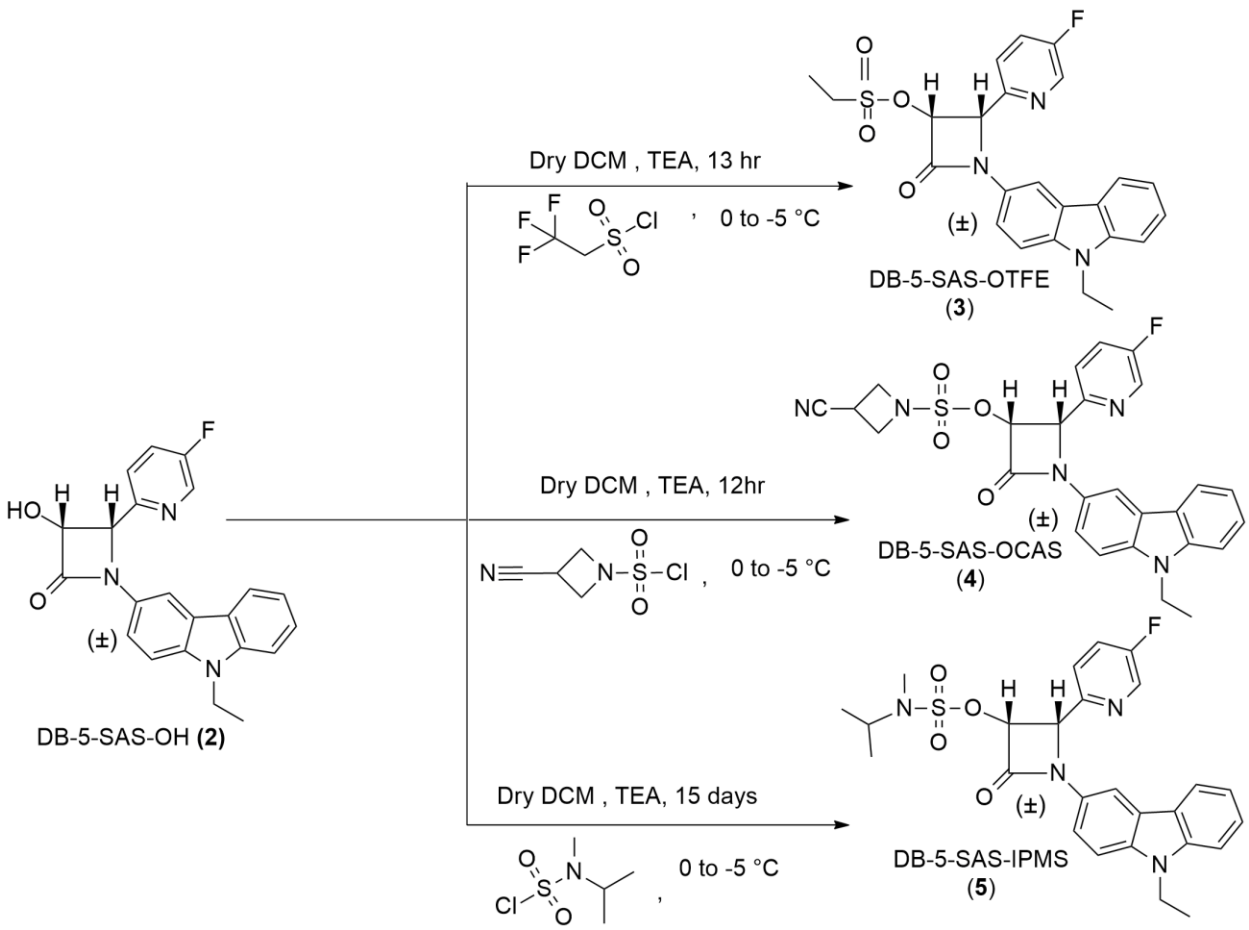


Figure 3.8: Synthesis of compound (3-5)

**Column chromatography for isolation**

Column chromatography was the method used in the isolation of compounds. This was completed by using 80.0 g of the diethyl ether leaf fraction in a gravity guided 2000 ml chromatography column. Ethyl acetate was used to increase the polarity of the mobile phase and elute more polar compounds. Through this process 5 compounds were isolated in a pure form. Purity of each compound was verified with Thin-Layer Chromatography viewed under a 254 nm wavelength UV lamp and in an iodine chamber. The Melting point, and the eluting solvent(s) of each compound was recorded on Table 3.6

Table 3.6. Characteristics of compound (1-5)

| Compound ID | Melting point | Eluting solvent |
|---|---|---|
| DB-5-SAS-OAC (1) | 185° C – 185.5° C | 20% Ethyl Acetate 80% Hexane |
| DB-5-SAS-OH (2) | 198.5° C – 198.8° C | 45% Ethyl Acetate 55% Hexane |
| DB-5-SAS-OTFE (3) | 198.7° C – 199.5° C | 25% Ethyl Acetate 75% Hexane |
| DB-5-SAS-OCAS (4) | 172.5° C – 174.7° C | 30% Ethyl Acetate 70% Hexane |
| DB-5-SAS-IPMS (5) | 169.8° C – 171.5° C | 20% Ethyl Acetate 80% Hexane |

**Characterization of Compound (1-5)**

*(2R,3R)-1-(9-ethyl-9H-carbazol-3-yl)-2-(5-fluoropyridin-2-yl)-4-oxoazetidin-3-yl acetate,* ***(DB-5-SAS-OAC, 1)***. White crystalline solid (352 mg, 84%); m.p. 185° C - 185.5° C; IR (KBr) 3086, 3052, 2967, 1737, 1630, 1602, 1580, 1485, 1468 $cm^{-1}$ (Figure 3.9); $^{1}H$ NMR ($CDCl_3$, 600 MHz) 8.52 (1H, s), 8.00 (2H, m), 7.39 (5H, m), 7.25 (1H, d, *J*=8.52), 7.18 (1H, t, *J*=7.44), 6.14 (1H, d, *J*=4.92), 5.60 (1H, d, *J*=4.92), 4.27 (2H, q, *J*=7.16), 1.80 (3H,brs), 1.3 (3H, t, *J*=7.17) (Figure 3.10); $^{13}C$ NMR (150 MHz, $CDCl_3$) 13.79, 20.00, 37.61, 61.84, 75.75, 108.71, 108. 92, 109.37, 115.85, 119.02, 120.79, 122.36, 123.03, 123.38, 126.34, 128.98, 137.23, 138.19, 140.49, 149.60, 158.32, 160.03, 161.35, 168.91. $^{13}C$ APT, DEPT 135° and 90° experiments clearly

established the presence of two methyl, one methylene, twelve methine and nine quaternary carbon in the molecule (Figure 11,12,13,14,15,16,17). Anal. Calcd for $C_{24}H_{20}FN_3O_3$: 417.15. Found 417.8 (Figure 3.18).

*(3R,4R)-1-(9-ethyl-9H-carbazol-3-yl)-4-(5-fluoropyridin-2-yl)-3-hydroxyazetidin-2-one* ***(DB-5-SAS-OH, 2)***. Light brown amorphous solid (348 mg, 77%); m.p. 198.5° C - 198.8° C; IR (KBr) 3235, 3056, 2937,2890, 1738, 1629,1592, 1487, 1471, 1453 $cm^{-1}$ (Figure 3.19.); $^1$H NMR (DMSO, 600 MHz) 8.60 (1H, d, *J*=2.76), 8.03 (2H, m), 7.70 (5H, td, *J*=4.054), 7.57 (2H, m), 7.43 (3H, m), 7.16 (1H, t, *J*=7.41), 7.2, 6.23 (1H, m), 5.55 (1H, d, *J*=5.04), 5.31 (1H, t, *J*=6.15), 4.39 (2H, q, *J*=6.38), 1.27 (3H, t, *J*=7.02) (Figure 3.20) ; $^{13}$C NMR (150 MHz, DMSO) 14.13, 37.47, 63.03, 77.32, 108.92, 109.74, 110.14, 116.30, 119.17, 120.89, 122.09, 123.98, 124.40, 126.61, 130.20, 136.80, 137.66, 137.81, 140.50, 152.15, 158.27, 166.73. $^{13}$C APT, DEPT 135° and 90° experiments clearly established the presence of one methyl, one methylene, twelve methine and eight quaternary carbon in the molecule (Figure 21,22,23,24,25,26,27). Anal. Calcd for $C_{22}H_{18}FN_3O_2$: 375.14. Found 375.8 (Figure 3.28).

*(2R,3R)-1-(9-ethyl-9H-carbazol-3-yl)-2-(5-fluoropyridin-2-yl)-4-oxoazetidin-3-yl 2,2,2-trifluoroethanesulfonate* ***(DB-5-SAS-OTFE, 3)***. Light pink fluffy solid (120mg, 23%); m.p. 198.7° C - 199.5° C; IR (KBr) 2994, 2976, 2927, 1763, 1624, 1587, 1484, 1463, 1444 $cm^{-1}$ (Figure 3.29), $^1$H NMR (DMSO, 600 MHz) 8.61 (1H, d, *J*=2.88), 8.04 (2H, m), 7.81(1H, td, *J*=3.39), 7.66 (1H, dd, *J*=4.34), 7.60 (2H, t, *J*=7.65), 7.44 (2H, m), 7.17 (1H, t, *J*=7.5), 6.26 (1H, d, *J*=5.04), 5.92 (1H, d, *J*=5.04), 5.03 (2H, m), 4.40 (2H, q, *J*=7.04), 1.27 (3H, t, *J*=7.11) (Figure 3.30); $^{13}$C NMR (150 MHz, DMSO) 14.11, 37.50, 52.20, 60.94, 80.74, 109.48, 109.84, 110.26, 116.53, 119.34, 120.99, 122.01, 122.49, 124.29, 124.41, 125.82, 126.80, 129.20, 137.20, 138.31, 138.47, 140.54, 149.10, 160.32. $^{13}$C APT, DEPT 135° and 90° experiments clearly established the

presence of one methyl, two methylene, twelve methine and nine quaternary carbons in the molecule (Figure 31,32,33,34,35,36,37). Anal. Calcd for $C_{24}H_{19}F_4N_3O_4S$: 521.10. Found 521.6 (Figure 3.38).

*(2R,3R)-1-(9-ethyl-9H-carbazol-3-yl)-2-(5-fluoropyridin-2-yl)-4-oxoazetidin-3-yl 3-cyanoazetidine-sulfonate* ***(DB-5-SAS-OCAS, 4)***. Light brown crystalline solid (414 mg, 39%); m.p. 172.5° C - 174.7° C; IR (KBr) 3082, 2968, 2926, 2896, 2249, 1620, 1600,1584, 1482 $cm^{-1}$ (Figure 3.39); $^1$H NMR (DMSO, 600 MHz) 8.65 (1H, d, J=2.88), 8.06 (2H, m), 7.81 (1H, td, J=4.032), 7.70 (1H, dd, *J*=4.90), 7.60 (2H, t, *J*=9.72), 7.46 (2H, m), 7.18 (1H, t, *J*=7.47), 6.17 (1H, d, *J*=5.10), 5.91 (1H, d, *J*=5.10), 4.40 (2H, q, *J*=7.10), 4.03 (3H, tt, *J*=9.315), 3.82 (2H, m), 1.27 (3H, t, *J*=7.11) (Figure 3.40), $^{13}$C NMR (150 MHz, DMSO) 14.13, 17.65, 37.50, 54.84, 54.89, 61.16, 80.30, 109.41, 109.84, 110.28, 116.47, 119.32, 119.39, 121.00, 122.04, 122.53, 124.47, 125.60, 126.75, 129.26, 137.19, 138.41, 140.55, 149.48, 158.57, 160.26. $^{13}$C APT, DEPT 135° and 90° experiments clearly established the presence of one methyl, three methylene, thirteen methine and nine quaternary carbons in the molecule (Figure 41,42,43,44,45,46,47). Anal. Calcd for $C_{26}H_{22}FN_5O_4S$: 519.14. Found 519.6 (Figure 3.48).

*(2R,3R)-1-(9-ethyl-9H-carbazol-3-yl)-2-(5-fluoropyridin-2-yl)-4-oxoazetidin-3-yl isopropyl(methyl)sulfamate*, ***(DB-5-SAS-IPMS, 5)***. Dark brown amorphous solid (30 mg, 5.88%); m.p. 169.8° C – 171.5° C; IR (KBr) 2978, 2938, 1760, 1599, 1588, 1493, 1484, 1472, 1460 $cm^{-1}$ (Figure 3.49); $^1$H NMR (DMSO, 600 MHz) 8.55 (1H, d, J=2.82), 7.97 (2H, m), 7.73 (1H, td, J=4.056), 7.58 (1H, dd, *J*=4.36), 7.52 (2H, m), 7.36 (2H, m), 7.10 (1H, t, J=7.455), 5.95 (1H, d, *J*=5.04), 5.78 (1H, d, *J*=5.04), 4.32 (2H, q, *J*=7.08), 3.66 (1H, septet *J*=6.72), 3.26 (3H, bs), 1.19 (3H, t, *J*=7.11), 0.91 (6H, dd, *J*=7.673) (Figure 3.50); $^{13}$C NMR (150 MHz, DMSO) 14.13, 19.95, 19.51, 28.57, 37.48, 50.73, 61.22, 79.38, 109.32, 109.82, 110.22, 116.42, 119.29, 120.96, 122.04,

122.50, 124.15, 125.74, 126.74, 129.44, 137.09, 160.26. $^{13}C$ APT, DEPT 135° and 90° experiments clearly established the presence of four methyl, one methylene, thirteen methine and eight quaternary carbon in the molecule (Figure 51,52,53,54,55,56,57,56,57). Anal. Calcd for $C_{26}H_{27}FN_4O_4S$: 510.17 (Figure 3.58).

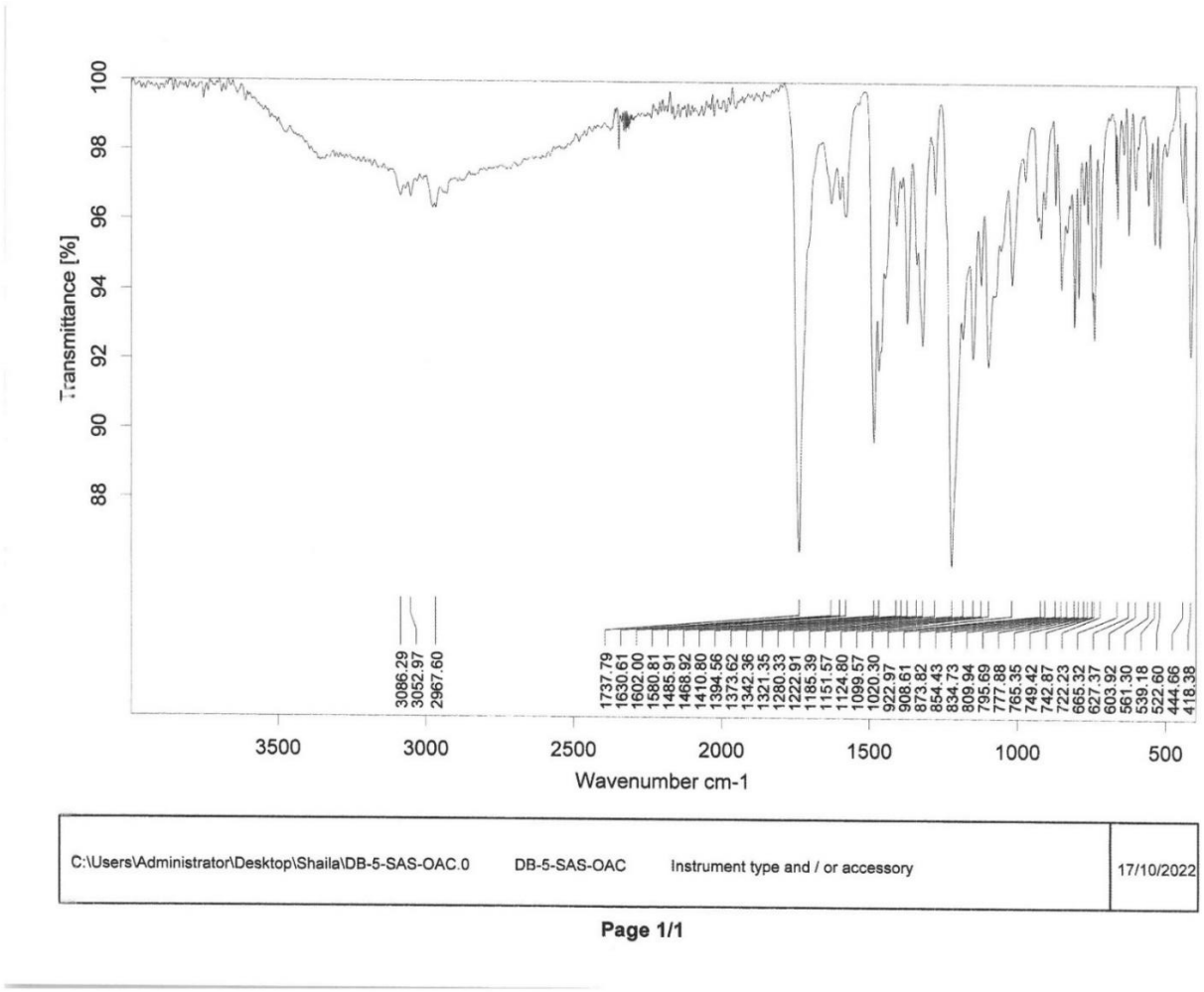


Figure 3.9: FTIR of DB-5-SAS-OAC (1)

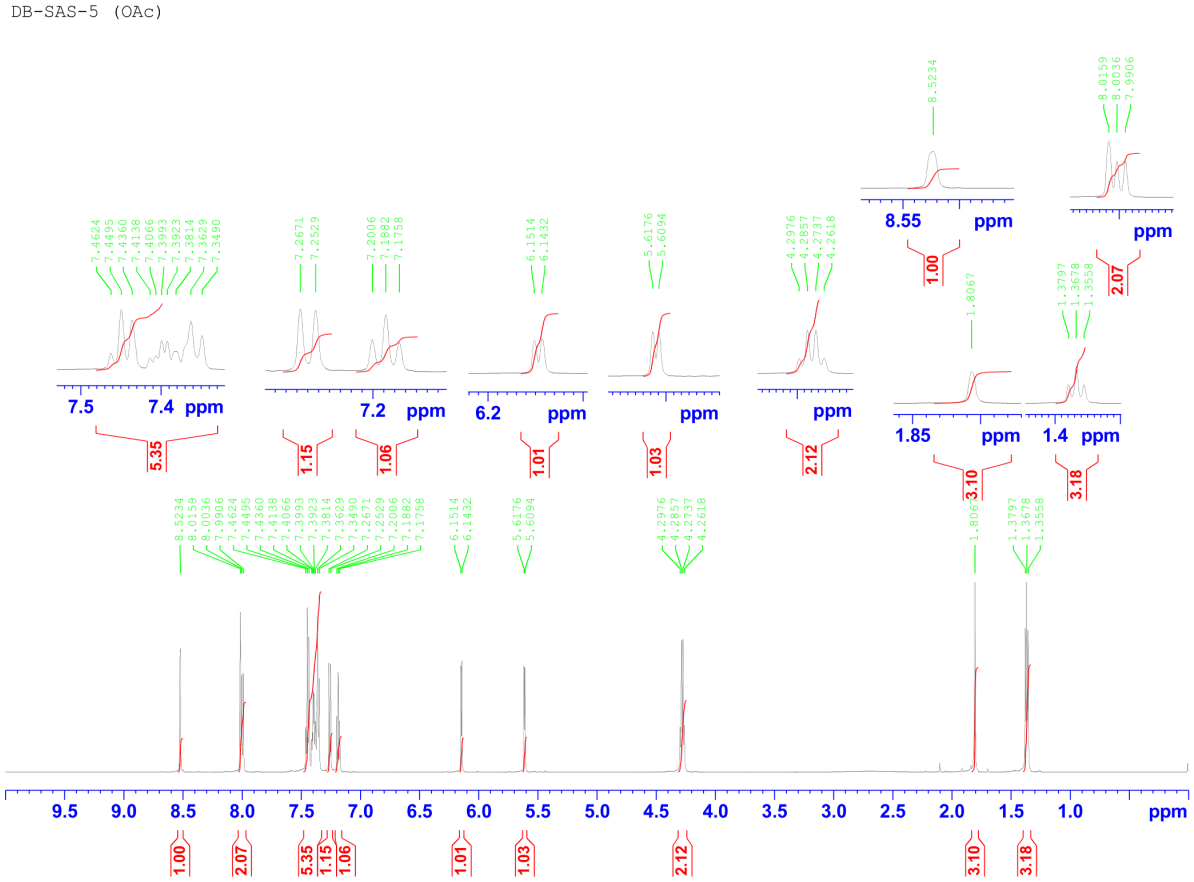


Figure 3.10: $^{1}$H NMR of DB-SAS-OAC (1)

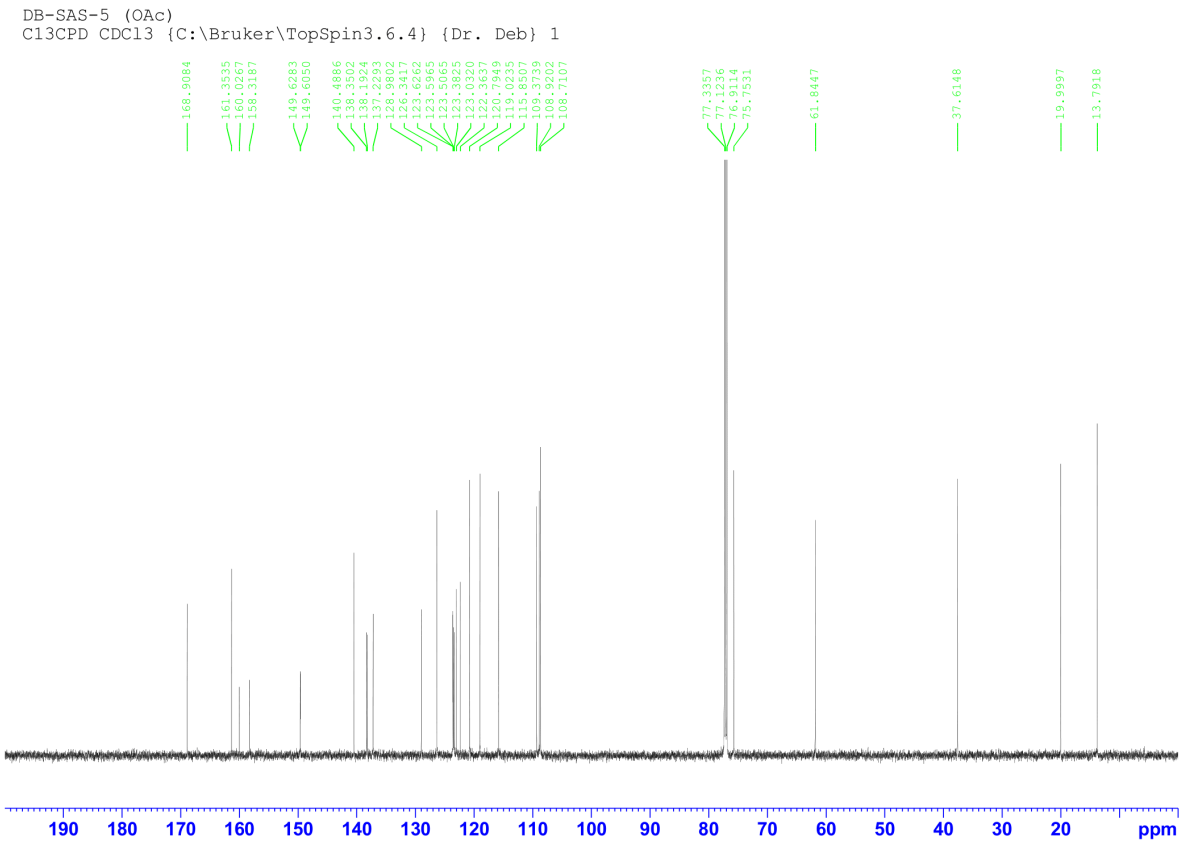


Figure 3.11: $^{13}C$ NMR of DB-SAS-OAC (1)

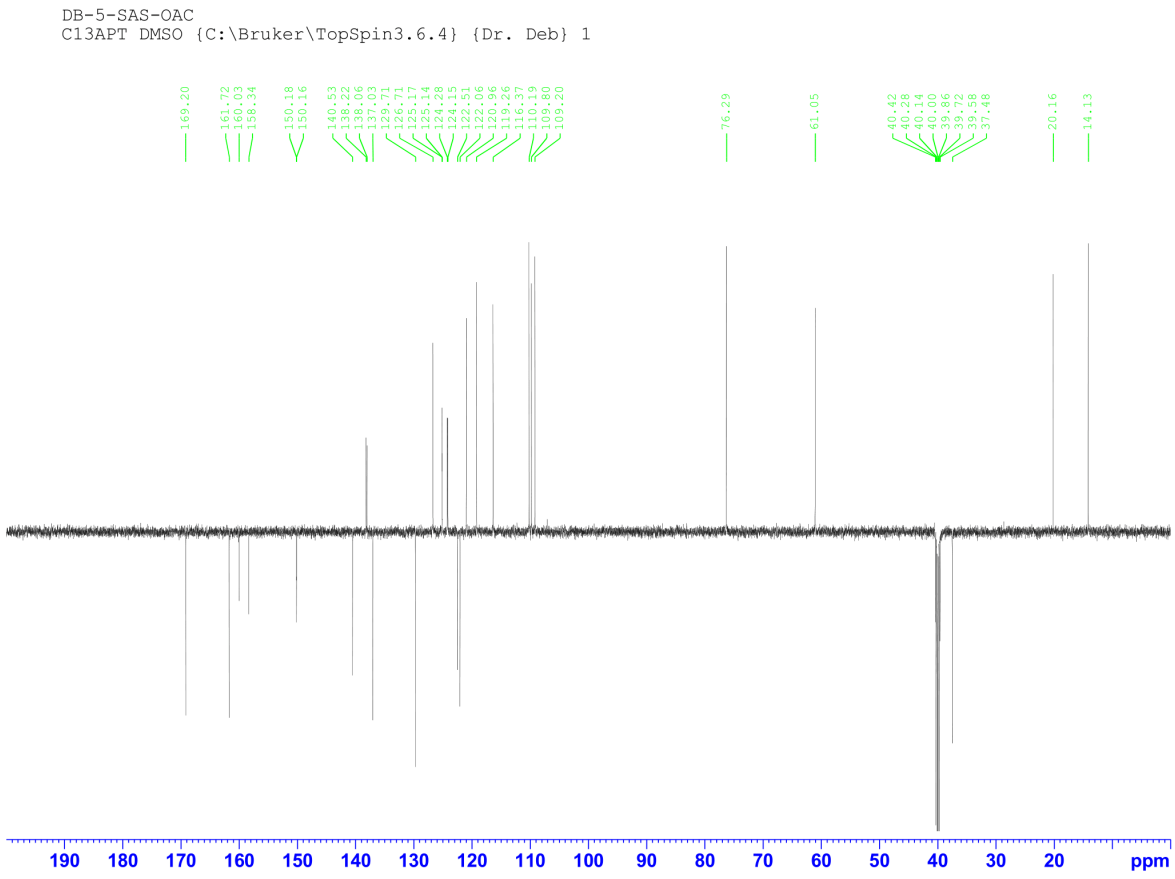


Figure 3.12: $^{13}$C APT NMR of DB-SAS-OAC (1)

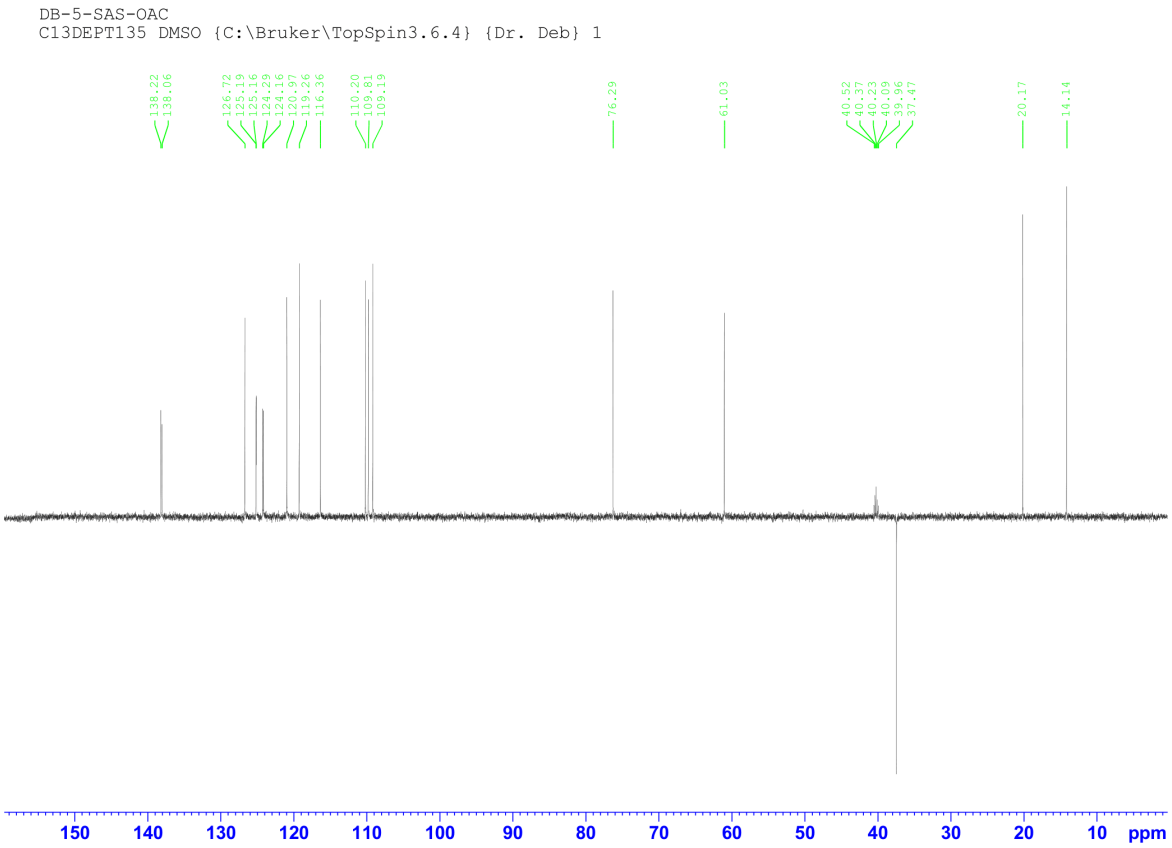


Figure 3.13: $^{13}C$ NMR of DB-SAS-OAC (1) (DFPT 135°)

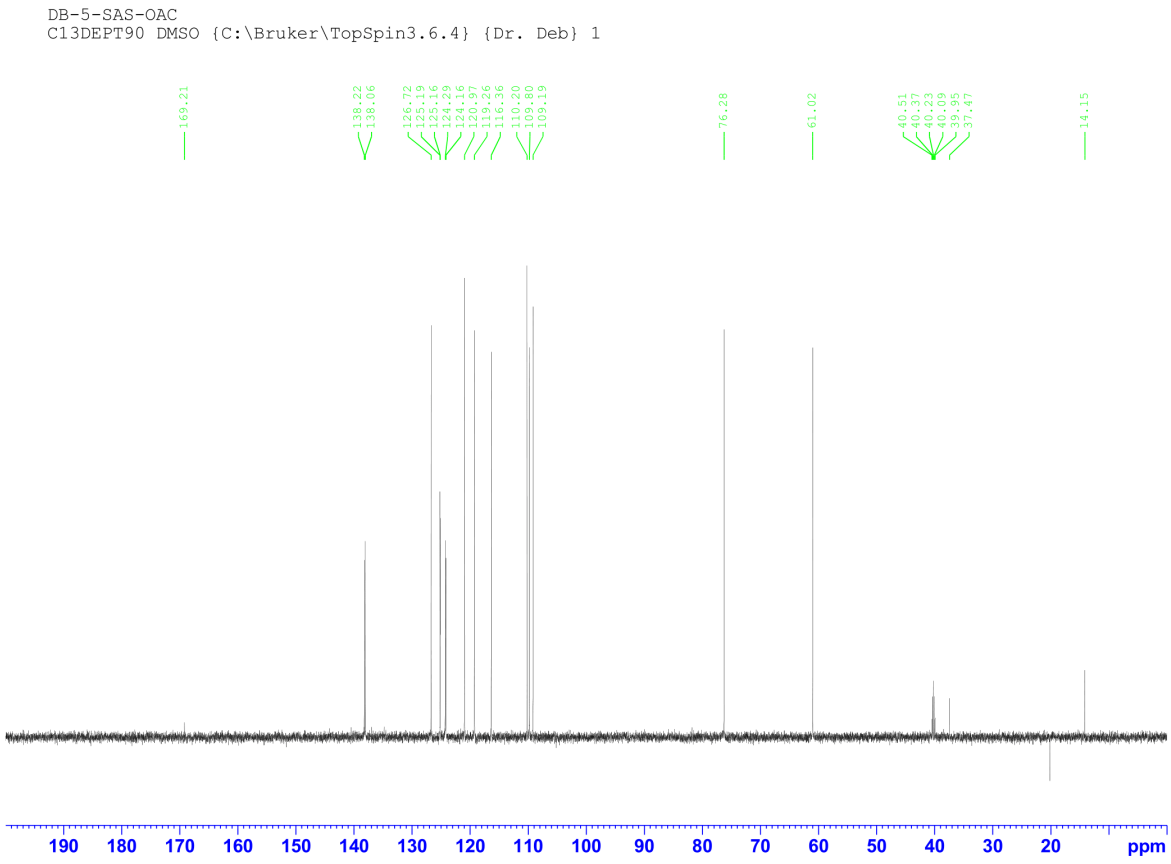


Figure 3.14: $^{13}C$ NMR of DB-SAS-OAC (1) (DFPT 90°)

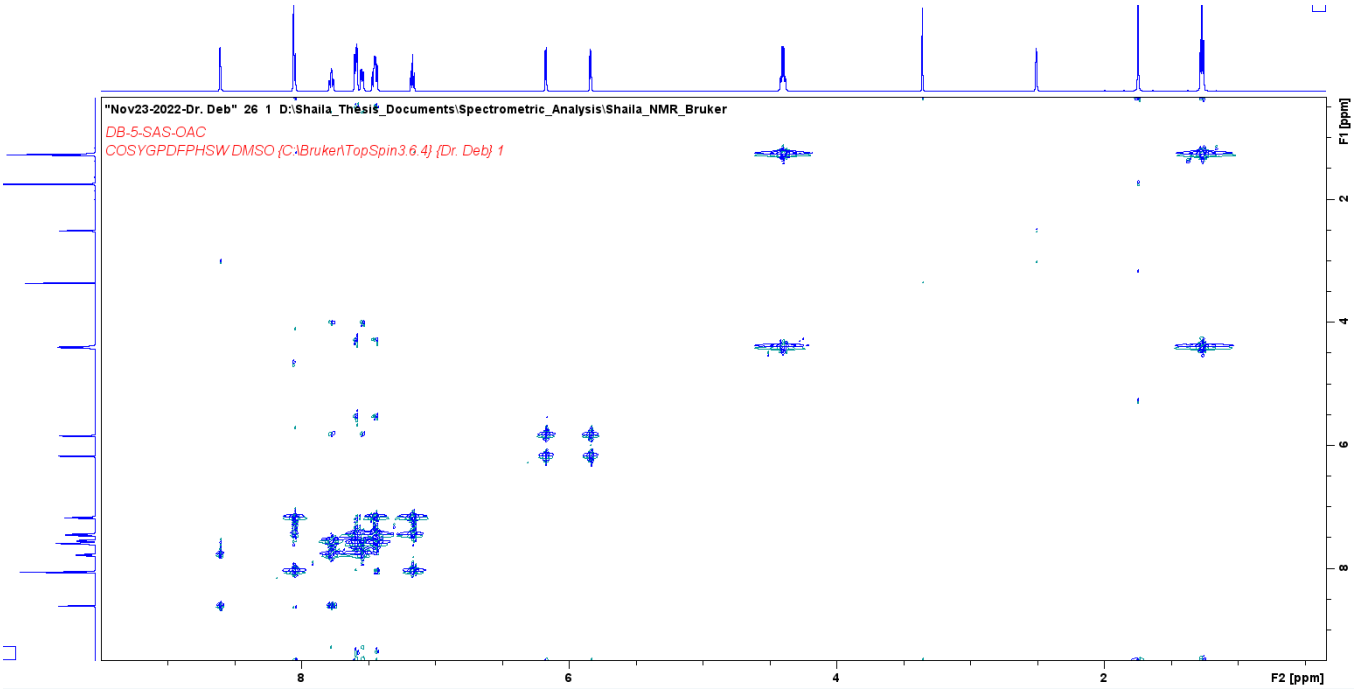


Figure 3.15: $^{1}H$-$^{1}H$ Correlation (COSY) NMR of DB-SAS-OAC (1)

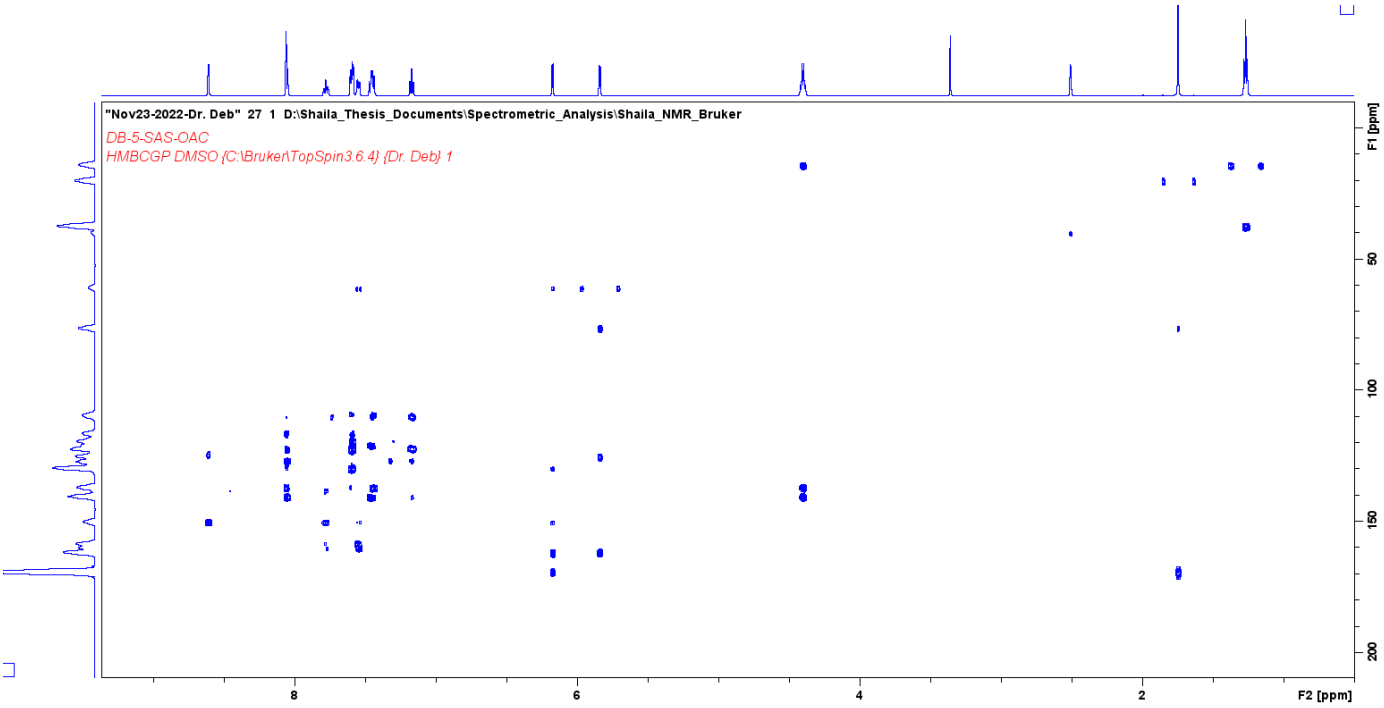


Figure 3.16: $^{1}H$-$^{13}C$ Correlation (HMBCGP) NMR of DB-SAS-OAC (1)

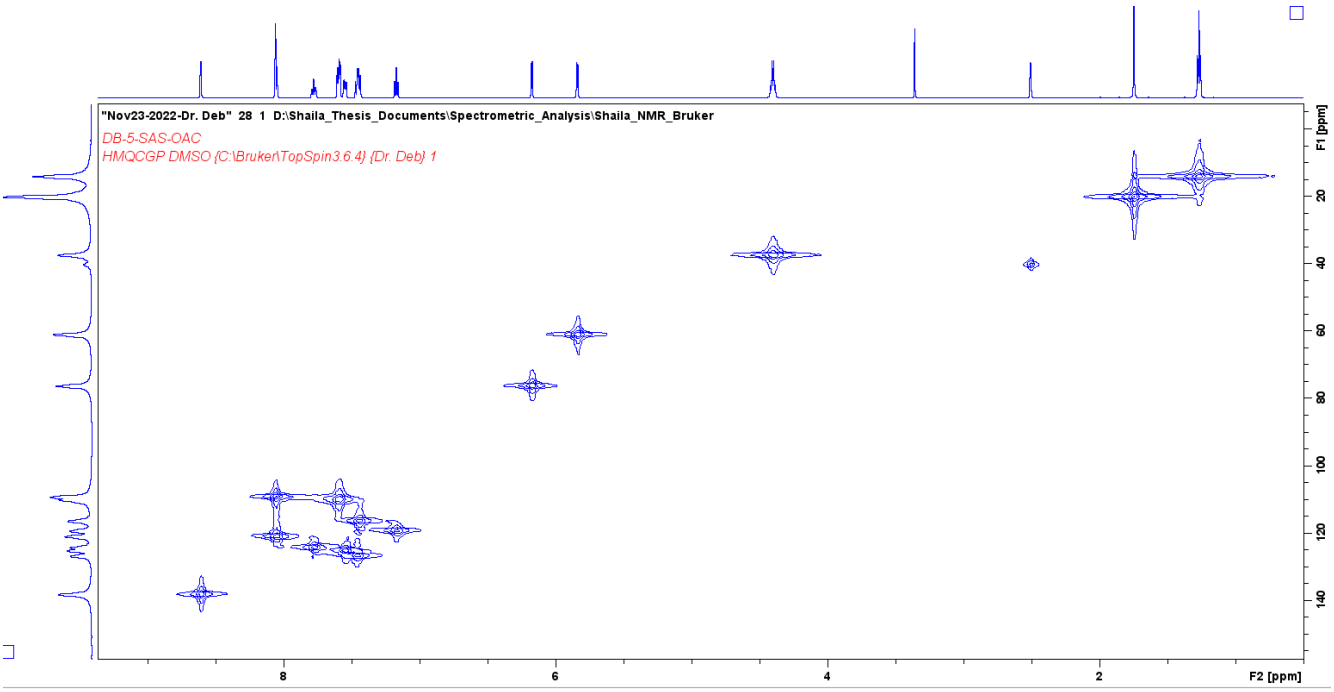


Figure 3.17: $^{1}H$-$^{13}C$ Correlation HMQCGP NMR of DB-SAS-OAC (1)

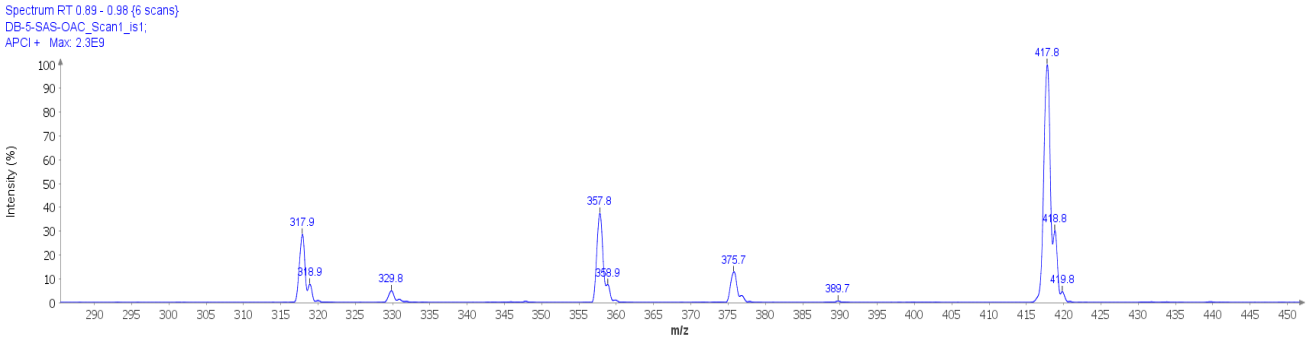


Figure 3.18: Mass spectrometry of DB-5-SAS-OAC (1)

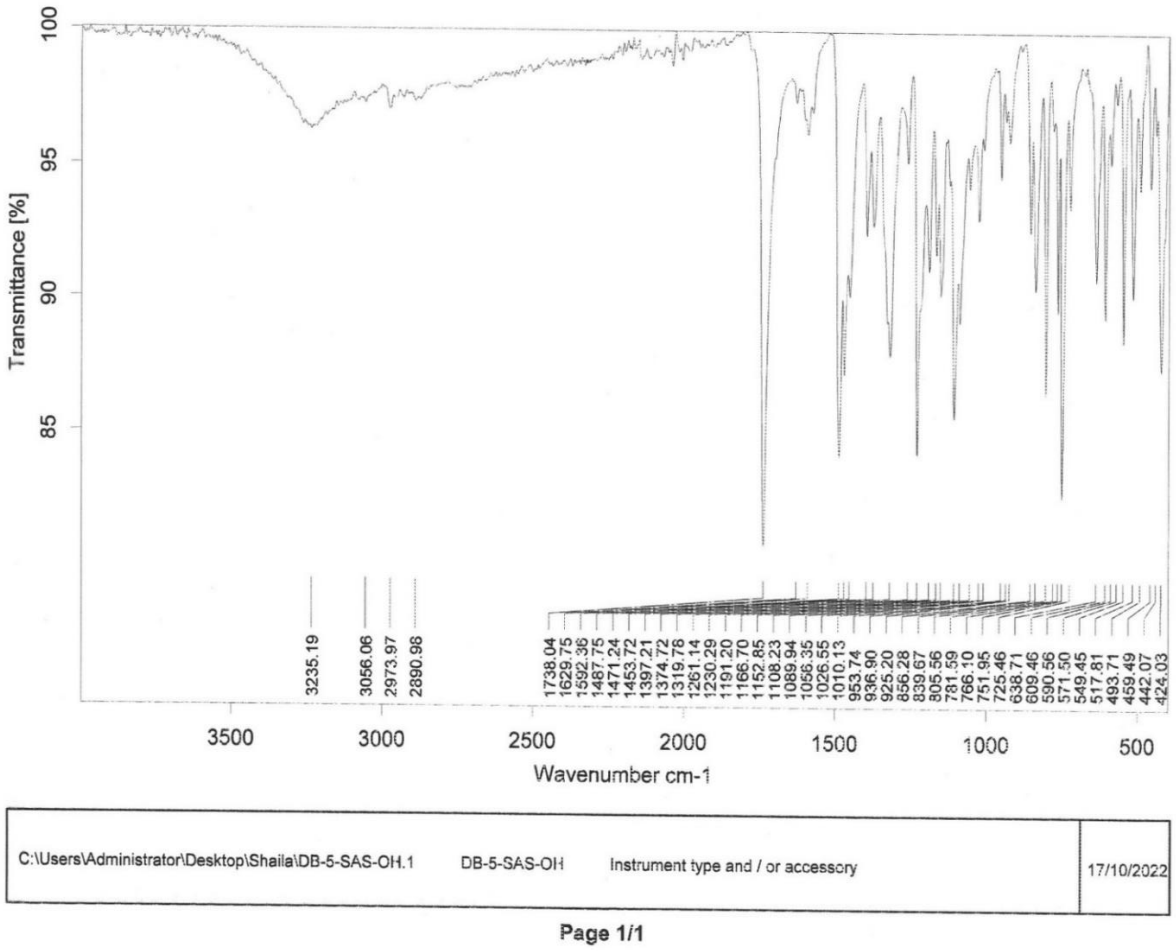


Figure 3.19: FTIR of DB-5-SAS-OH (2).

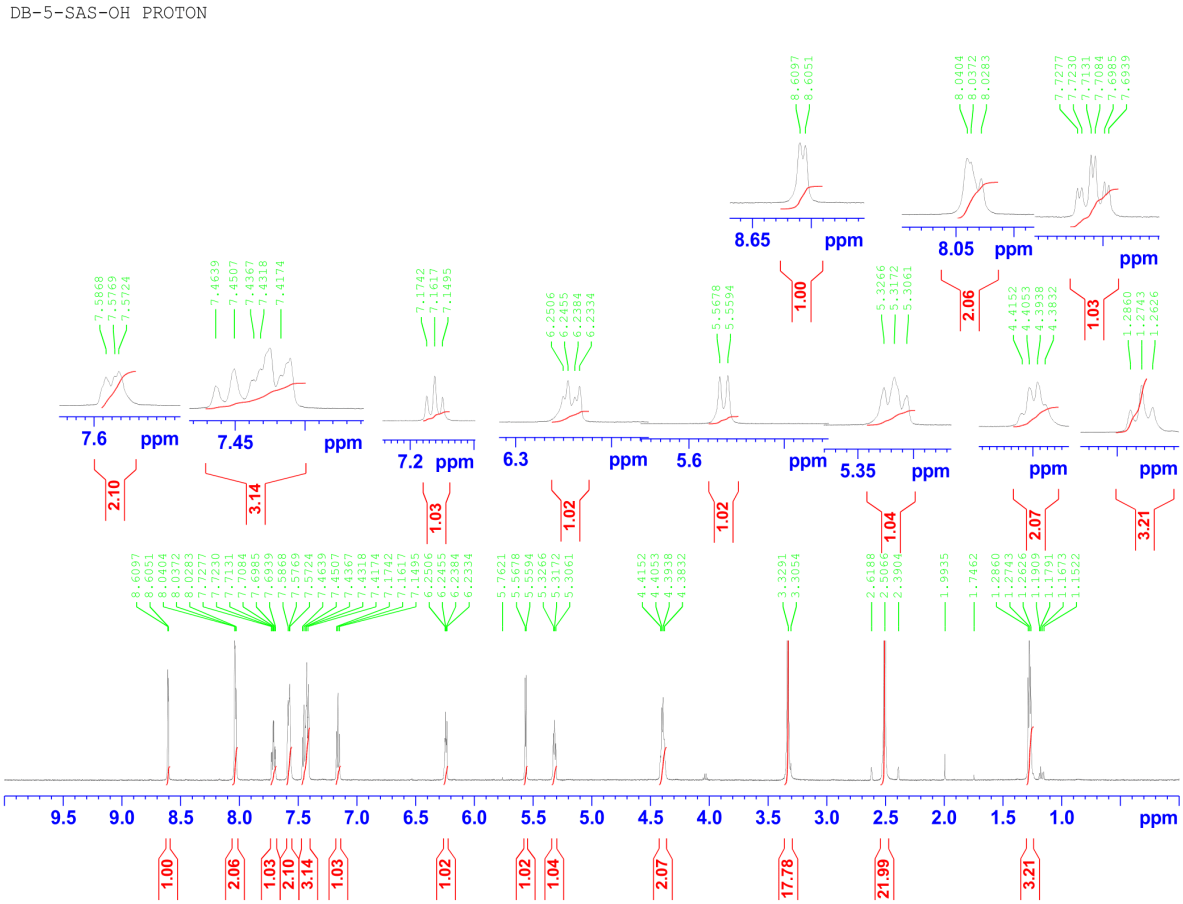


Figure 3.20: Proton NMR of compound DB-5-SAS-OH (2)

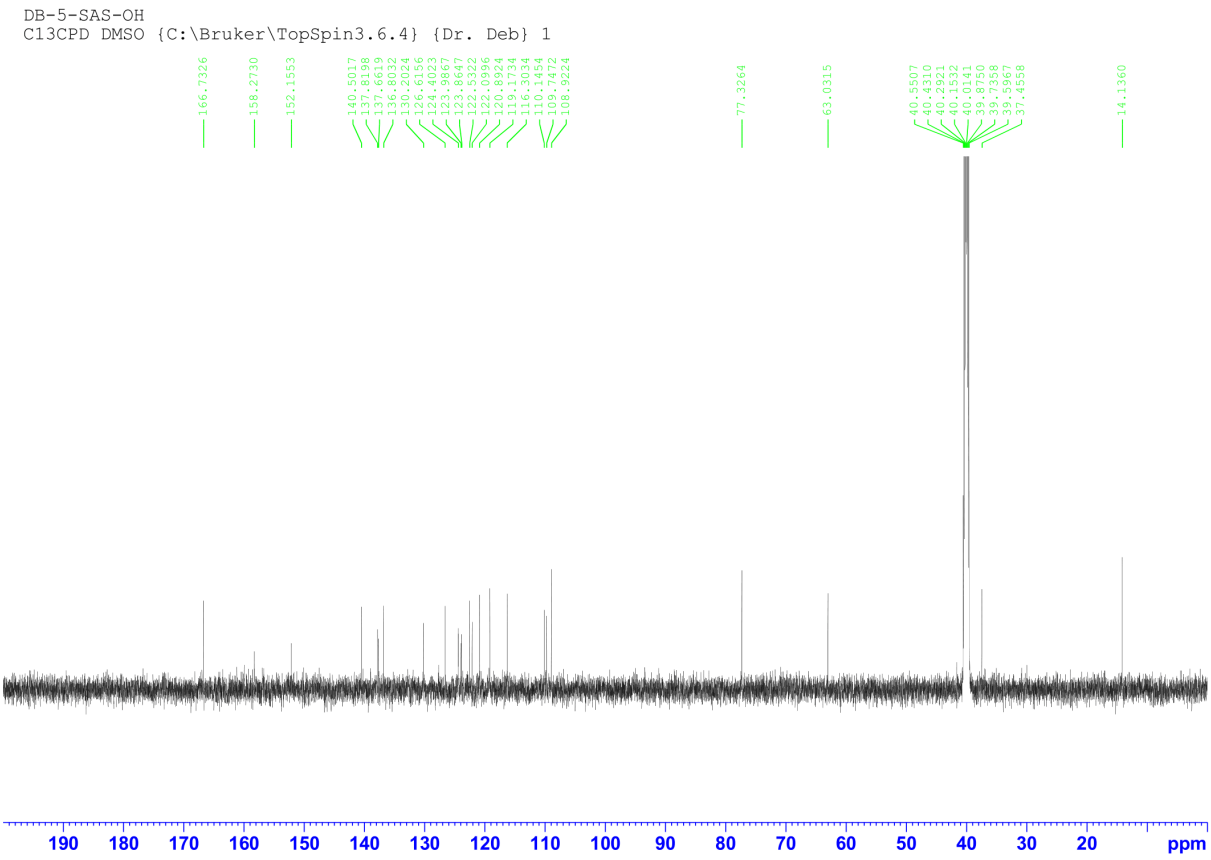


Figure 3.21: $^{13}$C NMR of DB-5-SAS-OH (2)

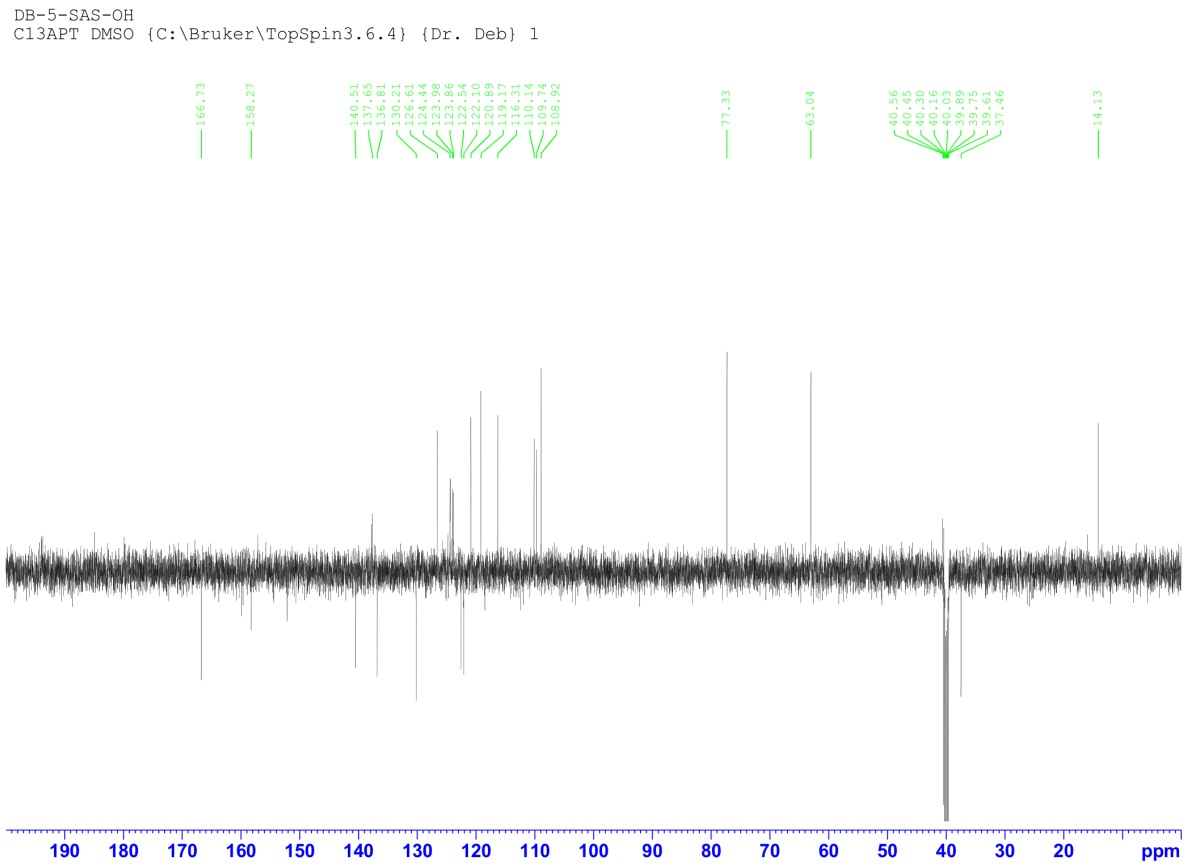


Figure 3.22: $^{13}$C APT NMR of DB-5-SAS-OH (2)

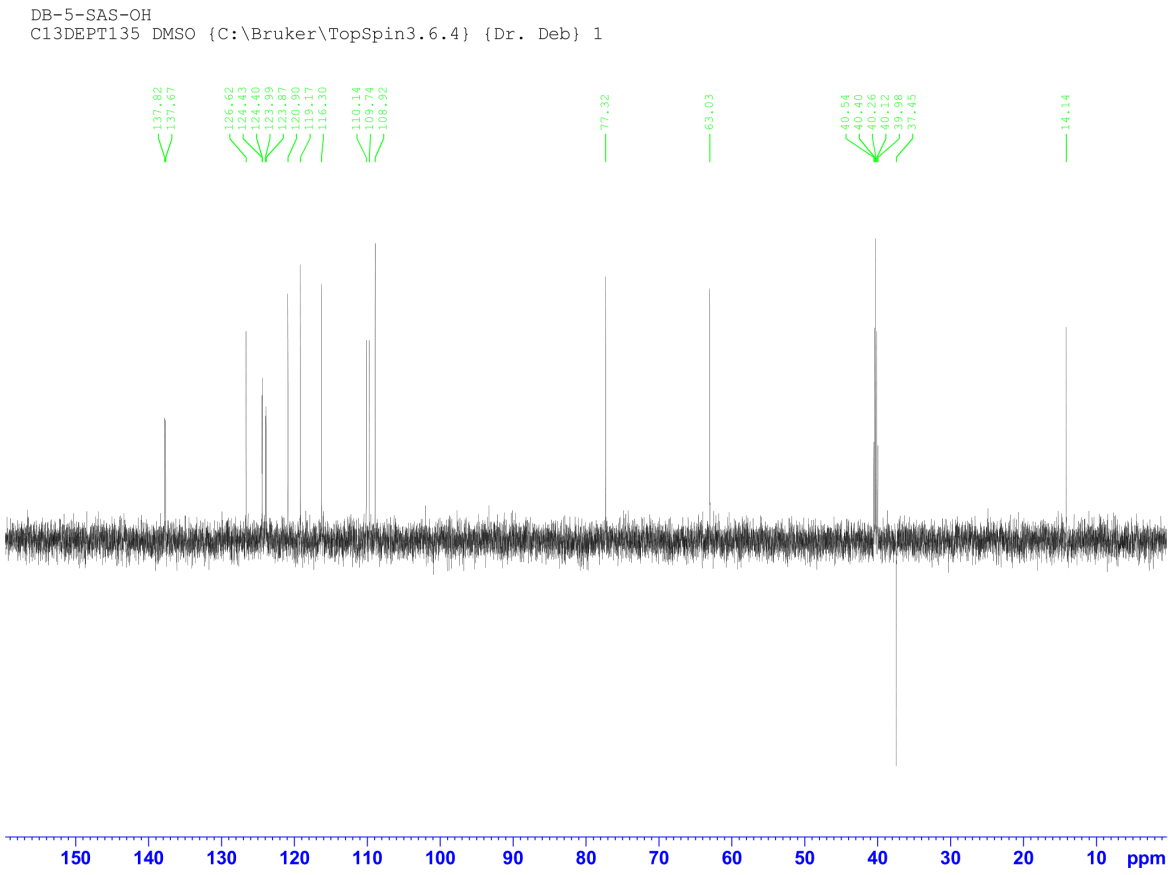


Figure 3.23: $^{13}C$ NMR of DB-5-SAS-OH (2) (DFPT 135)

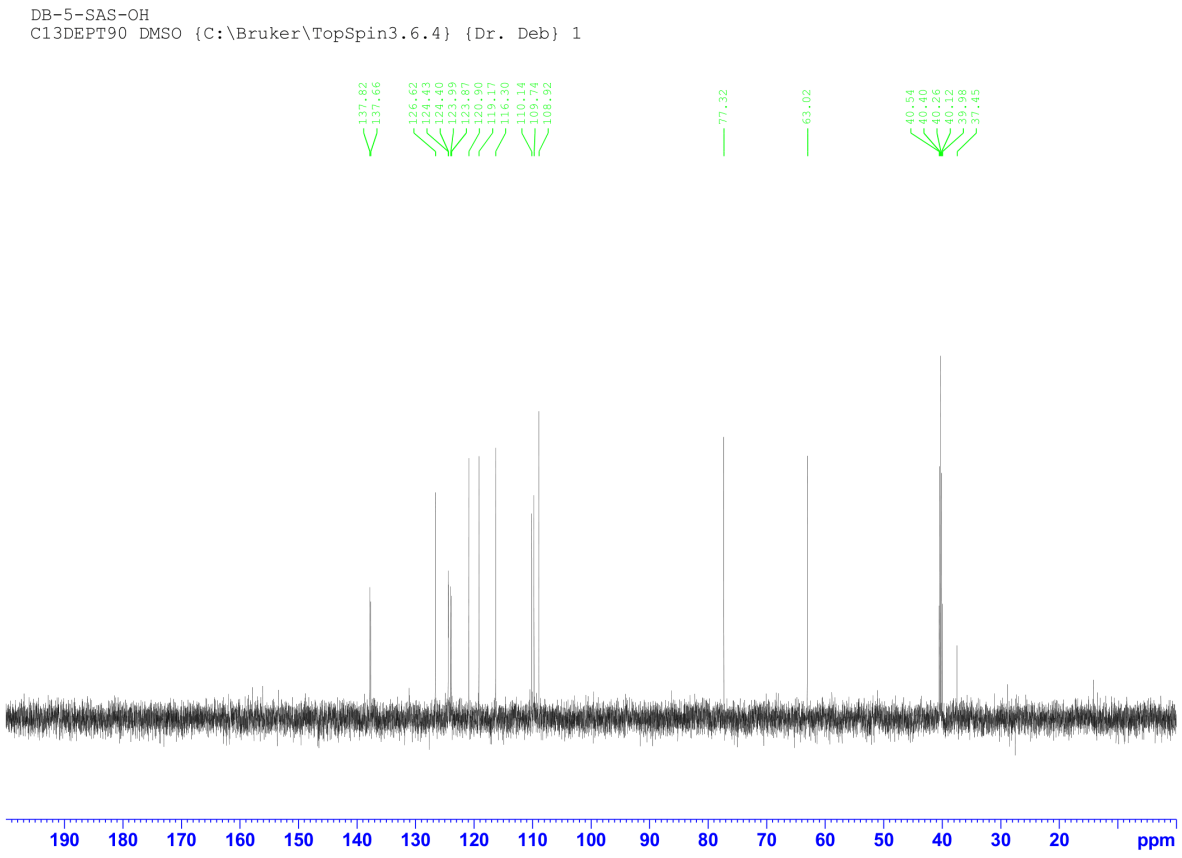


Figure 3.24: $^{13}C$ NMR of DB-5-SAS-OH (2) (DFPT 90°)

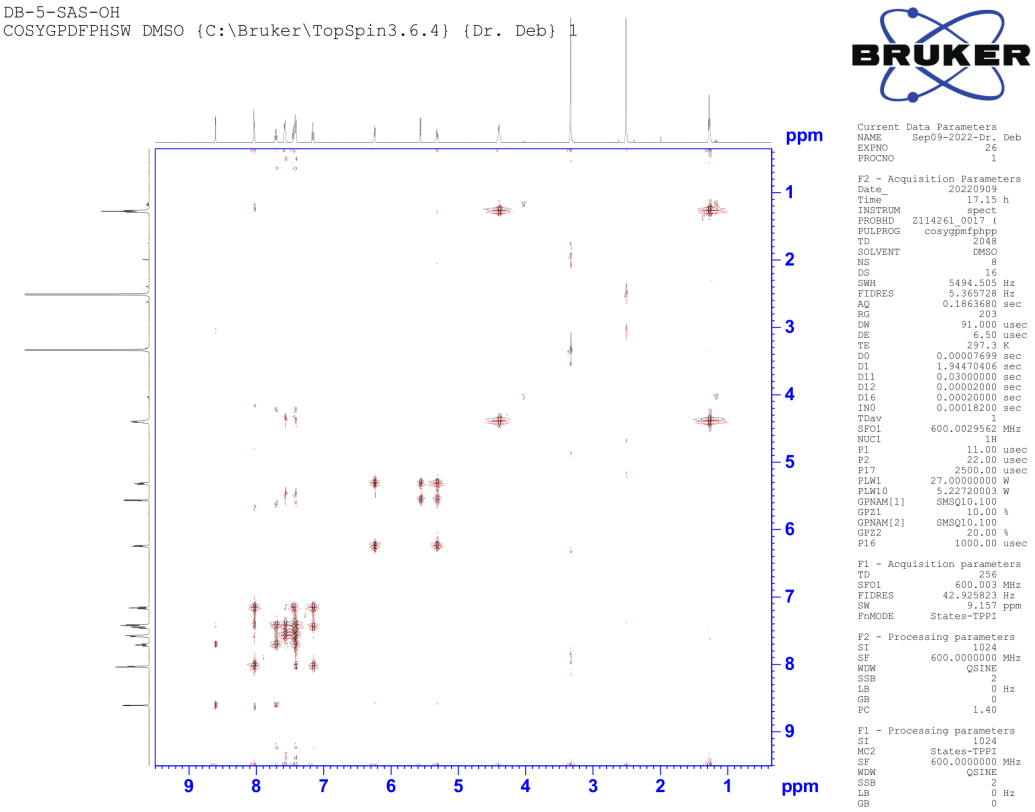


Figure 3.25: $^{1}$H-$^{1}$H Correlation (COSY) NMR of DB-5-SAS-OH (2)

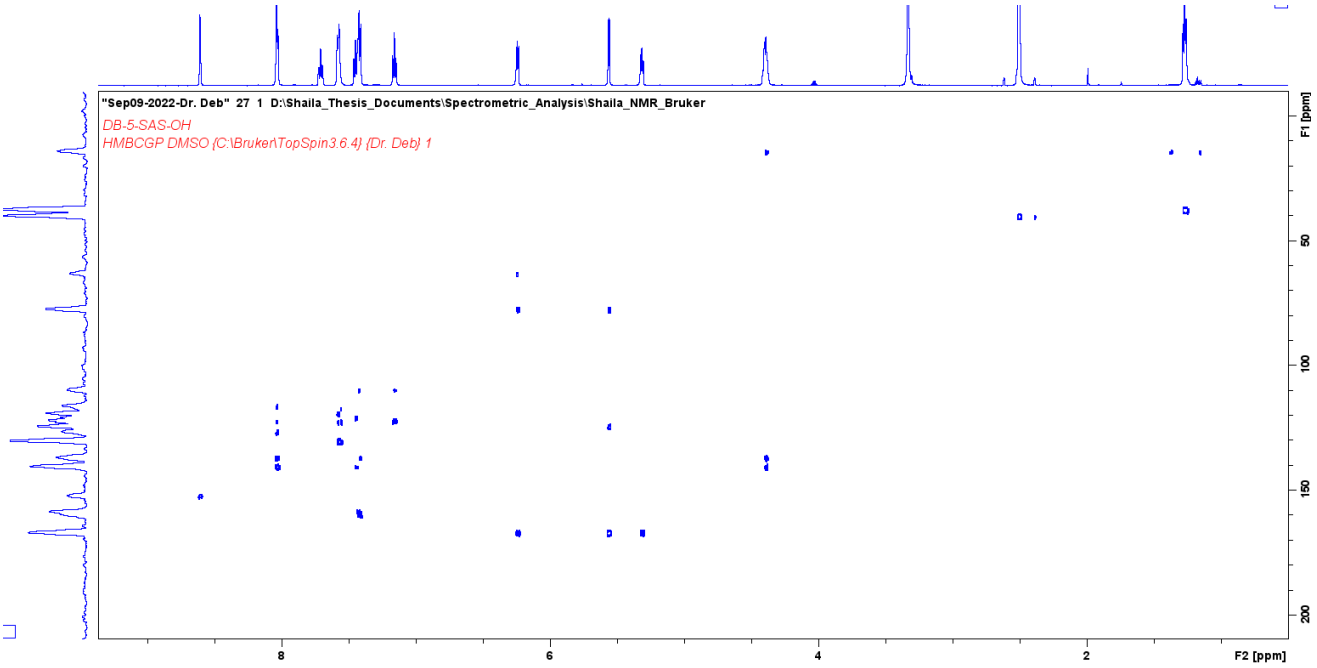


Figure 3.26: $^{1}H$-$^{13}C$ Correlation (HMBCGP) NMR of DB-5-SAS-OH (2)

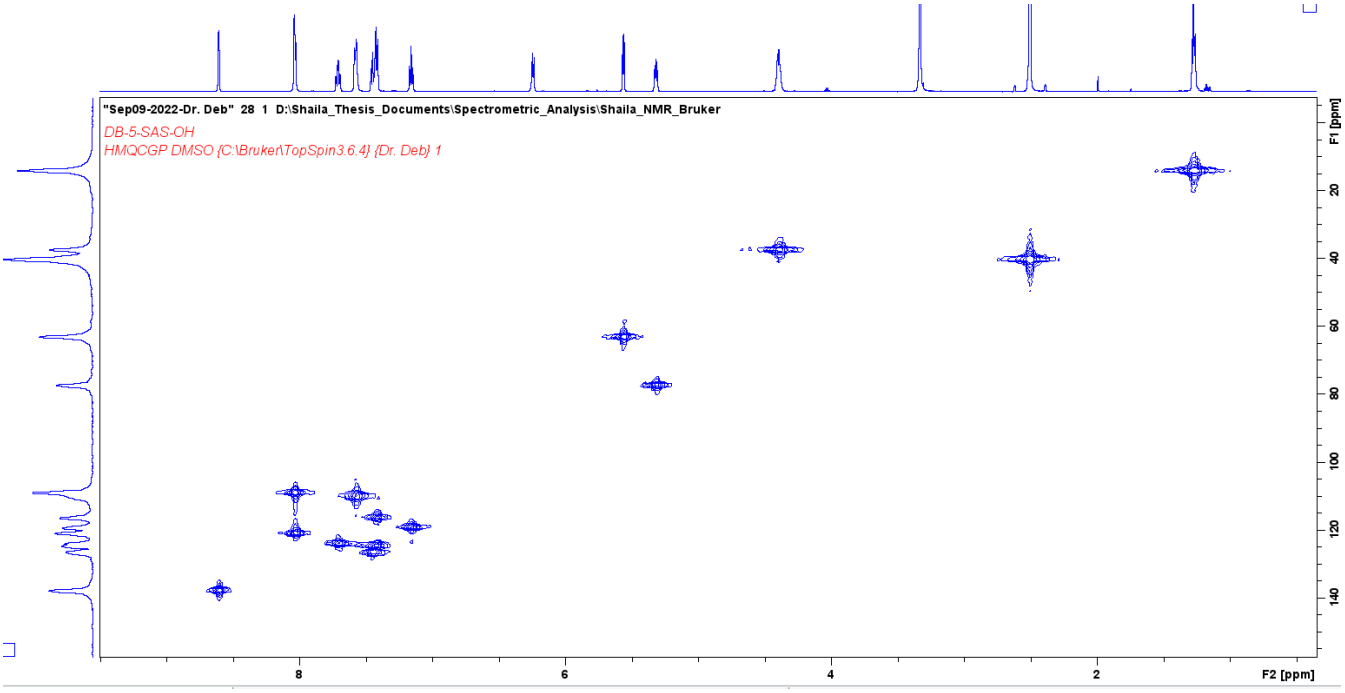


Figure 3.27: $^{1}H$-$^{13}C$ Correlation (HMQCGP) NMR of DB-5-SAS-OH (2)

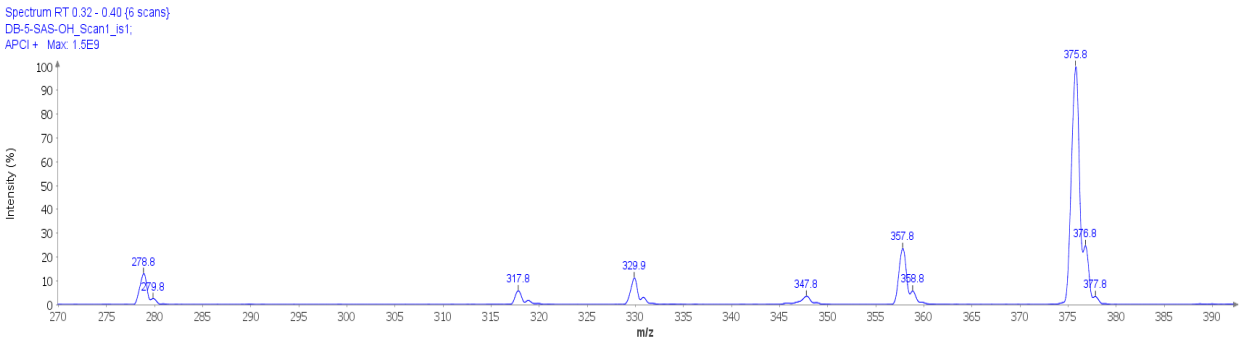


Figure 3.28: Mass spectrometry of DB-5-SAS-OH (2)

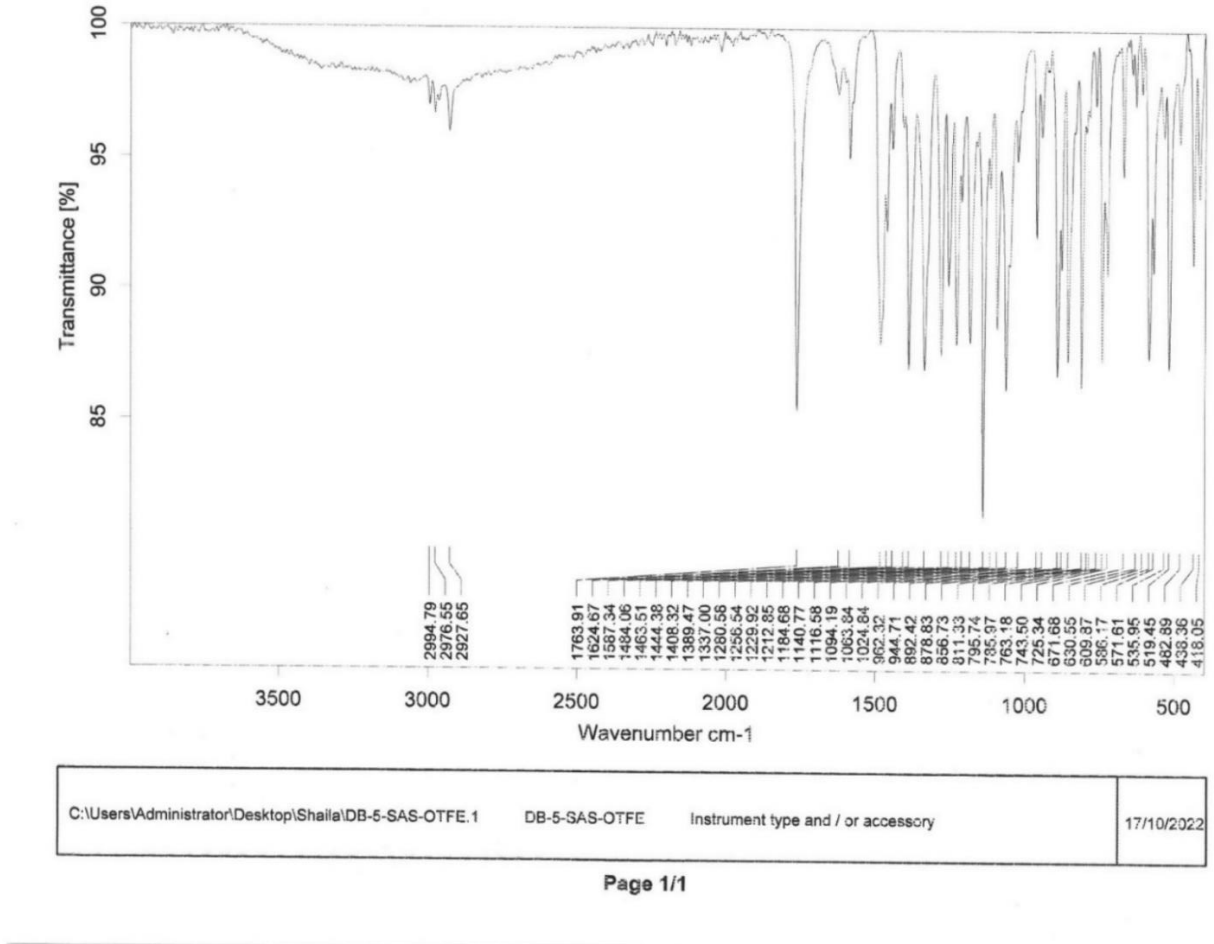


Figure 3.29: FTIR of DB-5-SAS-OTFE (3)

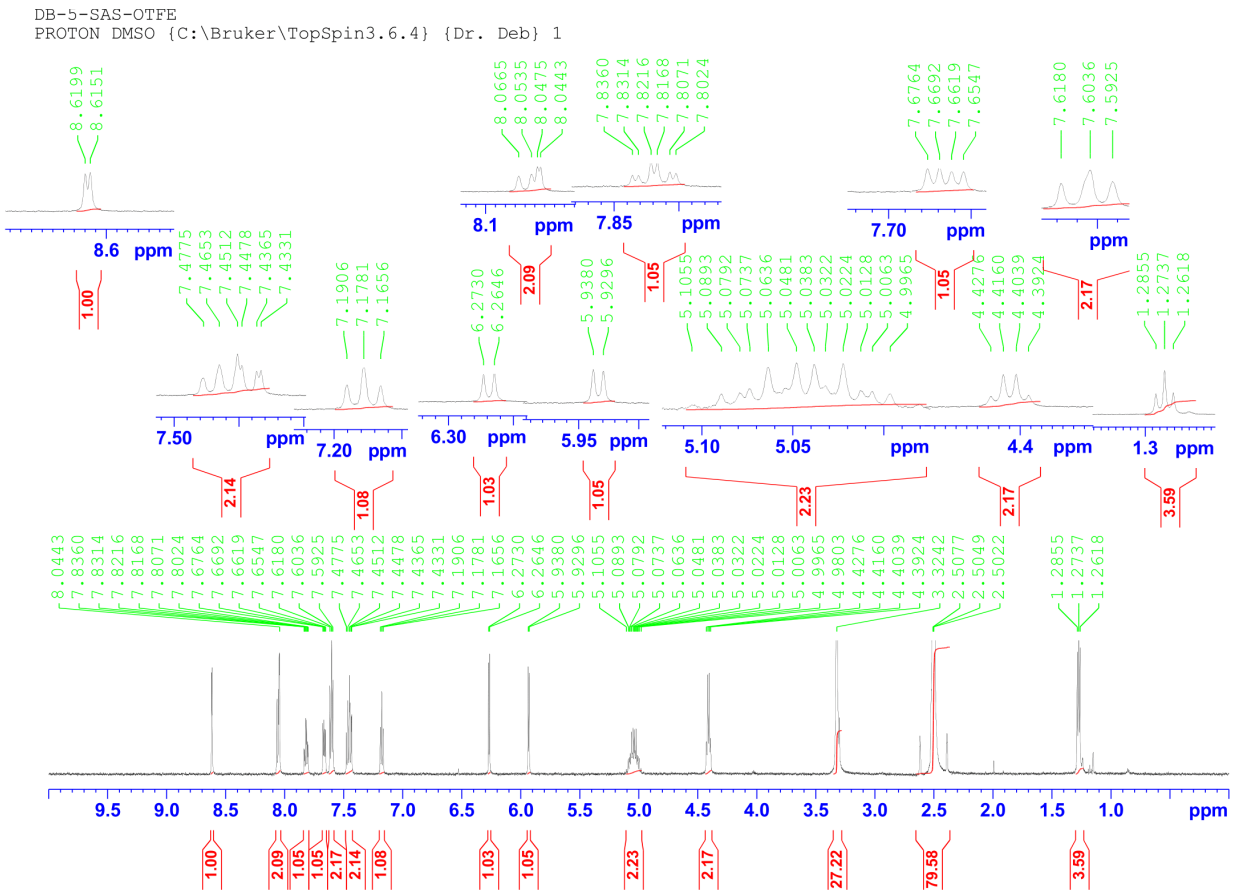


Figure:3.30: Proton NMR of compound DB-5-SAS-OTFE (3)

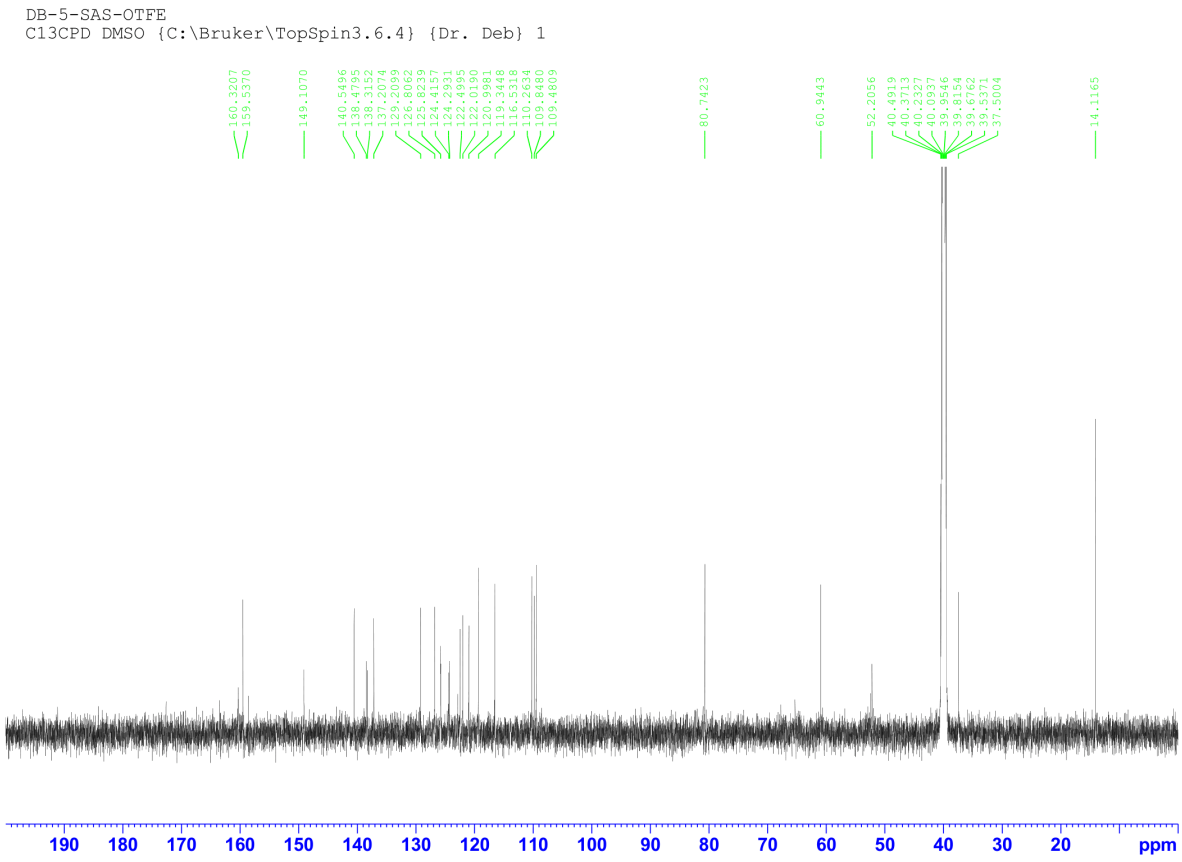


Figure 3.31: $^{13}C$ NMR of DB-5-SAS-OTFE (3)

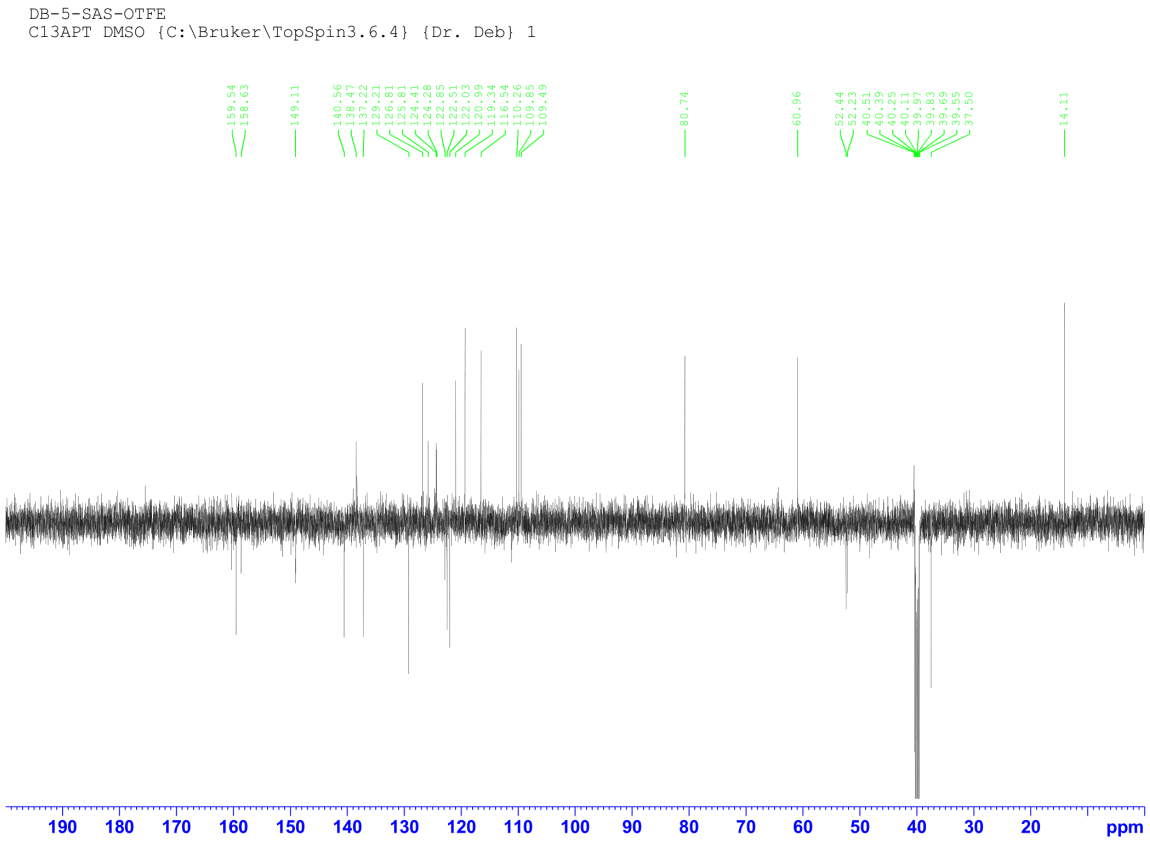


Figure 3.32: $^{13}$C APT NMR of DB-5-SAS-OTFE (3)

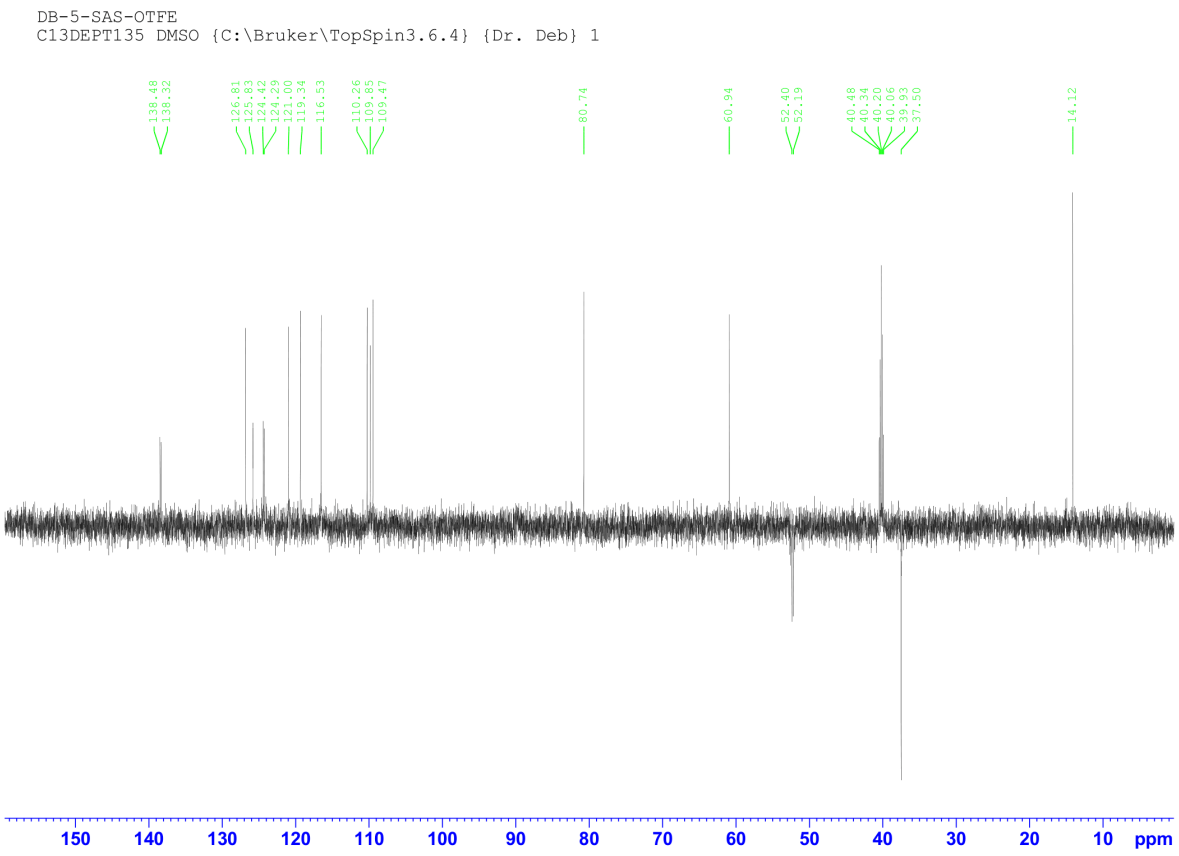


Figure 3.33: $^{13}$C DEPT of DB-5-SAS-OTFE (3) (DFPT 135°)

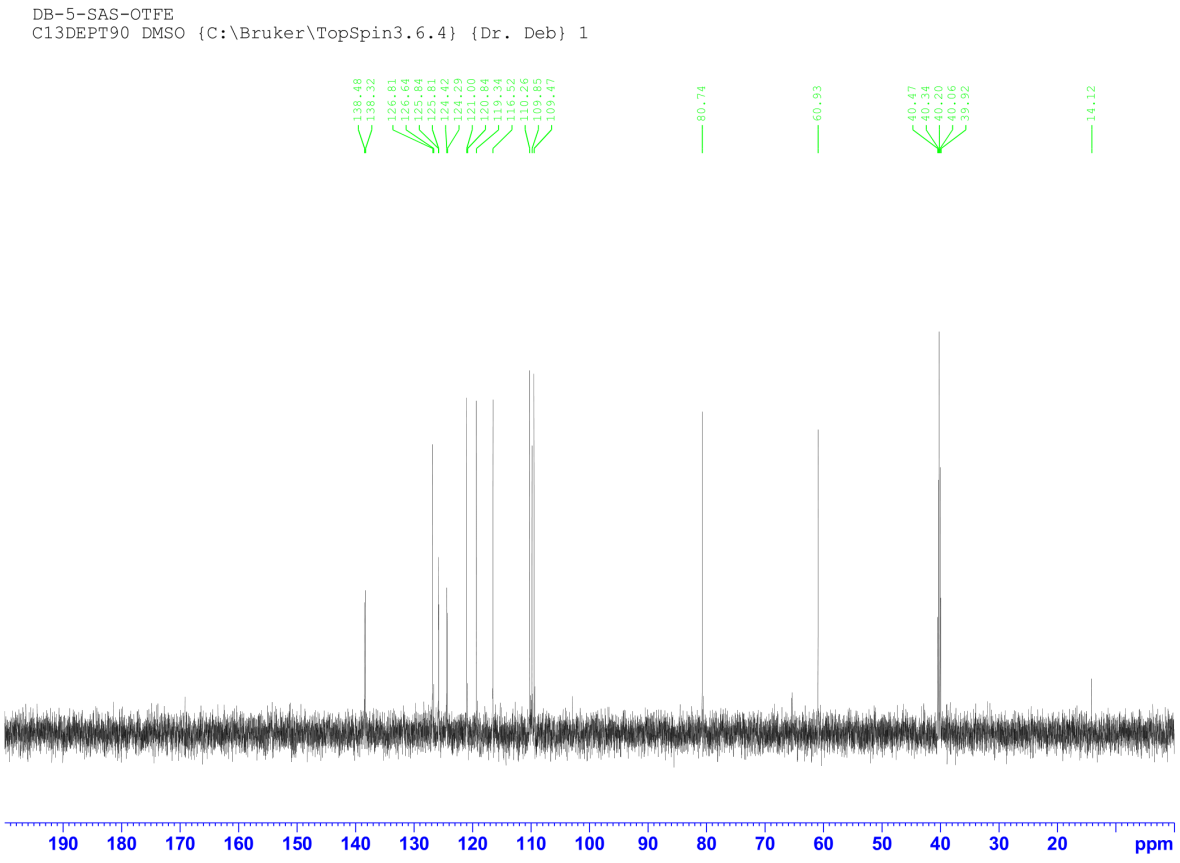


Figure 3.34: $^{13}C$ NMR of DB-5-SAS-OTFE (3) (DFPT 90°)

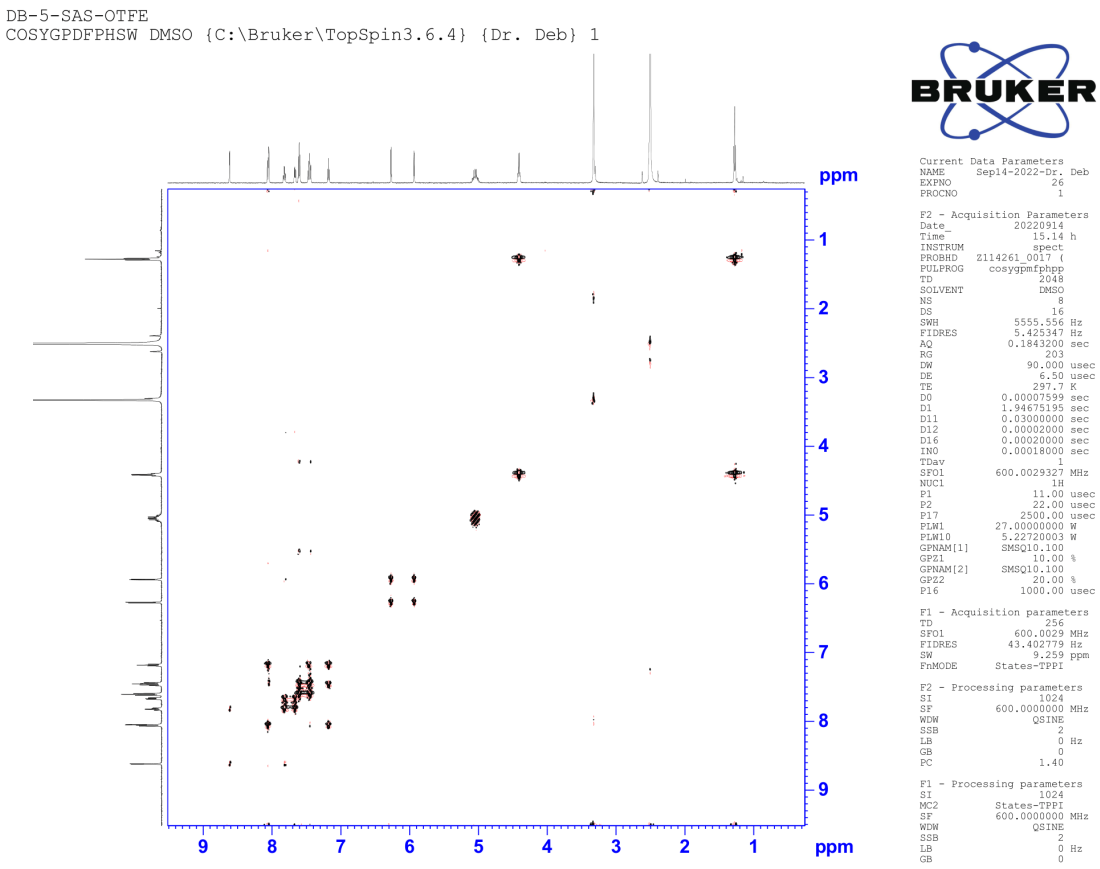


Figure 3.35: $^{1}$H-$^{1}$H Correlation (COSY) NMR of DB-5-SAS-OTFE (3)

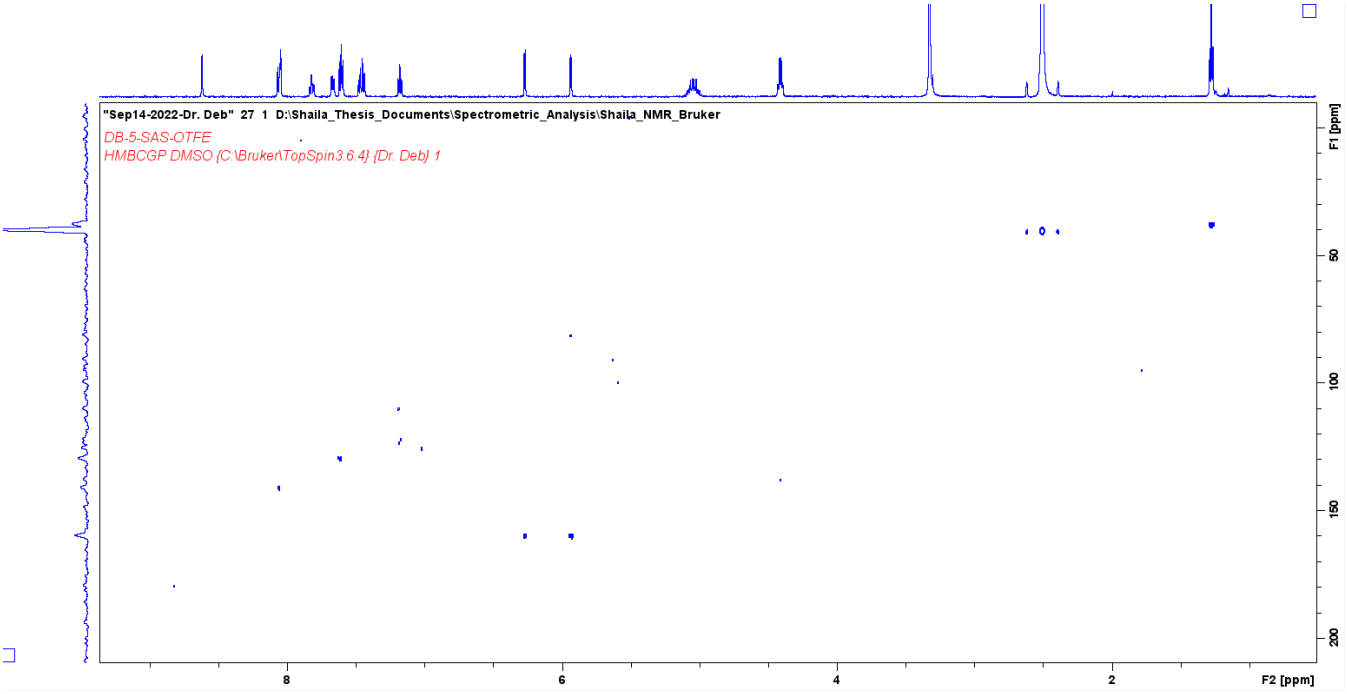


Figure 3.36: $^{1}H$-$^{13}C$ Correlation (HMBCGP) NMR of DB-5-SAS-OTFE (3)

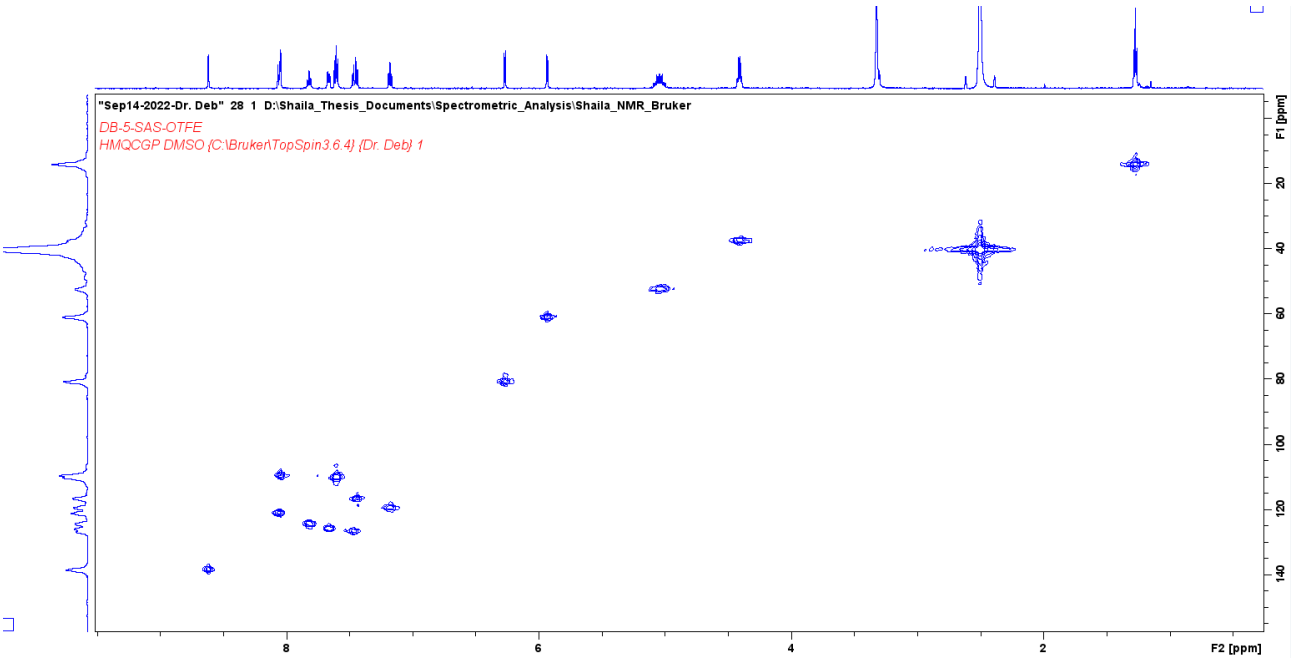


Figure 3.37: $^{1}H$-$^{13}C$ Correlation (HMQCGP) NMR of DB-5-SAS-OTFE (3)

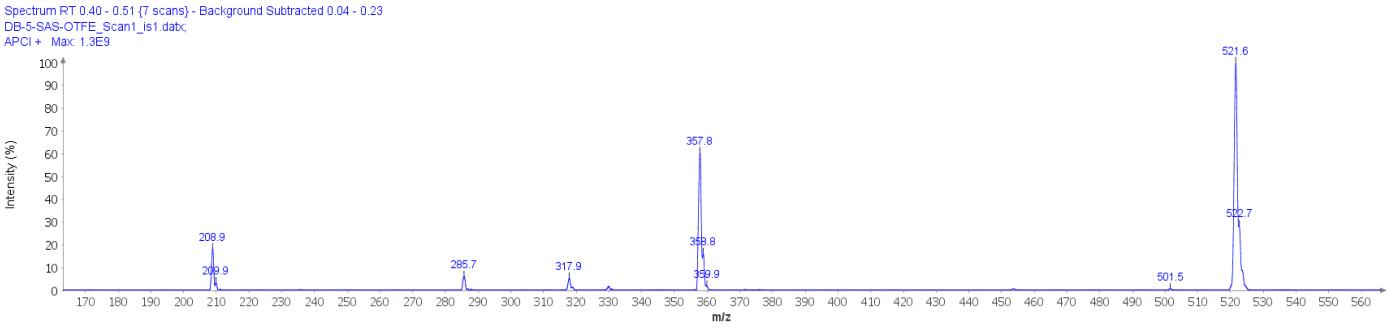


Figure 3.38: Mass spectrometry of DB-5-SAS-OTFE (3)

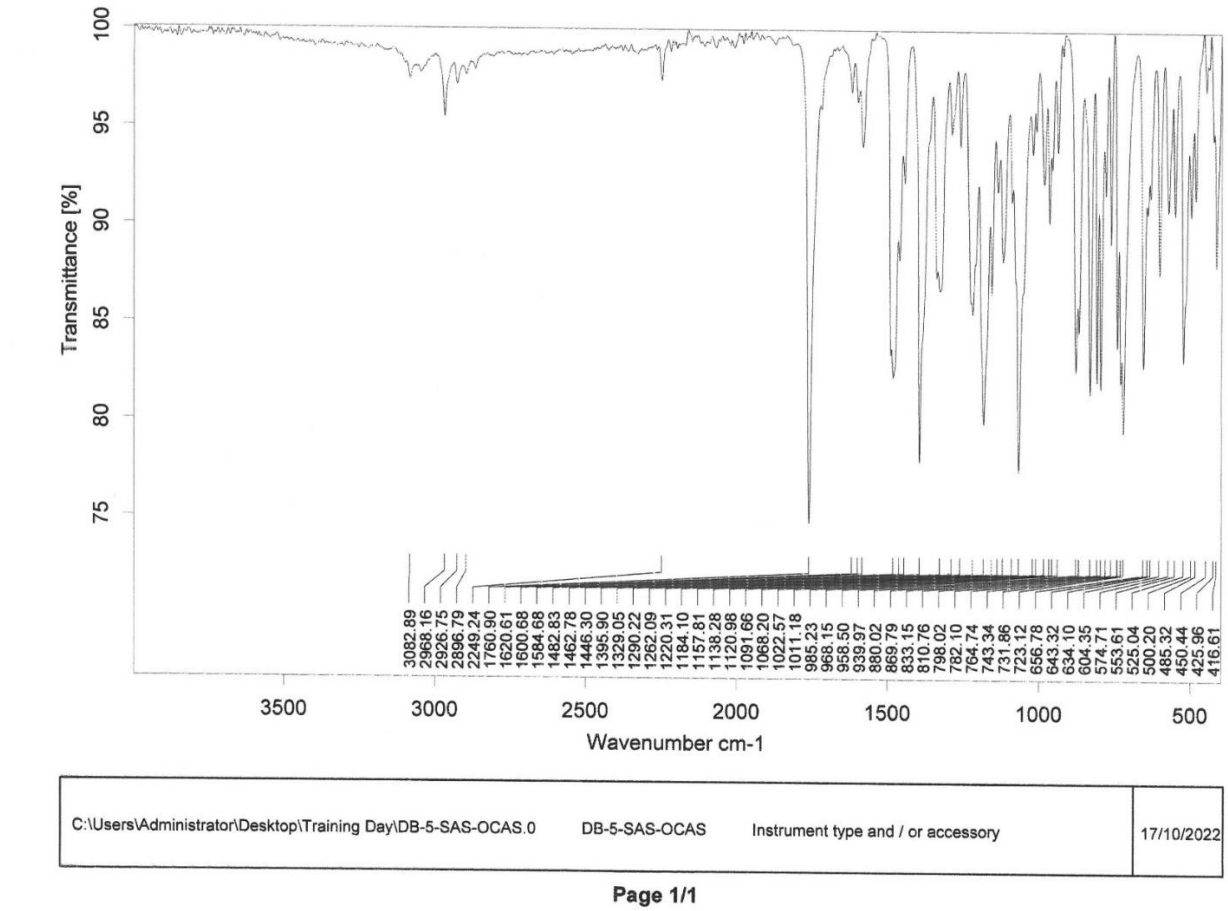


Figure 3.39: FTIR of DB-5-SAS-OCAS (4)

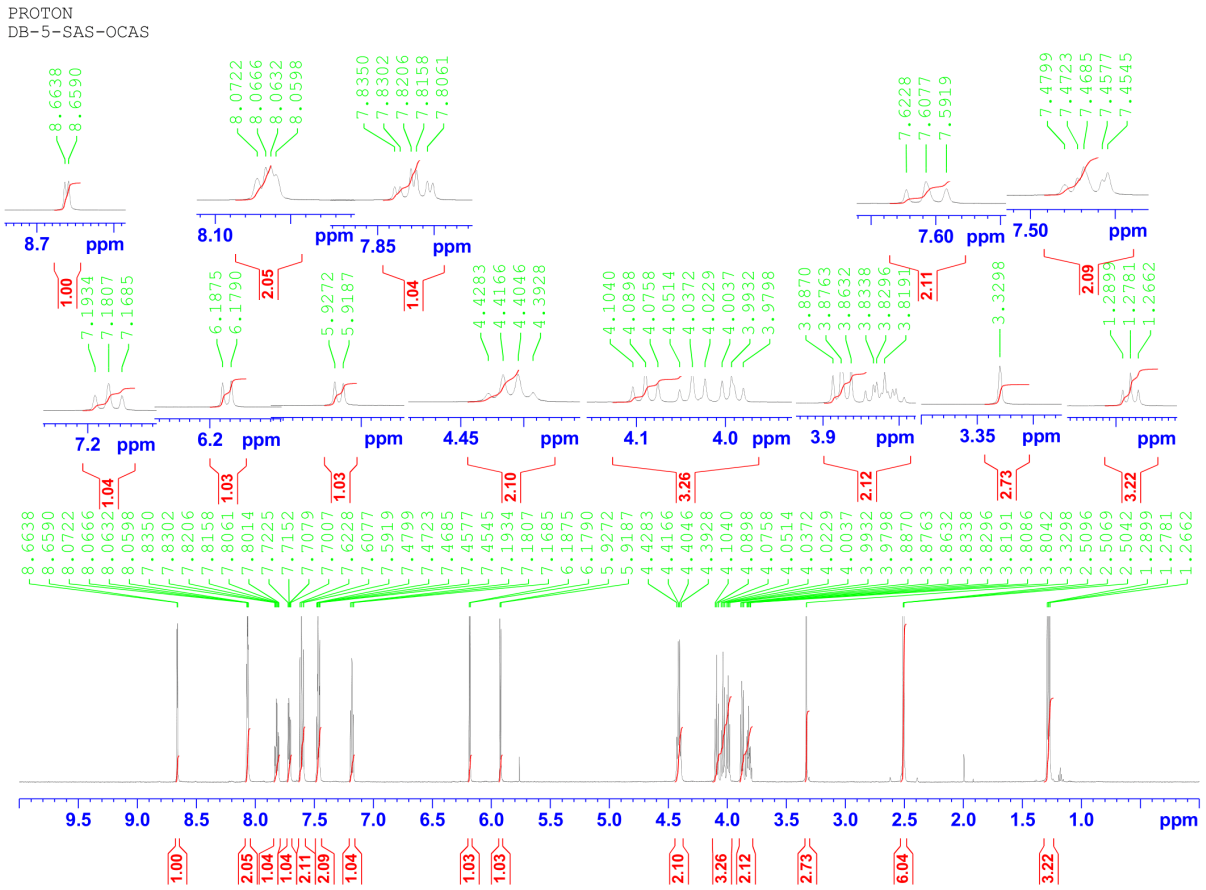


Figure. 3.40: Proton NMR of DB-5-SAS-OCAS (4)

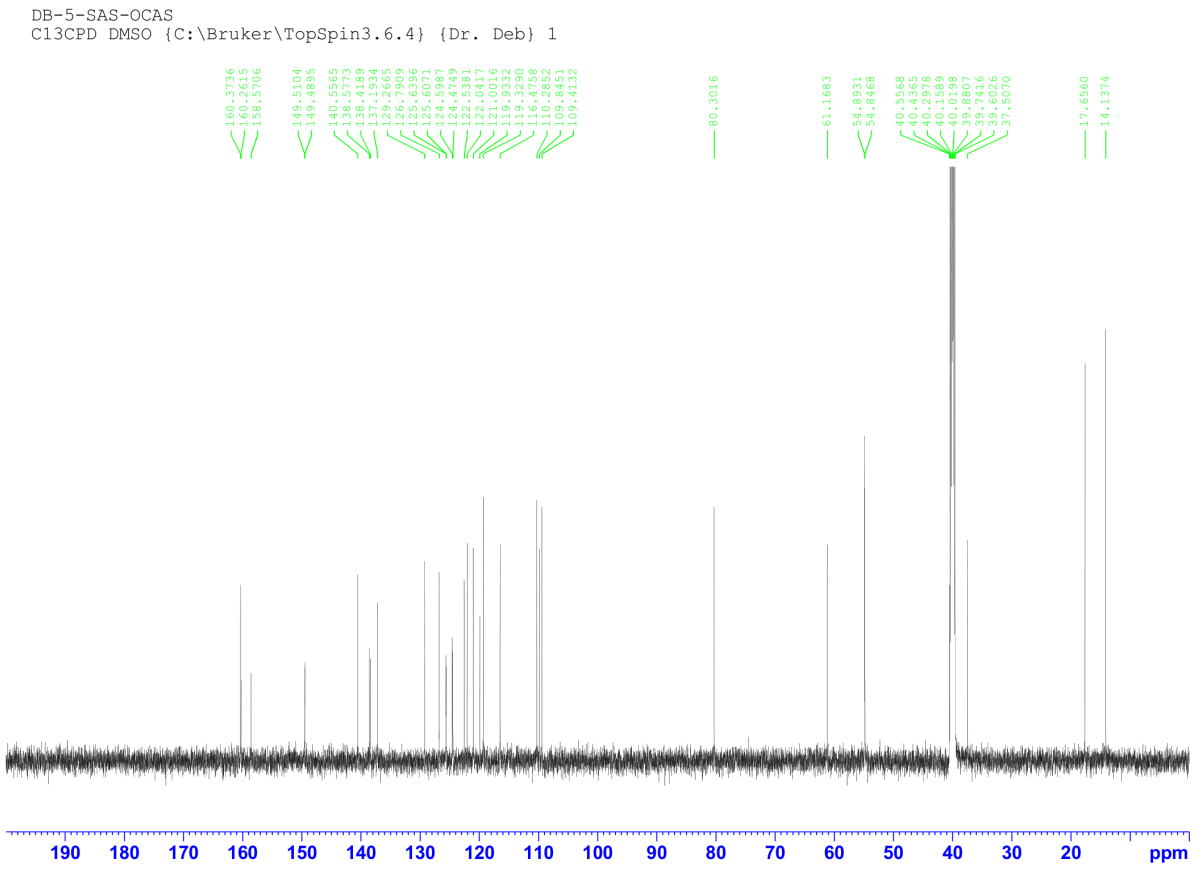


Figure 3.41: $^{13}$C NMR of DB-5-SAS-OCAS (4)

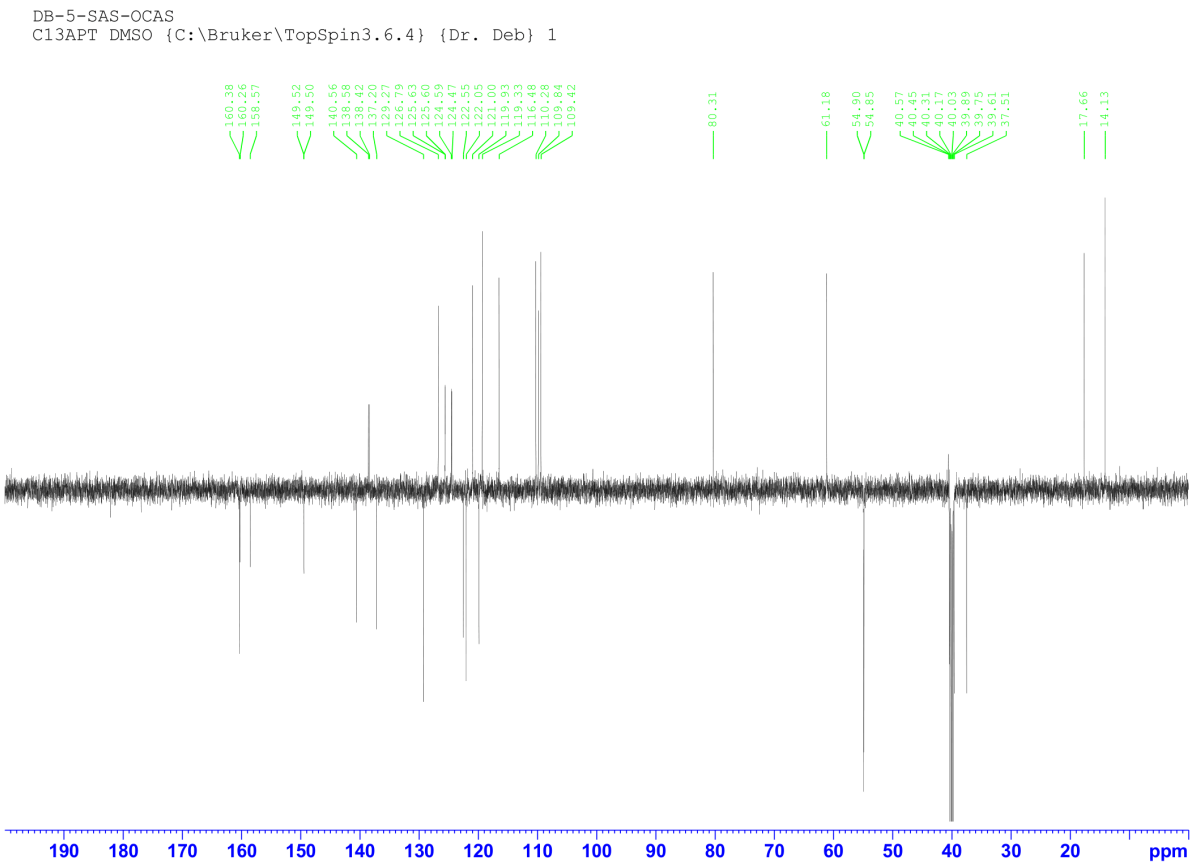


Figure 3.42: $^{13}$C APT NMR of DB-5-SAS-OCAS (4)

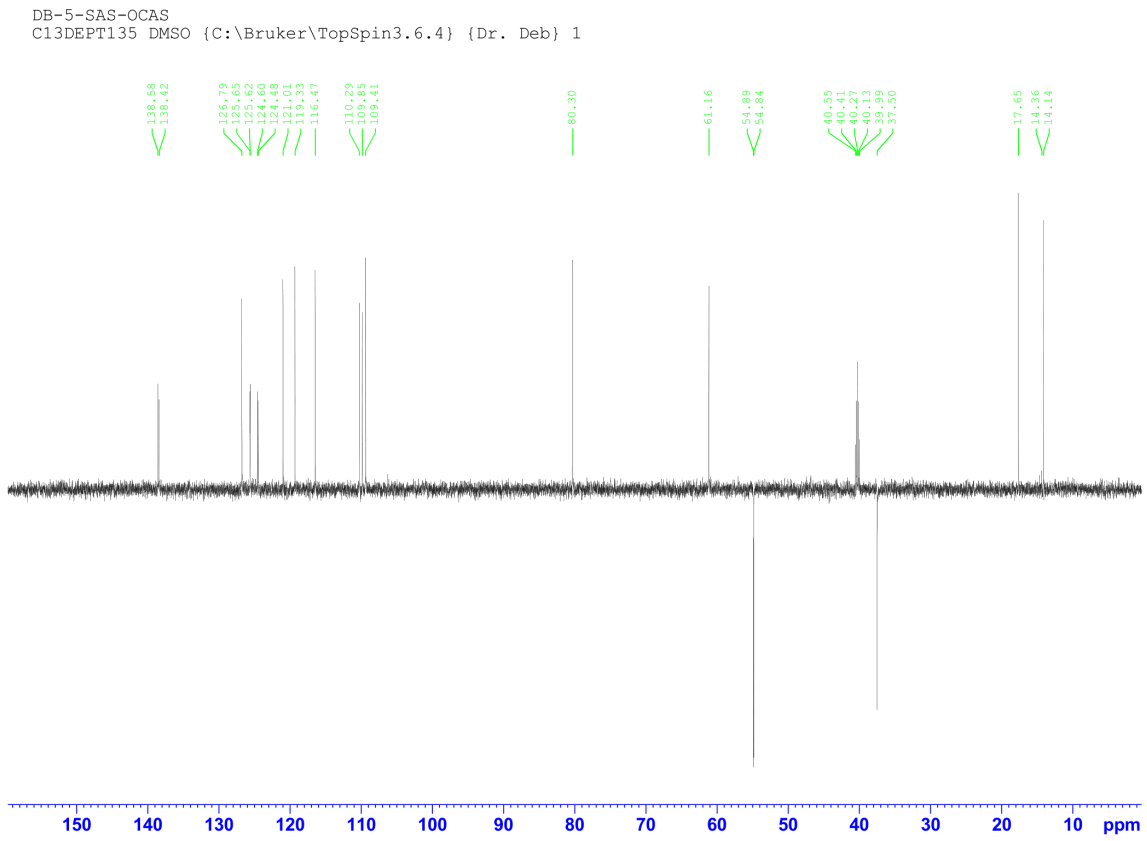


Figure 3.43: $^{13}$C DEPT of DB-5-SAS-OCAS (4) (DFPT 135)

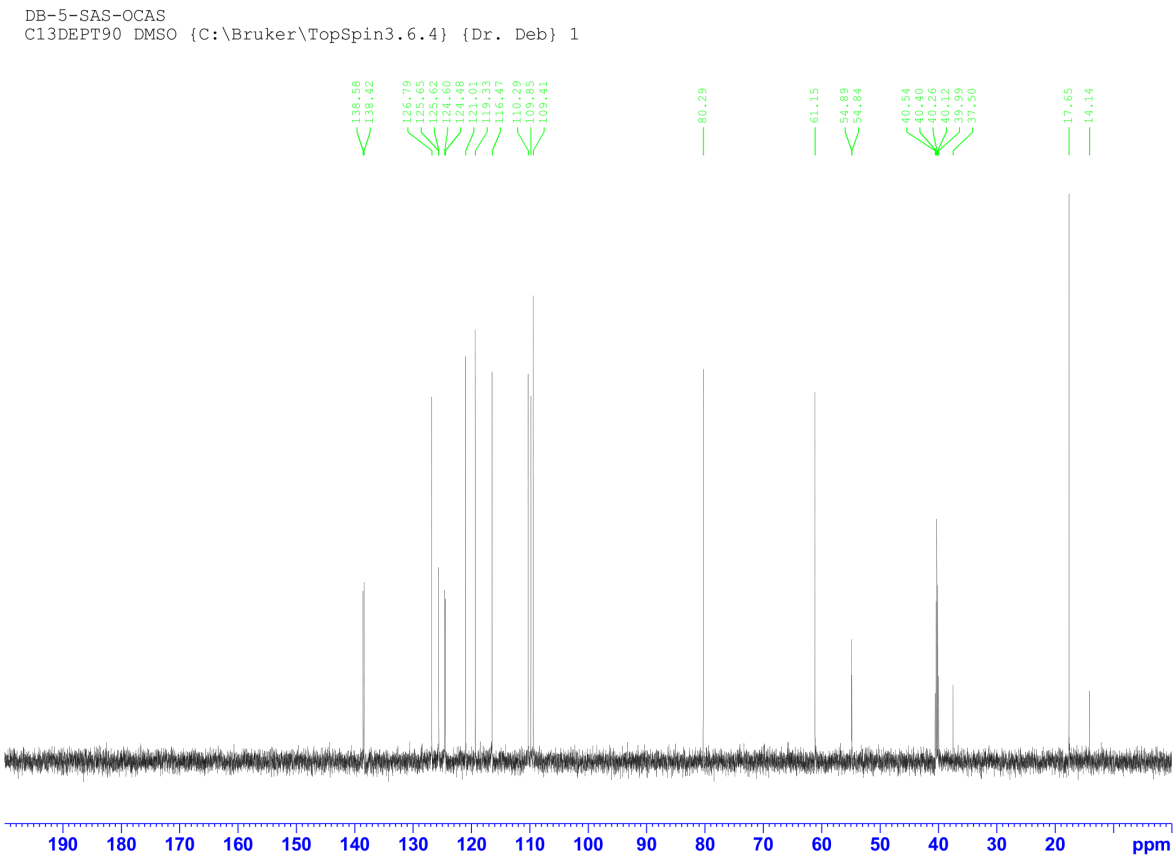


Figure 3.44: $^{13}C$ NMR of DB-5-SAS-OCAS (4) (DEPT 90°)

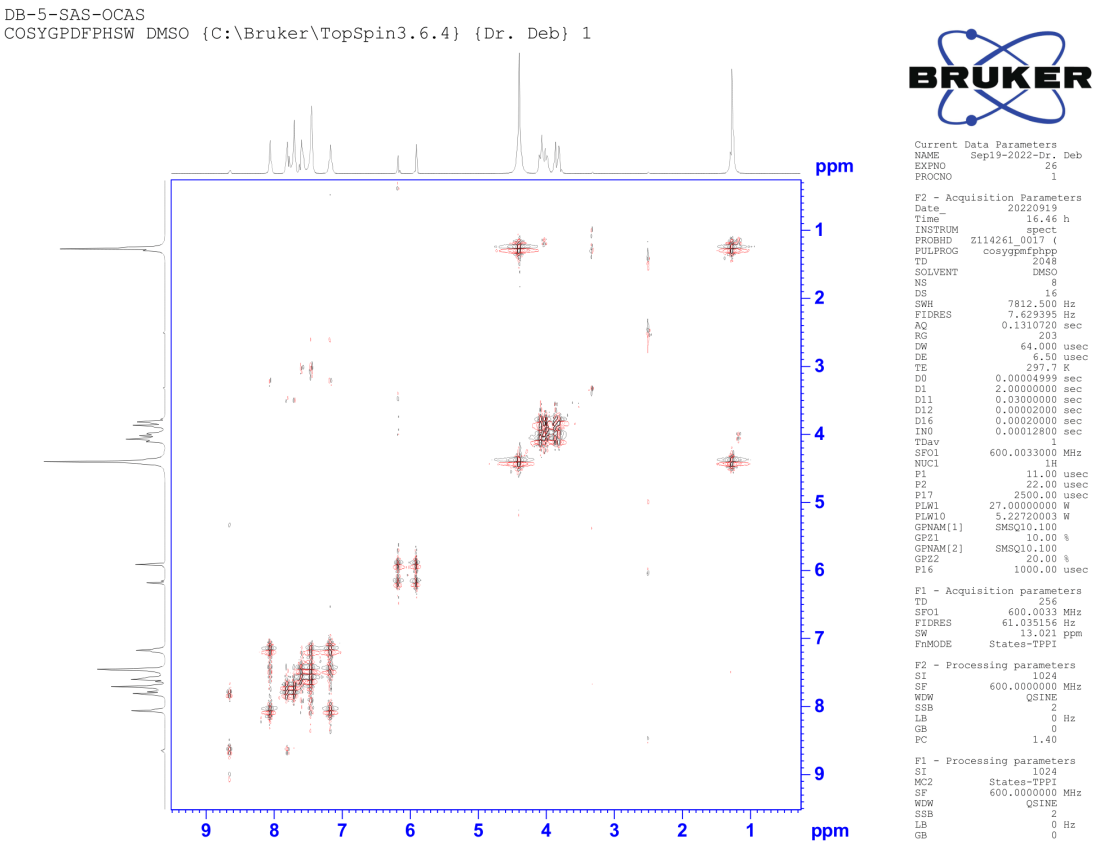


Figure 3.45: $^{1}H$-$^{1}H$ Correlation (COSY) of DB-5-SAS-OCAS (4)

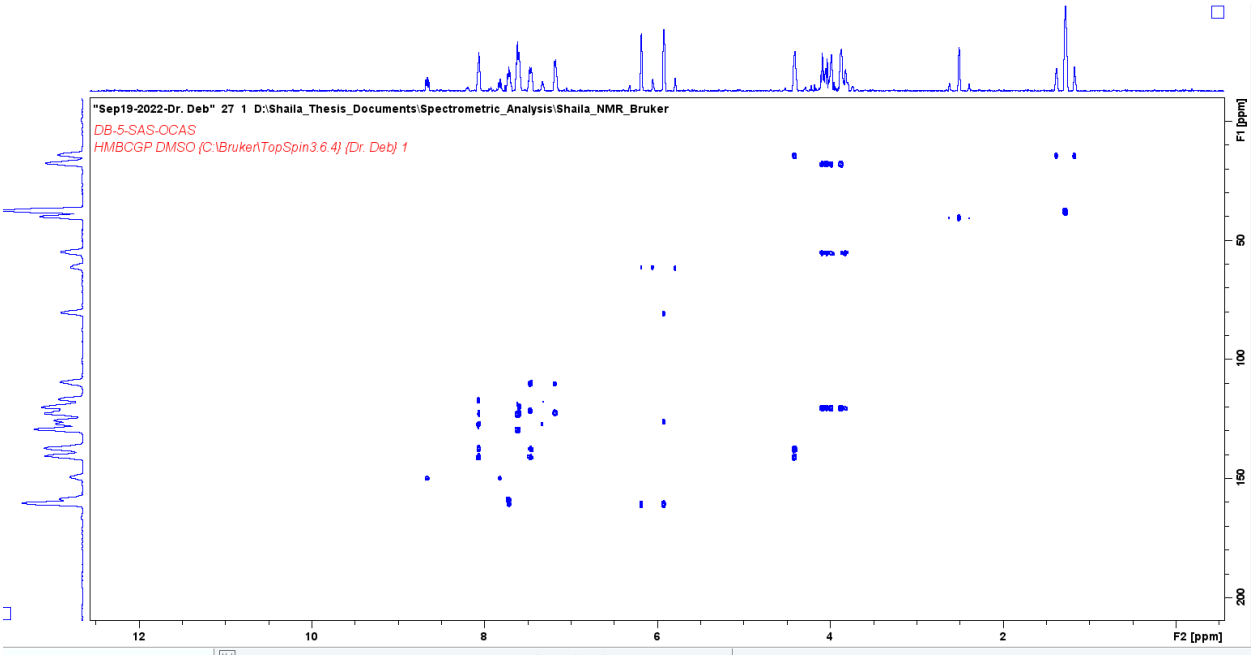


Figure 3.46: $^{1}H$-$^{13}C$ Correlation (HMBCGP) NMR of DB-5-SAS-OCAS (4)

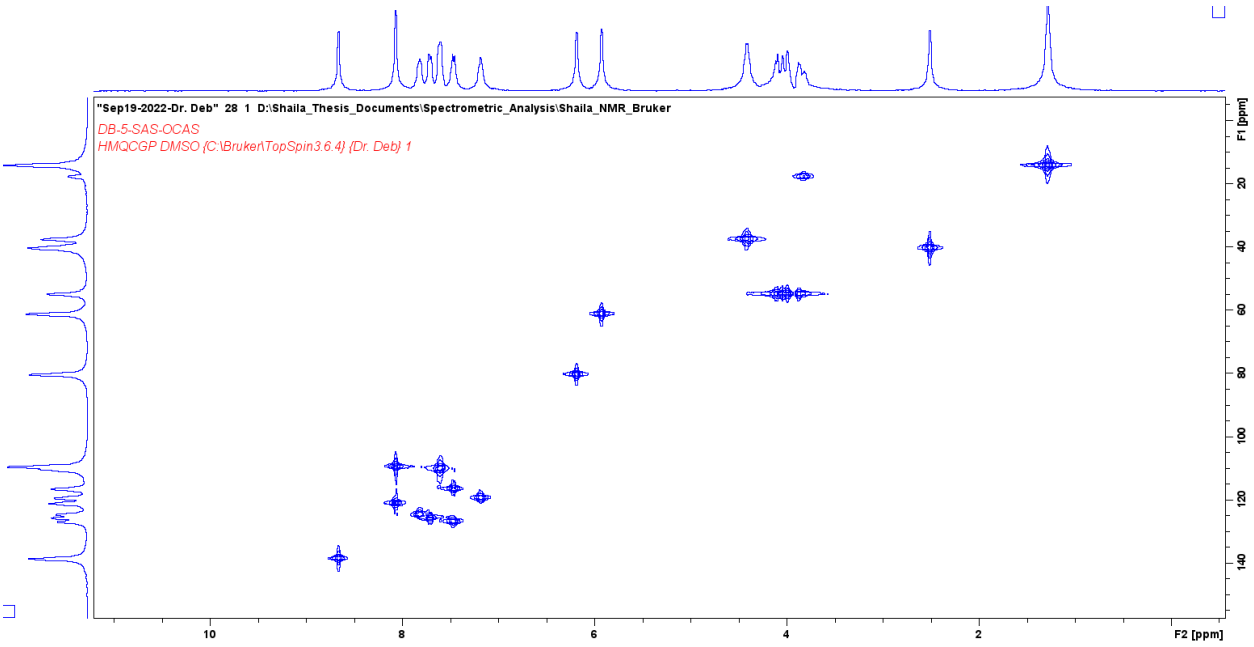


Figure 3.47: $^{1}H$-$^{13}C$ Correlation (HMQCGP) NMR of DB-5-SAS-OCAS (4)

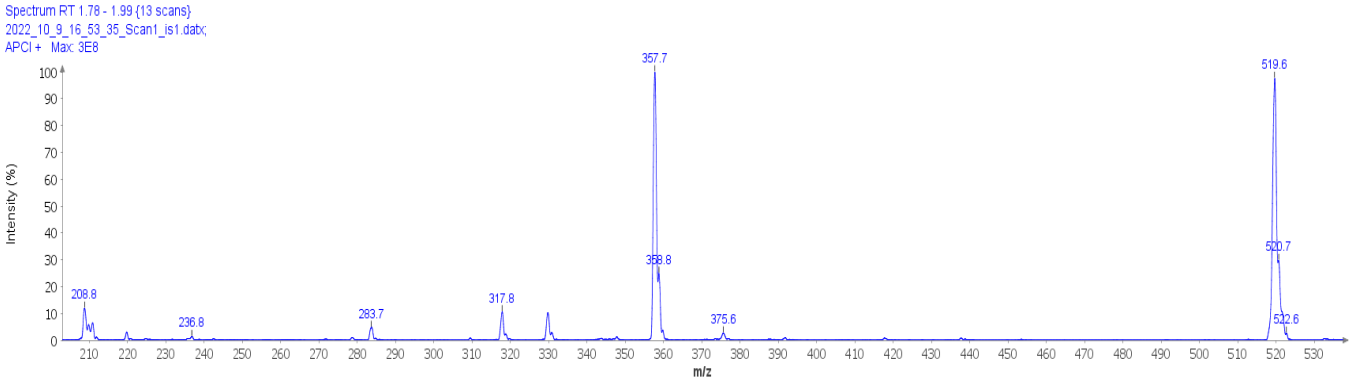


Figure 3.48: Mass spectrometry of DB-5-SAS-OCAS (4)

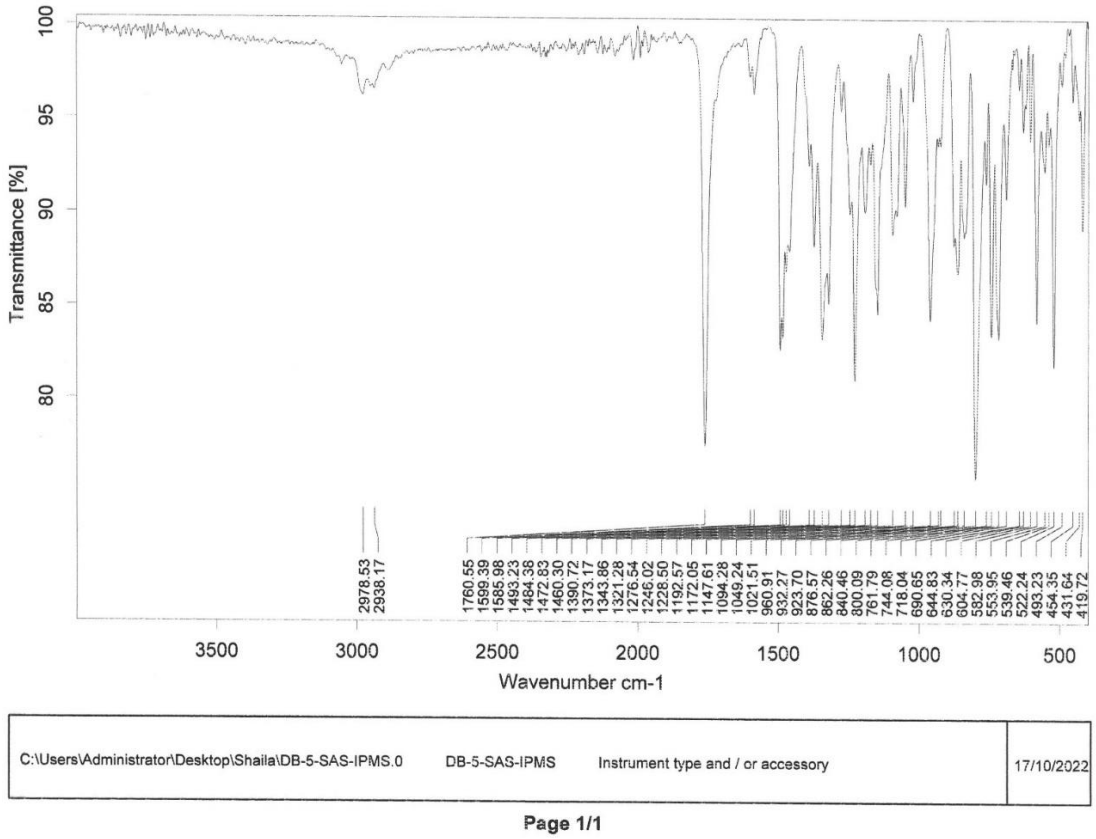


Figure 3.49: FTIR of DB-5-SAS-IPMS (5).

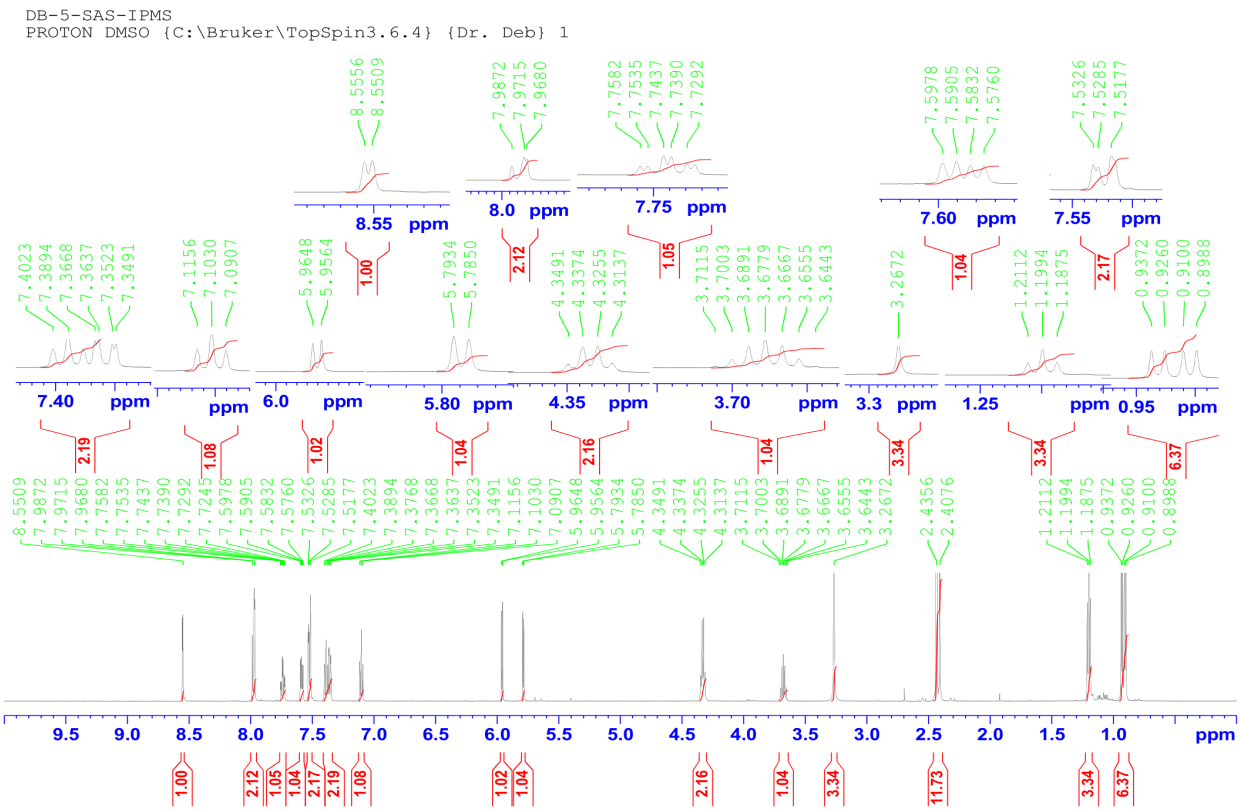


Figure 3.50: Proton NMR of DB-5-SAS-IPMS (5)

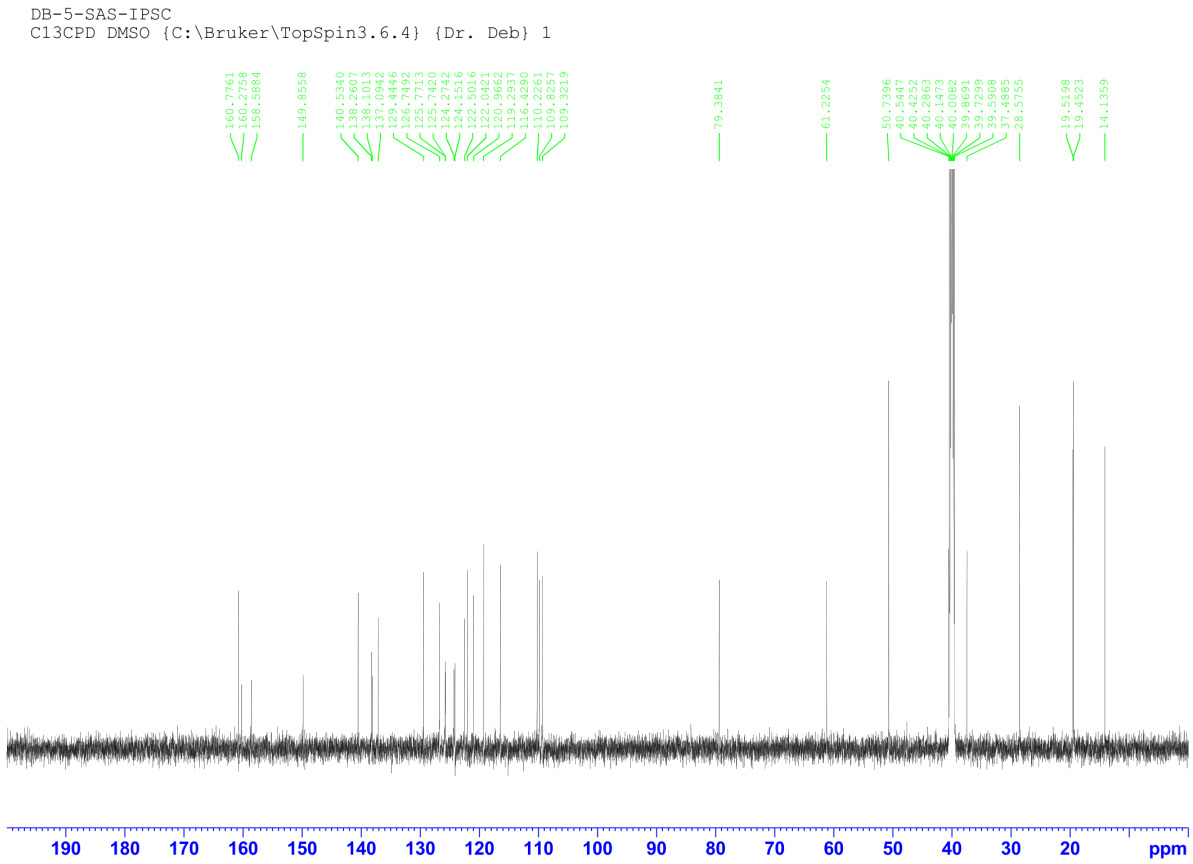


Figure 3.51: $^{13}$C NMR of DB-5-SAS-IPMS (5)

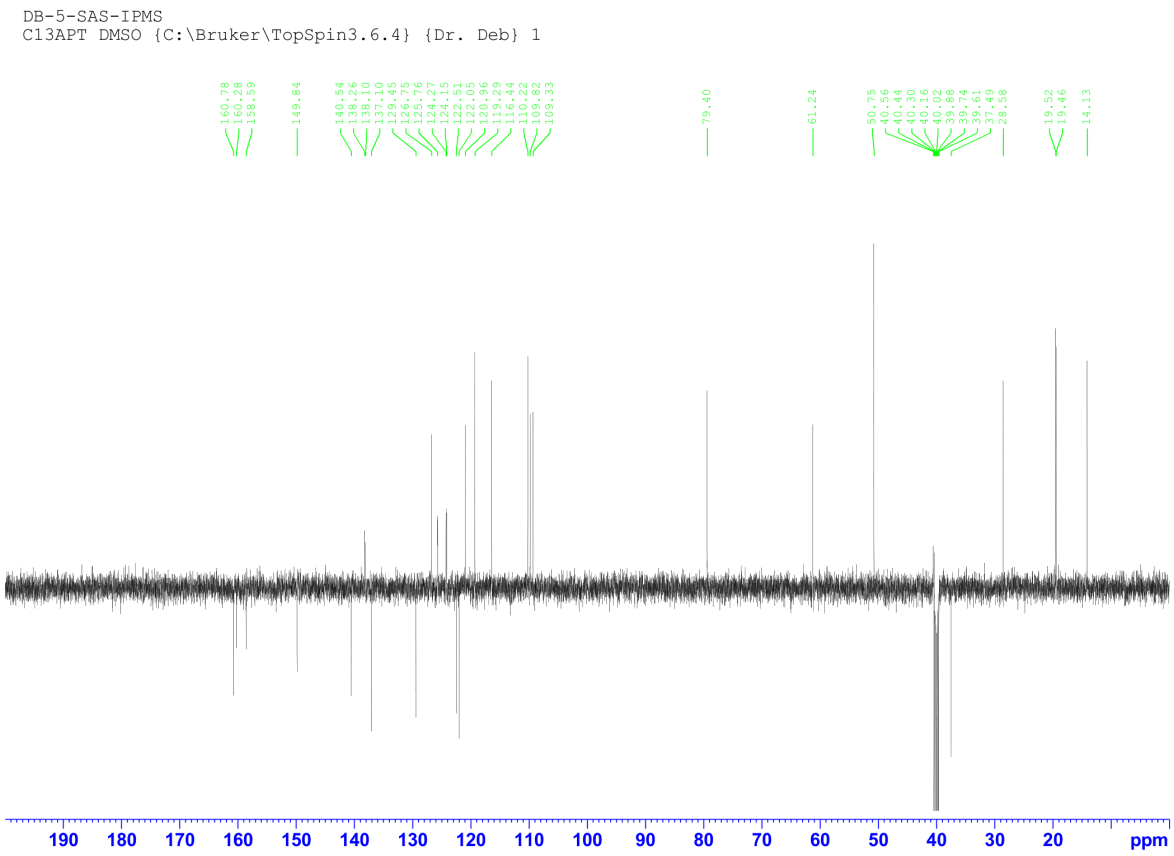


Figure 3.52: $^{13}$C APT NMR of DB-5-SAS-IPMS (5)

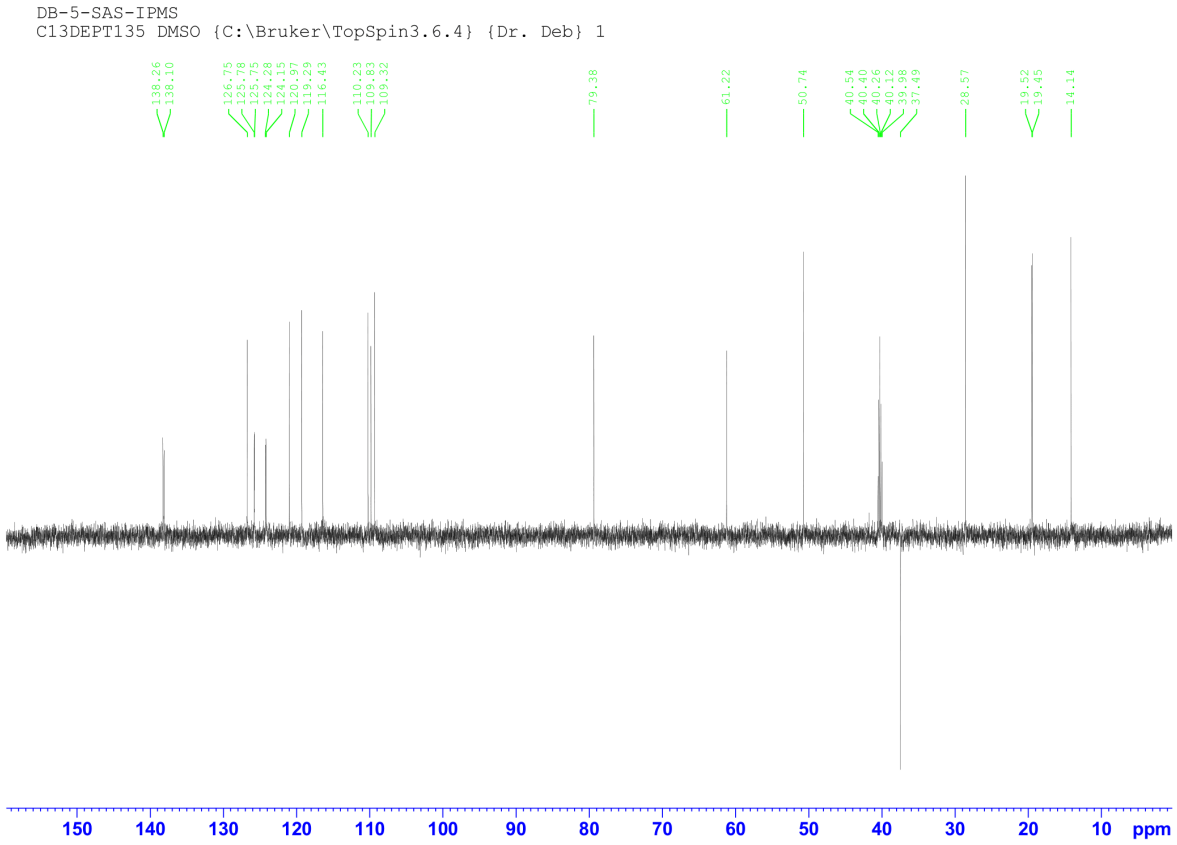


Figure 3.53: $^{13}$C NMR of DB-5-SAS-IPMS (5) (DFPT 135°)

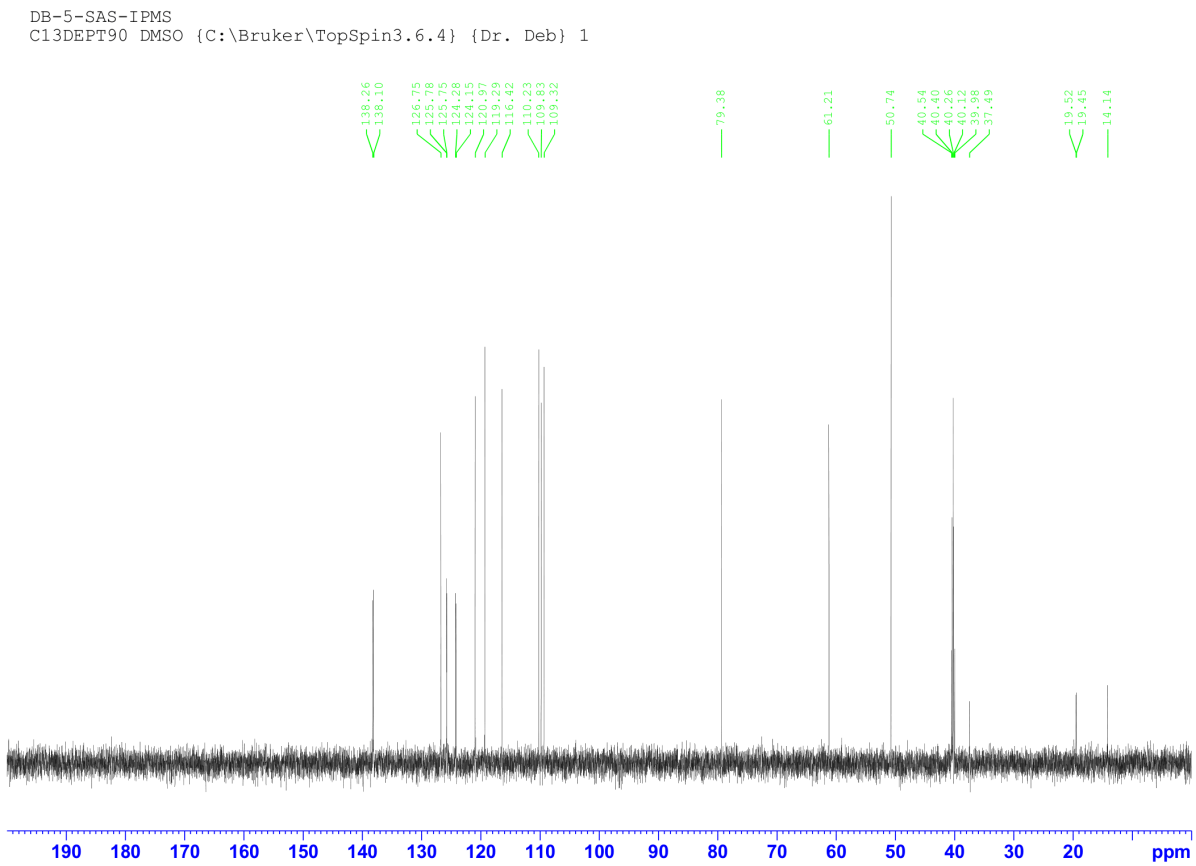


Figure 3.54: C13 NMR of DB-5-SAS-IPMS (5) (DFPT 90°)

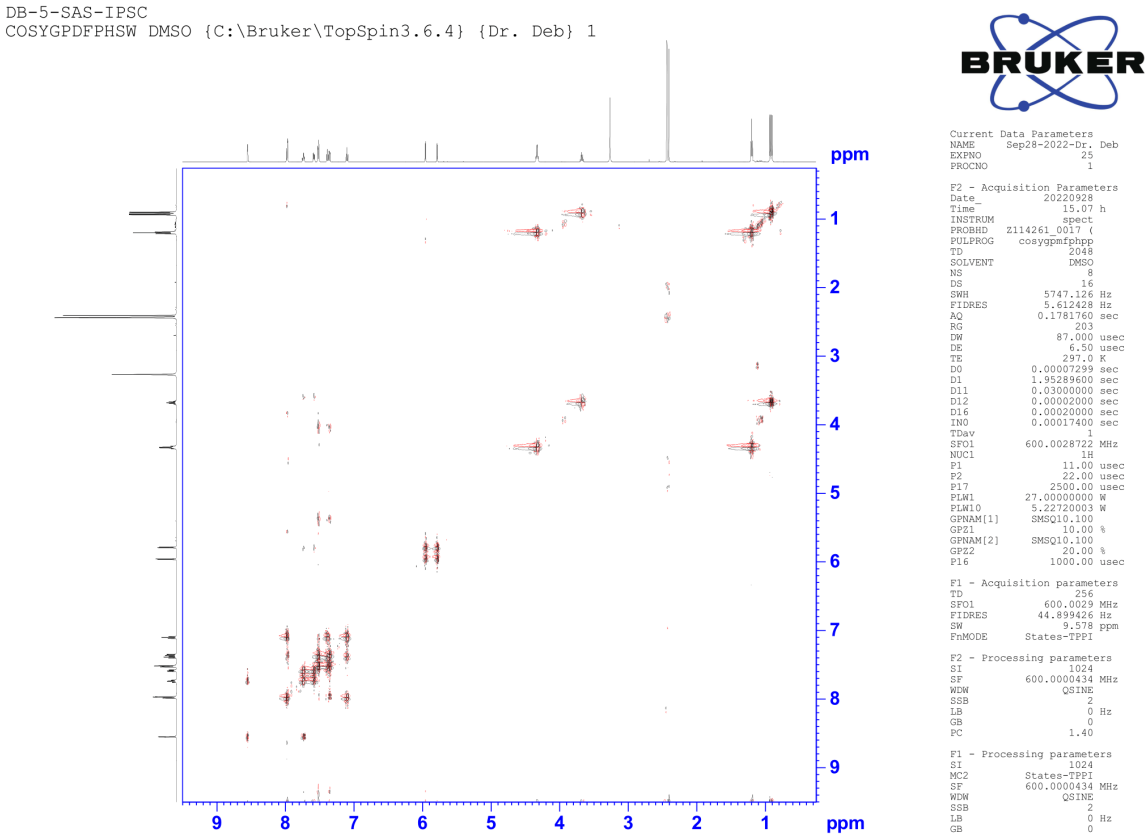


Figure 3.55: $^{1}$H-$^{1}$H Correlation (COSY) of DB-5-SAS-IPMS (5)

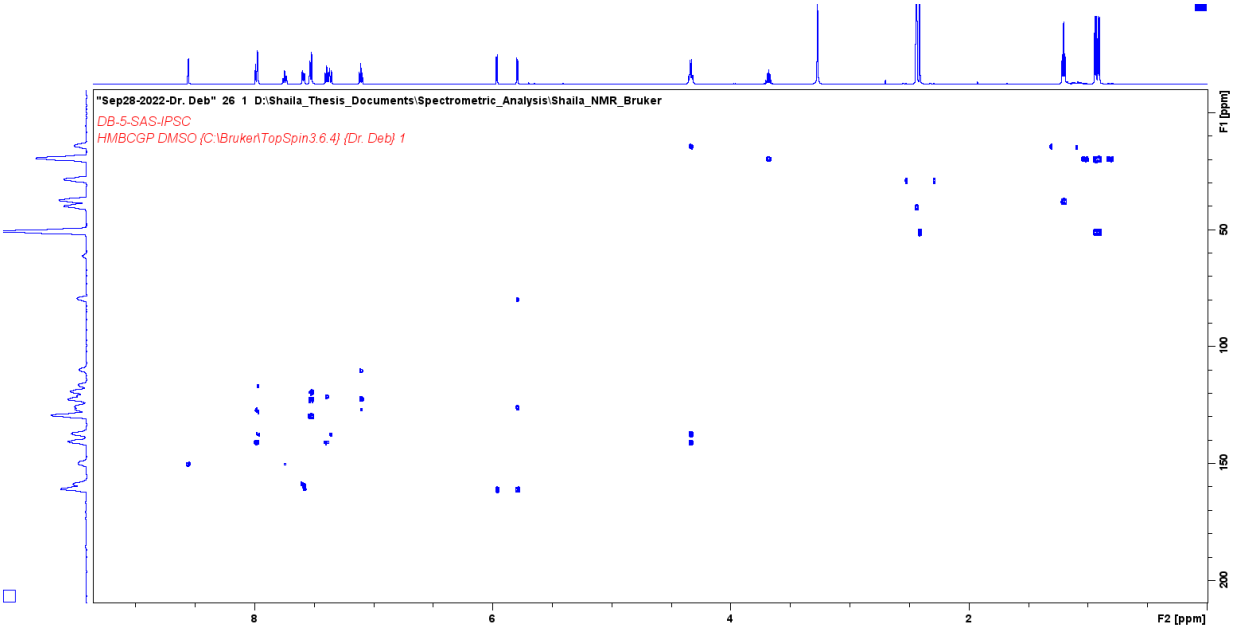


Figure 3.56: $^{1}H$-$^{13}C$ Correlation (HMBCGP) NMR of DB-5-SAS-IPMS (5)

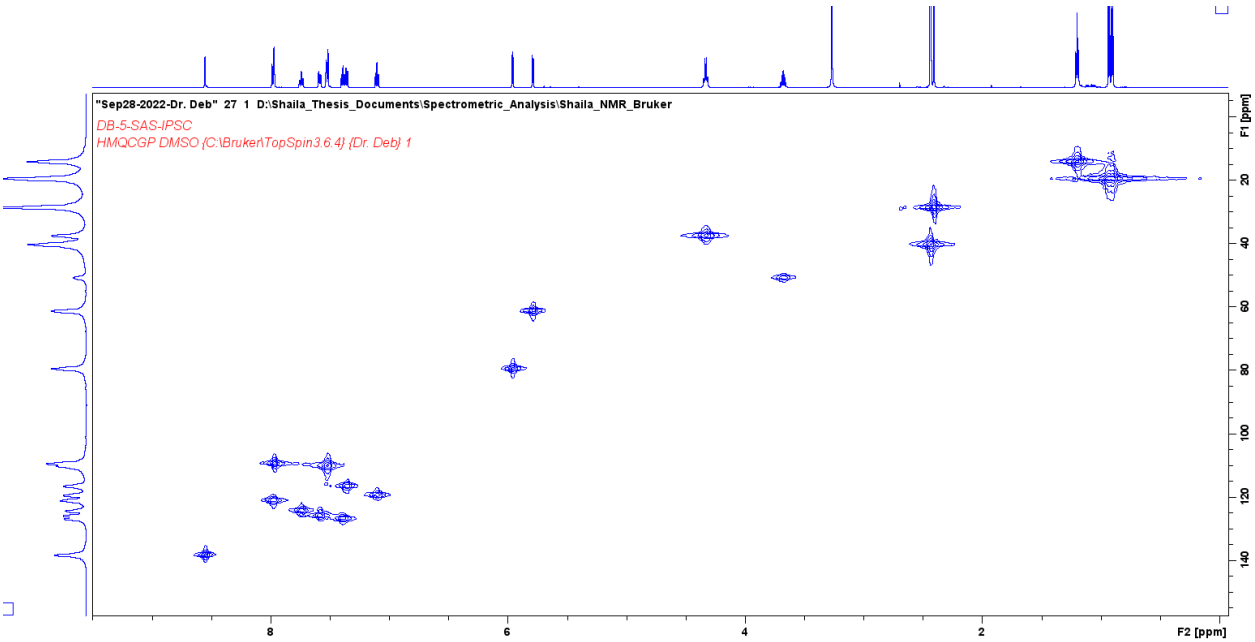


Figure 3.57: $^{1}H$-$^{13}C$ Correlation (HMQCGP) NMR of DB-5-SAS-IPMS (5)

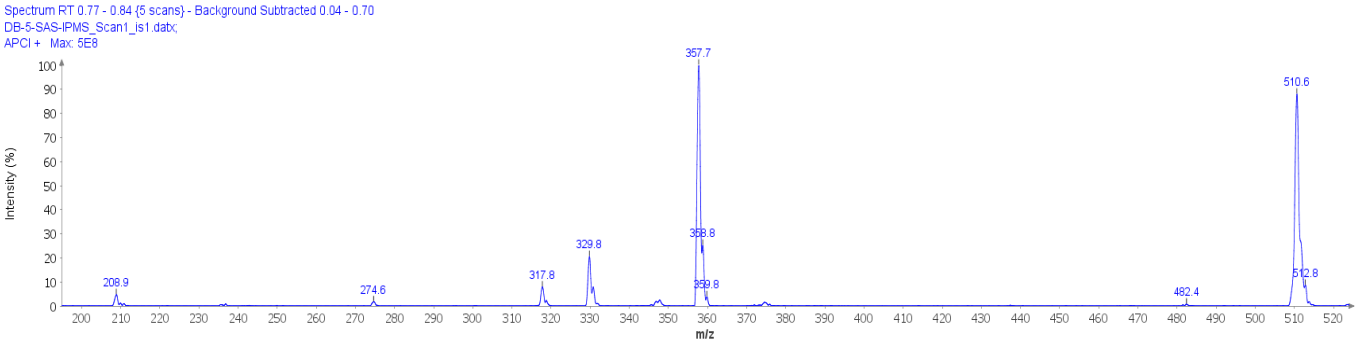


Figure 3.58: Mass spectrometry of DB-5-SAS-IPMS (5)

# CHAPTER IV

# CONCLUSION

It is obvious that our newly developed method satisfies several aspects of green chemistry, because we used greenest solvent water in our reactions and extracted with a recommended green solvent ethyl acetate and we also used ultra sound sonication that is a green energy source.

After analyzing all the result, we can say benzopyrazine **1** may find its application in the future drug development process against two major neglected tropical diseases: Chagas' disease and leishmaniasis.

The ever-increasing number of deaths caused by cancer is the alert that this field requires more attention from the researchers to the government in general. Though many chemotherapeutic drugs prevail in the market, most of them are incapable of selectively targeting the cancer cells. Beta-lactam is a promising candidate in this regard. It has proven antibacterial properties along with other biological effects. These characteristics drive the synthesis of a more potent and selective chemotherapeutic agent from beta-lactams.

## Future aspects

In future We want to do the chemical modification of our compounds (in particular benzopyrazine 1) (, so that it can target more binding sites. We also want to modify one or more functional groups to the existing molecule so that the new molecule can bind the target protein(s) more effectively than the currently available commercial drugs. Finally, our aim is to develop new drug(s) with higher potency and reduced side effects (toxicity) using this greener pathway and molecular docking studies.

From careful literature review it is found that carbazole compounds have potential anticancer effects. The next step is to do In vitro and in vivo study of carbazole compounds (1-5) on different cancer cells to identify anticancer effects. In silico molecular docking stud and in silico study to find the conformation and orientation (pose) of the compound (1-5) into the binding site of the target proteins.

REFERENCES


Achutha, L., Parameshwar, R., Reddy, B. M., & Babu, V. H. (2013). Microwave-Assisted Synthesis of Some Quinoxaline-Incorporated Schiff Bases and Their Biological Evaluation. *Journal of Chemistry*, *2013*, 578438. https://doi.org/10.1155/2013/578438

Are, C., Chowdhury, S., Ahmad, H., Ravipati, A., Song, T., Shrikandhe, S., & Smith, L. (2016). Predictive global trends in the incidence and mortality of pancreatic cancer based on geographic location, socio-economic status, and demographic shift. *J Surg Oncol*, *114*(6), 736-742. https://doi.org/10.1002/jso.24410

Awasthi, N., Zhang, C., Ruan, W., Schwarz, M. A., & Schwarz, R. E. (2012). BMS-754807, a small-molecule inhibitor of insulin-like growth factor-1 receptor/insulin receptor, enhances gemcitabine response in pancreatic cancer. *Mol Cancer Ther*, *11*(12), 2644-2653. https://doi.org/10.1158/1535-7163.Mct-12-0447

Bandyopadhyay, D., & Banik, B. K. (2021). Chapter 3 - Microwave-assisted synthesis of medicinally privileged heterocycles. In G. Brahmachari (Ed.), *Green Synthetic Approaches for Biologically Relevant Heterocycles (Second Edition)* (pp. 49-110). Elsevier. https://doi.org/https://doi.org/10.1016/B978-0-12-820586-0.00009-1

Bandyopadhyay, D., Cruz, J., Morales, L. D., Arman, H. D., Cuate, E., Lee, Y. S., Banik, B. K., & Kim, D. J. (2013). A green approach toward quinoxalines and bis-quinoxalines and their biological evaluation against A431, human skin cancer cell lines. *Future Med Chem*, *5*(12), 1377-1390. https://doi.org/10.4155/fmc.13.101

Bryant, K. L., Mancias, J. D., Kimmelman, A. C., & Der, C. J. (2014). KRAS: feeding pancreatic cancer proliferation. *Trends Biochem Sci*, *39*(2), 91-100. https://doi.org/10.1016/j.tibs.2013.12.004

Büchler, P., Reber, H. A., Roth, M. M., Shiroishi, M., Friess, H., & Hines, O. J. (2007). Target therapy using a small molecule inhibitor against angiogenic receptors in pancreatic cancer. *Neoplasia*, *9*(2), 119-127. https://doi.org/10.1593/neo.06616

Canon, J., Rex, K., Saiki, A. Y., Mohr, C., Cooke, K., Bagal, D., Gaida, K., Holt, T., Knutson, C. G., Koppada, N., Lanman, B. A., Werner, J., Rapaport, A. S., San Miguel, T., Ortiz, R., Osgood, T., Sun, J. R., Zhu, X., McCarter, J. D., . . . Lipford, J. R. (2019). The clinical KRAS(G12C) inhibitor AMG 510 drives anti-tumour immunity. *Nature*, *575*(7781), 217-223. https://doi.org/10.1038/s41586-019-1694-1

Carboni, J. M., Wittman, M., Yang, Z., Lee, F., Greer, A., Hurlburt, W., Hillerman, S., Cao, C., Cantor, G. H., Dell-John, J., Chen, C., Discenza, L., Menard, K., Li, A., Trainor, G., Vyas, D., Kramer, R., Attar, R. M., & Gottardis, M. M. (2009). BMS-754807, a small molecule inhibitor of insulin-like growth factor-1R/IR. *Mol Cancer Ther*, *8*(12), 3341-3349. https://doi.org/10.1158/1535-7163.Mct-09-0499

Carta, A., Sanna, P., Gherardini, L., Usai, D., & Zanetti, S. (2001). Novel functionalized pyrido[2,3-g]quinoxalinones as antibacterial, antifungal and anticancer agents. *Farmaco*, *56*(12), 933-938. https://doi.org/10.1016/s0014-827x(01)01161-2

Cox, A. D., Fesik, S. W., Kimmelman, A. C., Luo, J., & Der, C. J. (2014). Drugging the undruggable RAS: Mission possible? *Nat Rev Drug Discov*, *13*(11), 828-851. https://doi.org/10.1038/nrd4389

El-Attar, M. A. Z., Elbayaa, R. Y., Shaaban, O. G., Habib, N. S., Abdel Wahab, A. E., Abdelwahab, I. A., & El-Hawash, S. A. M. (2018). Design, synthesis, antibacterial evaluation and molecular docking studies of some new quinoxaline derivatives targeting dihyropteroate synthase enzyme. *Bioorg Chem*, *76*, 437-448. https://doi.org/10.1016/j.bioorg.2017.12.017

Evelyn, C. R., Duan, X., Biesiada, J., Seibel, W. L., Meller, J., & Zheng, Y. (2014). Rational design of small molecule inhibitors targeting the Ras GEF, SOS1. *Chem Biol*, *21*(12), 1618-1628. https://doi.org/10.1016/j.chembiol.2014.09.018

Ferro, R., & Falasca, M. (2014). Emerging role of the KRAS-PDK1 axis in pancreatic cancer. *World J Gastroenterol*, *20*(31), 10752-10757. https://doi.org/10.3748/wjg.v20.i31.10752

Garrido, C. M., Henkels, K. M., Rehl, K. M., Liang, H., Zhou, Y., Gutterman, J. U., & Cho, K. J. (2020). Avicin G is a potent sphingomyelinase inhibitor and blocks oncogenic K- and H-Ras signaling. *Sci Rep*, *10*(1), 9120. https://doi.org/10.1038/s41598-020-65882-5

Gbelcová, H., Rimpelová, S., Knejzlík, Z., Šáchová, J., Kolář, M., Strnad, H., Repiská, V., D'Acunto, W. C., Ruml, T., & Vítek, L. (2017). Isoprenoids responsible for protein prenylation modulate the biological effects of statins on pancreatic cancer cells. *Lipids in health and disease*, *16*(1), 250-250. https://doi.org/10.1186/s12944-017-0641-0

Geltz, N. R., & Augustine, J. A. (1998). The p85 and p110 subunits of phosphatidylinositol 3-kinase-alpha are substrates, in vitro, for a constitutively associated protein tyrosine kinase in platelets. *Blood*, *91*(3), 930-939.

Golan, T., Kanji, Z. S., Epelbaum, R., Devaud, N., Dagan, E., Holter, S., Aderka, D., Paluch-Shimon, S., Kaufman, B., Gershoni-Baruch, R., Hedley, D., Moore, M. J., Friedman, E., & Gallinger, S. (2014). Overall survival and clinical characteristics of pancreatic cancer in BRCA mutation carriers. *British journal of cancer*, *111*(6), 1132-1138. https://doi.org/10.1038/bjc.2014.418

Gonçalves, A., Gilabert, M., François, E., Dahan, L., Perrier, H., Lamy, R., Re, D., Largillier, R., Gasmi, M., Tchiknavorian, X., Esterni, B., Genre, D., Moureau-Zabotto, L., Giovannini, M., Seitz, J. F., Delpero, J. R., Turrini, O., Viens, P., & Raoul, J. L. (2012). BAYPAN study: a double-blind phase III randomized trial comparing gemcitabine plus sorafenib and gemcitabine plus placebo in patients with advanced pancreatic cancer. *Ann Oncol*, *23*(11), 2799-2805. https://doi.org/10.1093/annonc/mds135

Gysin, S., Salt, M., Young, A., & McCormick, F. (2011). Therapeutic strategies for targeting ras proteins. *Genes Cancer*, *2*(3), 359-372. https://doi.org/10.1177/1947601911412376

Hakam, A., Fang, Q., Karl, R., & Coppola, D. (2003). Coexpression of IGF-1R and c-Src proteins in human pancreatic ductal adenocarcinoma. *Dig Dis Sci*, *48*(10), 1972-1978. https://doi.org/10.1023/a:1026122421369

Hallin, J., Engstrom, L. D., Hargis, L., Calinisan, A., Aranda, R., Briere, D. M., Sudhakar, N., Bowcut, V., Baer, B. R., Ballard, J. A., Burkard, M. R., Fell, J. B., Fischer, J. P., Vigers, G. P., Xue, Y., Gatto, S., Fernandez-Banet, J., Pavlicek, A., Velastagui, K., . . . Christensen, J. G. (2020). The KRAS(G12C) Inhibitor MRTX849 Provides Insight toward Therapeutic Susceptibility of KRAS-Mutant Cancers in Mouse Models and Patients. *Cancer Discov*, *10*(1), 54-71. https://doi.org/10.1158/2159-8290.Cd-19-1167

Hidalgo, M. (2010). Pancreatic cancer. *N Engl J Med*, *362*(17), 1605-1617. https://doi.org/10.1056/NEJMra0901557

Hruban, R. H., Goggins, M., Parsons, J., & Kern, S. E. (2000). Progression model for pancreatic cancer. *Clinical cancer research : an official journal of the American Association for Cancer Research*, *6*(8), 2969-2972.

Ioka, T., Okusaka, T., Ohkawa, S., Boku, N., Sawaki, A., Fujii, Y., Kamei, Y., Takahashi, S., Namazu, K., Umeyama, Y., Bycott, P., & Furuse, J. (2015). Efficacy and safety of axitinib in combination with gemcitabine in advanced pancreatic cancer: subgroup analyses by region, including Japan, from the global randomized Phase III trial. *Jpn J Clin Oncol*, *45*(5), 439-448. https://doi.org/10.1093/jjco/hyv011

Itakura, J., Ishiwata, T., Shen, B., Kornmann, M., & Korc, M. (2000). Concomitant over-expression of vascular endothelial growth factor and its receptors in pancreatic cancer. *Int J Cancer*, *85*(1), 27-34. https://doi.org/10.1002/(sici)1097-0215(20000101)85:1<27::aid-ijc5>3.0.co;2-8

Janes, M. R., Zhang, J., Li, L. S., Hansen, R., Peters, U., Guo, X., Chen, Y., Babbar, A., Firdaus, S. J., Darjania, L., Feng, J., Chen, J. H., Li, S., Li, S., Long, Y. O., Thach, C., Liu, Y., Zarieh, A., Ely, T., . . . Liu, Y. (2018). Targeting KRAS Mutant Cancers with a Covalent G12C-Specific Inhibitor. *Cell*, *172*(3), 578-589.e517. https://doi.org/10.1016/j.cell.2018.01.006

Jones, S., Zhang, X., Parsons, D. W., Lin, J. C., Leary, R. J., Angenendt, P., Mankoo, P., Carter, H., Kamiyama, H., Jimeno, A., Hong, S. M., Fu, B., Lin, M. T., Calhoun, E. S., Kamiyama, M., Walter, K., Nikolskaya, T., Nikolsky, Y., Hartigan, J., . . . Kinzler, K. W. (2008). Core signaling pathways in human pancreatic cancers revealed by global genomic analyses. *Science*, *321*(5897), 1801-1806. https://doi.org/10.1126/science.1164368

Kamerkar, S., LeBleu, V. S., Sugimoto, H., Yang, S., Ruivo, C. F., Melo, S. A., Lee, J. J., & Kalluri, R. (2017). Exosomes facilitate therapeutic targeting of oncogenic KRAS in pancreatic cancer. *Nature*, *546*(7659), 498-503. https://doi.org/10.1038/nature22341

Kaur, S., Kumar, S., Momi, N., Sasson, A. R., & Batra, S. K. (2013). Mucins in pancreatic cancer and its microenvironment. *Nat Rev Gastroenterol Hepatol*, *10*(10), 607-620. https://doi.org/10.1038/nrgastro.2013.120

Khan, S., Ansarullah, Kumar, D., Jaggi, M., & Chauhan, S. C. (2013). Targeting microRNAs in pancreatic cancer: microplayers in the big game. *Cancer Res*, *73*(22), 6541-6547. https://doi.org/10.1158/0008-5472.Can-13-1288

Kim, C.-K., Wang, D., Bokesch, H. R., Fuller, R. W., Smith, E., Henrich, C. J., Durrant, D. E., Morrison, D. K., Bewley, C. A., & Gustafson, K. R. (2020). Swinhopeptolides A and B: Cyclic Depsipeptides from the Sponge Theonella swinhoei That Inhibit Ras/Raf Interaction. *Journal of Natural Products*, *83*(4), 1288-1294. https://doi.org/10.1021/acs.jnatprod.0c00136

Kordelas, L., Rebmann, V., Ludwig, A. K., Radtke, S., Ruesing, J., Doeppner, T. R., Epple, M., Horn, P. A., Beelen, D. W., & Giebel, B. (2014). MSC-derived exosomes: a novel tool to treat therapy-refractory graft-versus-host disease. *Leukemia*, *28*(4), 970-973. https://doi.org/10.1038/leu.2014.41

Kumar, S., & Agnihotri, N. (2019). Piperlongumine, a piper alkaloid targets Ras/PI3K/Akt/mTOR signaling axis to inhibit tumor cell growth and proliferation in DMH/DSS induced experimental colon cancer. *Biomed Pharmacother*, *109*, 1462-1477. https://doi.org/10.1016/j.biopha.2018.10.182

Kumar, V. B., Yuan, T. C., Liou, J. W., Yang, C. J., Sung, P. J., & Weng, C. F. (2011). Antroquinonol inhibits NSCLC proliferation by altering PI3K/mTOR proteins and miRNA expression profiles. *Mutat Res*, *707*(1-2), 42-52. https://doi.org/10.1016/j.mrfmmm.2010.12.009

Kumaresan, M., Saravanan, V., Sami, P., & Swaminathan, M. (2020). A green solid acid catalyst 12-tungstophosphoric acid H3[PW12O40] supported on g-C3N4 for synthesis of quinoxalines. *Research on Chemical Intermediates*, *46*(9), 4193-4209. https://doi.org/10.1007/s11164-020-04200-0

Lanfredini, S., Thapa, A., & O'Neill, E. (2019). RAS in pancreatic cancer. *Biochem Soc Trans*, *47*(4), 961-972. https://doi.org/10.1042/bst20170521

Lee, S. H., Lee, M.-Y., Kang, H.-M., Han, D. C., Son, K.-H., Yang, D. C., Sung, N.-D., Lee, C. W., Kim, H. M., & Kwon, B.-M. (2003). Anti-tumor activity of the farnesyl-protein transferase inhibitors arteminolides, isolated from Artemisa. *Bioorganic & medicinal chemistry*, *11*(21), 4545-4549. https://doi.org/10.1016/j.bmc.2003.08.008

Lee, Y. B., Gong, Y.-D., Kim, D. J., Ahn, C.-H., Kong, J.-Y., & Kang, N.-S. (2012). Synthesis, anticancer activity and pharmacokinetic analysis of 1-[(substituted 2-alkoxyquinoxalin-3-yl)aminocarbonyl]-4-(hetero)arylpiperazine derivatives. *Bioorganic & Medicinal Chemistry*, *20*(3), 1303-1309. https://doi.org/https://doi.org/10.1016/j.bmc.2011.12.026

Leung, E. L., Luo, L. X., Li, Y., Liu, Z. Q., Li, L. L., Shi, D. F., Xie, Y., Huang, M., Lu, L. L., Duan, F. G., Huang, J. M., Fan, X. X., Yuan, Z. W., Ding, J., Yao, X. J., Ward, D. C., & Liu, L. (2019). Identification of a new inhibitor of KRAS-PDEδ interaction targeting KRAS mutant nonsmall cell lung cancer. *Int J Cancer*, *145*(5), 1334-1345. https://doi.org/10.1002/ijc.32222

Loughran, H. M., Han, Z., Wrobel, J. E., Decker, S. E., Ruthel, G., Freedman, B. D., Harty, R. N., & Reitz, A. B. (2016). Quinoxaline-based inhibitors of Ebola and Marburg VP40 egress. *Bioorganic & medicinal chemistry letters*, *26*(15), 3429-3435. https://doi.org/10.1016/j.bmcl.2016.06.053

Ludwig, K. F., Du, W., Sorrelle, N. B., Wnuk-Lipinska, K., Topalovski, M., Toombs, J. E., Cruz, V. H., Yabuuchi, S., Rajeshkumar, N. V., Maitra, A., Lorens, J. B., & Brekken, R. A. (2018). Small-Molecule Inhibition of Axl Targets Tumor Immune Suppression and Enhances Chemotherapy in Pancreatic Cancer. *Cancer Res*, *78*(1), 246-255. https://doi.org/10.1158/0008-5472.Can-17-1973

Mackenzie, G. G., Bartels, L. E., Xie, G., Papayannis, I., Alston, N., Vrankova, K., Ouyang, N., & Rigas, B. (2013). A novel Ras inhibitor (MDC-1016) reduces human pancreatic tumor growth in mice. *Neoplasia*, *15*(10), 1184-1195. https://doi.org/10.1593/neo.131368

Maheshwari, K. K., & Bandyopadhyay, D. (2021). Heterocycles in the Treatment of Neglected Tropical Diseases. *Curr Med Chem*, *28*(3), 472-495. https://doi.org/10.2174/0929867327666200219141652

Martínez-Bosch, N., Guerrero, P. E., Moreno, M., José, A., Iglesias, M., Munné-Collado, J., Anta, H., Gibert, J., Orozco, C. A., Vinaixa, J., Fillat, C., Viñals, F., & Navarro, P. (2016). The pancreatic niche inhibits the effectiveness of sunitinib treatment of pancreatic cancer. *Oncotarget*, *7*(30), 48265-48279. https://doi.org/10.18632/oncotarget.10199

McCarthy, M. J., Pagba, C. V., Prakash, P., Naji, A. K., van der Hoeven, D., Liang, H., Gupta, A. K., Zhou, Y., Cho, K. J., Hancock, J. F., & Gorfe, A. A. (2019). Discovery of High-Affinity Noncovalent Allosteric KRAS Inhibitors That Disrupt Effector Binding. *ACS Omega*, *4*(2), 2921-2930. https://doi.org/10.1021/acsomega.8b03308

Melisi, D., Garcia-Carbonero, R., Macarulla, T., Pezet, D., Deplanque, G., Fuchs, M., Trojan, J., Oettle, H., Kozloff, M., Cleverly, A., Smith, C., Estrem, S. T., Gueorguieva, I., Lahn, M. M. F., Blunt, A., Benhadji, K. A., & Tabernero, J. (2018). Galunisertib plus gemcitabine vs. gemcitabine for first-line treatment of patients with unresectable pancreatic cancer. *British journal of cancer*, *119*(10), 1208-1214. https://doi.org/10.1038/s41416-018-0246-z

Melo, S. A., Luecke, L. B., Kahlert, C., Fernandez, A. F., Gammon, S. T., Kaye, J., LeBleu, V. S., Mittendorf, E. A., Weitz, J., Rahbari, N., Reissfelder, C., Pilarsky, C., Fraga, M. F., Piwnica-Worms, D., & Kalluri, R. (2015). Glypican-1 identifies cancer exosomes and detects early pancreatic cancer. *Nature*, *523*(7559), 177-182. https://doi.org/10.1038/nature14581

Middleton, G., Palmer, D. H., Greenhalf, W., Ghaneh, P., Jackson, R., Cox, T., Evans, A., Shaw, V. E., Wadsley, J., Valle, J. W., Propper, D., Wasan, H., Falk, S., Cunningham, D., Coxon, F., Ross, P., Madhusudan, S., Wadd, N., Corrie, P., . . . Neoptolemos, J. P. (2017). Vandetanib plus gemcitabine versus placebo plus gemcitabine in locally advanced or metastatic pancreatic carcinoma (ViP): a prospective, randomised, double-blind, multicentre phase 2 trial. *Lancet Oncol*, *18*(4), 486-499. https://doi.org/10.1016/s1470-2045(17)30084-0

Miguel-García, A., Orero, T., Matutes, E., Carbonell, F., Miguel-Sosa, A., Linares, M., Tarín, F., Herrera, M., García-Talavera, J., & Carbonell-Ramón, F. (1998). bcl-2 expression in plasma cells from neoplastic gammopathies and reactive plasmacytosis: a comparative study. *Haematologica*, *83*(4), 298-304.

Mizrahi, J. D., Surana, R., Valle, J. W., & Shroff, R. T. (2020). Pancreatic cancer. *Lancet*, *395*(10242), 2008-2020. https://doi.org/10.1016/s0140-6736(20)30974-0

Mosolits, S., Ullenhag, G., & Mellstedt, H. (2005). Therapeutic vaccination in patients with gastrointestinal malignancies. A review of immunological and clinical results. *Ann Oncol*, *16*(6), 847-862. https://doi.org/10.1093/annonc/mdi192

Moss, R. A., Moore, D., Mulcahy, M. F., Nahum, K., Saraiya, B., Eddy, S., Kleber, M., & Poplin, E. A. (2012). A Multi-institutional Phase 2 Study of Imatinib Mesylate and Gemcitabine for First-Line Treatment of Advanced Pancreatic Cancer. *Gastrointest Cancer Res*, *5*(3), 77-83.

Murphy, J. E., Wo, J. Y., Ryan, D. P., Clark, J. W., Jiang, W., Yeap, B. Y., Drapek, L. C., Ly, L., Baglini, C. V., Blaszkowsky, L. S., Ferrone, C. R., Parikh, A. R., Weekes, C. D., Nipp, R. D., Kwak, E. L., Allen, J. N., Corcoran, R. B., Ting, D. T., Faris, J. E., . . . Hong, T. S. (2019). Total Neoadjuvant Therapy With FOLFIRINOX in Combination With Losartan Followed by Chemoradiotherapy for Locally Advanced Pancreatic Cancer: A Phase 2 Clinical Trial. *JAMA Oncol*, *5*(7), 1020-1027. https://doi.org/10.1001/jamaoncol.2019.0892

Panja, D., Paul, B., Balasubramaniam, B., Gupta, R. K., & Kundu, S. (2020). Application of a reusable Co-based nanocatalyst in alcohol dehydrogenative coupling strategy: Synthesis of quinoxaline and imine scaffolds. *Catalysis Communications*, *137*, 105927. https://doi.org/https://doi.org/10.1016/j.catcom.2020.105927

Patricelli, M. P., Janes, M. R., Li, L. S., Hansen, R., Peters, U., Kessler, L. V., Chen, Y., Kucharski, J. M., Feng, J., Ely, T., Chen, J. H., Firdaus, S. J., Babbar, A., Ren, P., & Liu, Y. (2016). Selective Inhibition of Oncogenic KRAS Output with Small Molecules

Targeting the Inactive State. *Cancer Discov*, *6*(3), 316-329. https://doi.org/10.1158/2159-8290.Cd-15-1105

Phan, A. T., Halperin, D. M., Chan, J. A., Fogelman, D. R., Hess, K. R., Malinowski, P., Regan, E., Ng, C. S., Yao, J. C., & Kulke, M. H. (2015). Pazopanib and depot octreotide in advanced, well-differentiated neuroendocrine tumours: a multicentre, single-group, phase 2 study. *The Lancet Oncology*, *16*(6), 695-703. https://doi.org/10.1016/s1470-2045(15)70136-1

Phan, A. T., Halperin, D. M., Chan, J. A., Fogelman, D. R., Hess, K. R., Malinowski, P., Regan, E., Ng, C. S., Yao, J. C., & Kulke, M. H. (2015). Pazopanib and depot octreotide in advanced, well-differentiated neuroendocrine tumours: a multicentre, single-group, phase 2 study. *Lancet Oncol*, *16*(6), 695-703. https://doi.org/10.1016/s1470-2045(15)70136-1

Putta, R. R., Chun, S., Lee, S. B., Hong, J., Oh, D.-C., & Hong, S. (2021). Iron-catalyzed one-pot synthesis of quinoxalines: transfer hydrogenative condensation of 2-nitroanilines with vicinal diols [10.1039/D1RA02532E]. *RSC Advances*, *11*(30), 18225-18230. https://doi.org/10.1039/D1RA02532E

Qi, J., Dong, H., Huang, J., Zhang, S., Niu, L., Zhang, Y., & Wang, J. (2018). Synthesis and biological evaluation of N-substituted 3-oxo-1,2,3,4-tetrahydro-quinoxaline-6-carboxylic acid derivatives as tubulin polymerization inhibitors. *Eur J Med Chem*, *143*, 8-20. https://doi.org/10.1016/j.ejmech.2017.08.018

Quandt, J., Schlude, C., Bartoschek, M., Will, R., Cid-Arregui, A., Schölch, S., Reissfelder, C., Weitz, J., Schneider, M., Wiemann, S., Momburg, F., & Beckhove, P. (2018). Long-peptide vaccination with driver gene mutations in p53 and Kras induces cancer mutation-specific effector as well as regulatory T cell responses. *Oncoimmunology*, *7*(12), e1500671. https://doi.org/10.1080/2162402x.2018.1500671

Rao, C. V., Janakiram, N. B., Madka, V., Kumar, G., Scott, E. J., Pathuri, G., Bryant, T., Kutche, H., Zhang, Y., Biddick, L., Gali, H., Zhao, Y. D., Lightfoot, S., & Mohammed, A. (2016). Small-Molecule Inhibition of GCNT3 Disrupts Mucin Biosynthesis and Malignant Cellular Behaviors in Pancreatic Cancer. *Cancer Res*, *76*(7), 1965-1974. https://doi.org/10.1158/0008-5472.Can-15-2820

Rawla, P., Sunkara, T., & Gaduputi, V. (2019). Epidemiology of Pancreatic Cancer: Global Trends, Etiology and Risk Factors. *World J Oncol*, *10*(1), 10-27. https://doi.org/10.14740/wjon1166

Renouf, D. J., Tang, P. A., Hedley, D., Chen, E., Kamel-Reid, S., Tsao, M. S., Tran-Thanh, D., Gill, S., Dhani, N., Au, H. J., Wang, L., & Moore, M. J. (2014). A phase II study of erlotinib in gemcitabine refractory advanced pancreatic cancer. *Eur J Cancer*, *50*(11), 1909-1915. https://doi.org/10.1016/j.ejca.2014.04.008

Román, M., Baraibar, I., López, I., Nadal, E., Rolfo, C., Vicent, S., & Gil-Bazo, I. (2018). KRAS oncogene in non-small cell lung cancer: clinical perspectives on the treatment of an old target. *Mol Cancer*, *17*(1), 33. https://doi.org/10.1186/s12943-018-0789-x

Schutte, M., Hruban, R. H., Geradts, J., Maynard, R., Hilgers, W., Rabindran, S. K., Moskaluk, C. A., Hahn, S. A., Schwarte-Waldhoff, I., Schmiegel, W., Baylin, S. B., Kern, S. E., & Herman, J. G. (1997). Abrogation of the Rb/p16 tumor-suppressive pathway in virtually all pancreatic carcinomas. *Cancer Res*, *57*(15), 3126-3130.

Sharma, A., Dixit, R., Sharma, S., Dutta, S., Yadav, S., Arora, B., Gawande, M. B., & Sharma, R. K. (2021). Efficient and sustainable Co3O4 nanocages based nickel catalyst: A

suitable platform for the synthesis of quinoxaline derivatives. *Molecular Catalysis*, *504*, 111454. https://doi.org/https://doi.org/10.1016/j.mcat.2021.111454

Sturm, S., Gil, R. R., Chai, H.-B., Ngassapa, O. D., Santisuk, T., Reutrakul, V., Howe, A., Moss, M., Besterman, J. M., Yang, S.-L., Farthing, J. E., Tait, R. M., Lewis, J. A., O'Neill, M. J., Farnsworth, N. R., Cordell, G. A., Pezzuto, J. M., & Kinghorn, A. D. (1996). Lupane Derivatives from Lophopetalum wallichii with Farnesyl Protein Transferase Inhibitory Activity. *Journal of Natural Products*, *59*(7), 658-663. https://doi.org/10.1021/np960370u

Tinder, T. L., Subramani, D. B., Basu, G. D., Bradley, J. M., Schettini, J., Million, A., Skaar, T., & Mukherjee, P. (2008). MUC1 enhances tumor progression and contributes toward immunosuppression in a mouse model of spontaneous pancreatic adenocarcinoma. *J Immunol*, *181*(5), 3116-3125. https://doi.org/10.4049/jimmunol.181.5.3116

Wallis, N., Oberman, F., Shurrush, K., Germain, N., Greenwald, G., Gershon, T., Pearl, T., Abis, G., Singh, V., Singh, A., Sharma, A. K., Barr, H. M., Ramos, A., Spiegelman, V. S., & Yisraeli, J. K. (2022). Small molecule inhibitor of Igf2bp1 represses Kras and a pro-oncogenic phenotype in cancer cells. *RNA Biol*, *19*(1), 26-43. https://doi.org/10.1080/15476286.2021.2010983

Wang, M. T., Holderfield, M., Galeas, J., Delrosario, R., To, M. D., Balmain, A., & McCormick, F. (2015). K-Ras Promotes Tumorigenicity through Suppression of Non-canonical Wnt Signaling. *Cell*, *163*(5), 1237-1251. https://doi.org/10.1016/j.cell.2015.10.041

Wang, Y.-B., Shi, L., Zhang, X., Fu, L.-R., Hu, W., Zhang, W., Zhu, X., Hao, X.-Q., & Song, M.-P. (2021). NaOH-Mediated Direct Synthesis of Quinoxalines from o-Nitroanilines and Alcohols via a Hydrogen-Transfer Strategy. *The Journal of Organic Chemistry*, *86*(1), 947-958. https://doi.org/10.1021/acs.joc.0c02453

Waters, A. M., & Der, C. J. (2018). KRAS: The Critical Driver and Therapeutic Target for Pancreatic Cancer. *Cold Spring Harb Perspect Med*, *8*(9). https://doi.org/10.1101/cshperspect.a031435

Weissmueller, S., Manchado, E., Saborowski, M., Morris, J. P. t., Wagenblast, E., Davis, C. A., Moon, S. H., Pfister, N. T., Tschaharganeh, D. F., Kitzing, T., Aust, D., Markert, E. K., Wu, J., Grimmond, S. M., Pilarsky, C., Prives, C., Biankin, A. V., & Lowe, S. W. (2014). Mutant p53 drives pancreatic cancer metastasis through cell-autonomous PDGF receptor β signaling. *Cell*, *157*(2), 382-394. https://doi.org/10.1016/j.cell.2014.01.066

Wu, Z., Gabrielson, A., Hwang, J. J., Pishvaian, M. J., Weiner, L. M., Zhuang, T., Ley, L., Marshall, J. L., & He, A. R. (2015). Phase II study of lapatinib and capecitabine in second-line treatment for metastatic pancreatic cancer. *Cancer Chemother Pharmacol*, *76*(6), 1309-1314. https://doi.org/10.1007/s00280-015-2855-z

Xie, C., Li, Y., Li, L. L., Fan, X. X., Wang, Y. W., Wei, C. L., Liu, L., Leung, E. L., & Yao, X. J. (2017). Identification of a New Potent Inhibitor Targeting KRAS in Non-small Cell Lung Cancer Cells. *Front Pharmacol*, *8*, 823. https://doi.org/10.3389/fphar.2017.00823

Yang, H. H., Liu, J. W., Lee, J. H., Harn, H. J., & Chiou, T. W. (2021). Pancreatic Adenocarcinoma Therapeutics Targeting RTK and TGF Beta Receptor. *International journal of molecular sciences*, *22*(15). https://doi.org/10.3390/ijms22158125

Yaqoob, A., Li, W. M., Liu, V., Wang, C., Mackedenski, S., Tackaberry, L. E., Massicotte, H. B., Egger, K. N., Reimer, K., & Lee, C. H. (2020). Grifolin, neogrifolin and confluentin from the terricolous polypore Albatrellus flettii suppress KRAS expression in human

colon cancer cells. *PLoS One*, *15*(5), e0231948-e0231948. https://doi.org/10.1371/journal.pone.0231948

Yonemori, K., Kurahara, H., Maemura, K., & Natsugoe, S. (2017). MicroRNA in pancreatic cancer. *Journal of Human Genetics*, *62*(1), 33-40. https://doi.org/10.1038/jhg.2016.59

Zimmermann, G., Schultz-Fademrecht, C., Küchler, P., Murarka, S., Ismail, S., Triola, G., Nussbaumer, P., Wittinghofer, A., & Waldmann, H. (2014). Structure guided design and kinetic analysis of highly potent benzimidazole inhibitors targeting the PDEδ prenyl binding site. *Journal of Medicinal Chemistry*, *57*(12), 5435-5448. https://doi.org/10.1021/jm500632s

Zorde Khvalevsky, E., Gabai, R., Rachmut, I. H., Horwitz, E., Brunschwig, Z., Orbach, A., Shemi, A., Golan, T., Domb, A. J., Yavin, E., Giladi, H., Rivkin, L., Simerzin, A., Eliakim, R., Khalaileh, A., Hubert, A., Lahav, M., Kopelman, Y., Goldin, E., . . . Galun, E. (2013). Mutant KRAS is a druggable target for pancreatic cancer. *Proceedings of the National Academy of Sciences of the United States of America*, *110*(51), 20723-20728. https://doi.org/10.1073/pnas.1314307110

# BIOGRAPHICAL SKETCH

Shaila Akter Shetu was born in Bangladesh on July 7, 1995. She received her Bachelor of Pharmacy and Master of Pharmacy degree from Gono University, Bangladesh in 2017 and 2018. In 2021, she enrolled at the University of Texas Rio Grande Valley (UTRGV), Edinburg Texas for her Master of Science degree in Chemistry and was awarded Sustainability Fellowship from the Institution for the duration of her study program. Working under the supervision of Dr. Debasish Bandyopadhyay, her research focused on synthesis of bioactive heterocycles. She obtained her Master of Science degree in Chemistry from UTRGV in December 2022. Author can be reached via email at: Shaila.pharmacy@gmail.com